2009

Study Of Film Cooling Effectiveness: Conical, Trenched And Asymmetrical Shaped Holes

Humberto Zuniga
University of Central Florida

STUDY OF FILM COOLING EFFECTIVENESS: CONICAL, TRENCHED AND ASYMMETRICAL SHAPED HOLES

by

HUMBERTO ANTONIO ZÚNIGA
M.S.M.E. University of Central Florida, 2006
B.S.A.E. University of Central Florida, 2000

A dissertation submitted in partial fulfillment of the requirements
for the degree of Doctor of Philosophy
in the Department of Mechanical, Materials & Aerospace Engineering
in the College of Engineering and Computer Science
at the University of Central Florida
Orlando, Florida

Summer Term
2009

Major Professor: Jayanta S. Kapat

ABSTRACT

Film cooling is a technique whereby air from the compressor stage of a gas turbine engine is diverted for cooling purposes to parts, such as the turbine stage, that operate at very high temperatures. Cooling arrangements include impingement jets, finned, ribbed and turbulated channels, and rows of film cooling holes, all of which over the years have become progressively more complex. This costly, but necessary complexity is a result of the industry's push to run engines at increasingly higher turbine inlet temperatures. Higher temperatures mean higher efficiency, but they also mean that the turbine first stage operates hundreds of degrees Kelvin above the melting point of the metal core of the vanes and blades. Existing cooling technology and materials make it possible to protect these parts and allow them to function for extended periods of time—but this comes at a price: the compressed air that is used for cooling represents a considerable penalty in overall turbine efficiency. The aim of current cooling research is threefold: to improve the protection of components from extreme fluxes in order to extend the life of the parts; to increase the inlet turbine operating temperature; and to reduce the amount of air that is diverted from the compressor for cooling.

Current film cooling schemes consist of forcing air through carefully machined holes on a part and ejecting it at an angle with the intent of cooling that part by blanketing the surface downstream of the point of ejection. The last major development in the field has been the use of expanded hole exits, which reduce coolant momentum and allow for greater surface coverage. Researchers and designers are continuously looking for novel geometries and arrangements that would increase the level of protection or maintain it while using less coolant. This dissertation investigates such novel methods which one day may include combinations of cylindrical and fan-shaped holes embedded inside trenches, conical holes, or even rows of asymmetric fan-shaped holes.

The review of current literature reveals that very few investigations have been done on film cooling effectiveness for uniformly diffusing conical holes. They have been treated as a sort of side novelty since industrial partners often say they are hard to manufacture. To extend our understanding of

effectiveness of conical holes, the present study investigates the effect of increasing diffusion angle, as well as the effect of adding a cylindrical entrance length to a conical hole. The measurements were made in the form of film cooling effectiveness and the technique used was temperature sensitive paint. Eight different conical geometries were tested in the form of coupons with rows of holes. The geometry of the holes changed from pure cylindrical holes, a 0° cylindrical baseline, to an 8° pure cone. The coupons were tested in a closed loop wind tunnel at blowing ratios varying from 0.5 to 1.5, and the coolant employed was nitrogen gas. Results indicate that the larger conical holes do, in fact offer appropriate protection and that the holes with the higher expansion angles perform similar to fan-shaped baseline holes, even at the higher blower ratios.

The study was also extended to two other plates in which the conical hole was preceded by a cylindrical entry length. The performance of the conical holes improves as a result of the entry length and this is seen at the higher blowing ratios in the form of a delay in the onset of jet detachment. The results of this study show that conical expanding holes are a viable geometry and that their manufacturing can be made easier with a cylindrical entry length, at the same time improving the performance of these holes.

Trench cooling consists of having film cooling holes embedded inside a gap, commonly called a trench. The walls of this gap are commonly vertical with respect to the direction of the main flow and are directly in the path of the coolant. The coolant hits the downstream trench wall which forces it to spread laterally, resulting in more even film coverage downstream than that of regular holes flush with the surface. Recent literature has focused on the effect that trenching has on cylindrical cooling holes only. While the results indicate that trenches are an exciting, promising new geometry derived from the refurbishing process of thermal barrier ceramic coatings, not all the parameters affecting film cooling have been investigated relating to trenched holes. For example, nothing has been said about how far apart holes inside the trench will need to be placed for them to stop interacting. Nothing has been said about shaped holes inside a trench, either. This dissertation explores the extent to which trenching is useful by expanding the PI/D from 4 to 12 for rows of round and fan holes. In addition the effect that trenching has

on fan-shaped holes is studied by systematically increasing the trench depth. Values of local, laterally-averaged and spatially-averaged film cooling effectiveness are reported.

It is found that placing the cylinders inside the trench and doubling the distance between the holes provides better performance than the cylindrical, non-trenched baseline, especially at the higher blowing ratios, M > 1.0. At these higher coolant flow rates, the regular cylindrical jets show detachment, while those in the trench do not. They, in fact perform very well. The importance of this finding implies that the number of holes, and coolant, can be cut in half while still improving performance over regular holes. The trenched cylindrical holes did not, however, perform like the fan shaped holes. It was found that the performance of fan-shaped holes inside trenches is actually diminished by the presence of the trench. It is obvious, since the fan diffuses the flow, reducing the momentum of the coolant; the addition of the trench further slows the flow down. This, in turn, leads to the quicker ingestion of the main flow by the jets resulting in lower effectiveness.

The next part of the study consisted of systematically increasing the depth of the trench for the fan-shaped holes. The purpose of this was to quantify the effect of the trench on the film cooling effectiveness. It was found that the presence of the trench significantly reduces the film effectiveness, especially for the deeper cases. At the higher blowing ratios, the overall performance of the fans collapses to the same value signifying insensitivity to the blowing ratio.

A recent study suggests that having a compound angle could reduce the protective effect of the film due to the elevated interaction between the non-co-flowing coolant jet and the mainstream. Although it has been suggested that a non-symmetric lateral diffusion could mitigate the ill effects of having a compound angle, little has been understood on the effect this non-symmetry has on film cooling effectiveness. The last part of this study investigates the effect of non-symmetric lateral diffusion on film cooling effectiveness by systematically varying one side of a fan-shaped hole. For this part of the study, one of the lateral angles of diffusion of a fan-shaped hole was changed from 5° to 13°, while the other side was kept at 7°. It was found that a lower angle of diffusion hurts performance, while a larger

diffusion angle improves it. However, the more significant result was that the jet seemed to be slightly turning. This suggests that the jets actually have two regions: one region with reduced momentum, ideal for protecting a large area downstream of the point of injection; and another region with more integrity which could withstand more aggressive main flow conditions. A further study should be conducted for this geometry at compound angles with the main flow to test this theory.

The studies conducted show that the temperature sensitive paint technique can be used to study the performance of film cooling holes for various geometries. The studies also show the film cooling performance of novel geometries and explain why, in some cases, such new arrangements are desirable, and in others, how they can hurt performance. The studies also point in the direction of further investigations in order to advance cooling technology to more effective applications and reduced coolant consumption, the main goal of applied turbine cooling research.

As I reflect on the journey, and what it has taken to arrive to this moment, I stop and look back to a faraway time and see the people who sent me off. They fed me, clothed me—sacrificed for me. They walked with my brother and me to school and were waiting there at the end of the day. I left my country and they stayed behind, their faces shrouded by the years, the distance and their eventual passing. They were my grandmother and my aunt and I will never forget them. I dedicate this work to their memory and as a thank you for their unfailing love and support. I know that as continue the journey, they walk with me.

ACKNOWLEDGMENTS

Thanks to Dr. Kapat, who started out as my enthusiastic Thermodynamics professor and who over the years has encouraged and guided me to achieve great heights. In my life, he has played the role of teacher, advisor, mentor, cheerleader, champion, moral support, parent, friend. I can look forward to a rewarding professional career with endless possibilities because of all the lessons I have learned since I joined his lab and started on this journey. Thank you, Dr. Kapat.

I thank the members of the committee, Dr. Ruey-Hung Chen, Dr. Saptarshi Basu, and Dr. Bhimsen Shivamoggi. I am grateful for their participation in the dissertation process and for their valuable input in my candidacy presentation, emails, and conversations.

I would like to acknowledge all those with whom I have worked directly in the lab in Building 44. These are, in a sort-of-chronological order: Vaidy, Quan, Sylvette, Sanjeev, Kevin, Anil, Ahmad, Tony, Yunis, Stephanie, John, Mark, Jeff, An, Jason, Billy, Jan, Nghia, Carson, Jared, Monica, Bryan. Each offered a unique perspective, enriching my lab experience.

I also thank my family and loved ones for all their support throughout my college career: My parents, my brother Milton, my family back in Managua, Aaron, the Kohls and all my other friends who have cheered me on my journey and are cheering even more now that I am transitioning to the professional world.

Thanks, everybody—you do not know how much I have needed your support.

TABLE OF CONTENTS

LIST OF FIGURES

LIST OF TABLES

LIST OF ABBREVIATIONS

C_D	Discharge Coefficient
D	Metering diameter of hole inlet
DA	Diffusion Angle – DA6 refers to coupon with diffusion angle of 6º w/r/t hole axis
DR	Density ratio
I	Momentum flux ratio,
IR	Intensity Ratio
L	Length of hole
M	Blowing ratio, M=
N	Number of holes
P	Pressure
PI	Pitch
R	Fluid's gas constant
T	Temperature
U	Velocity
U_T	Total uncertainty (followed by a temperature subscript)
h	trench height
m	Mass flow rate through the hole
x	Distance downstream of center of the hole

Greek

α	Angle of hole-axis inclination
η	Film cooling effectiveness
κ	Ratio of specific heats
ρ	Density

Subscripts

0	Stagnation value
aw	Adiabatic wall
c	Coolant
i	Inlet
e	Exit
la	Laterally averaged
m	Main flow
rec	Recovery
T	Temperature

Other

=	Double bar indicates spatial averaging

CHAPTER ONE: INTRODUCTION

Film Cooling in Industry

Film cooling is a technique used in the gas turbine industry to protect component surfaces exposed to high-temperature gas streams. It consists of forcing air through carefully machined holes on a part and ejecting it, often at an angle, with the intent of cooling said part by blanketing the surface downstream of the point of ejection. This technique is effective in keeping turbine components cool, as these operate continuously for extended periods of time.

Over the last six decades, film cooling research has been a joint effort between industry and academia with the aim at improving the technology and its implementation. The purpose of such effort is to improve aerodynamics, increase internal and external rates of heat removal, extend the life of the components, increase turbine inlet temperature, save fuel, and reduce NO_x—for environmental reasons (and government regulations). Improvement in any of these areas can often be translated into higher turbine efficiency. However, this does not imply that having the best cooling scheme will lead to the highest efficiency. One of the main thrusts of film cooling research has been the continuous increase in the temperature at the inlet to the turbine stage as a means of increasing cycle efficiency.

According to Çengel and Boles, 2008, the simple-cycle efficiency of a gas turbine power plant in the 1940s and early 1950s was in the neighborhood of 17%. The approach to increasing the efficiency of gas turbines operating on the Brayton Cylcle, has focused on three areas: increasing the turbine inlet temperature, increasing the efficiency of the individual power plant components, and modifying the basic cycle. In practice, the easiest way to increase the efficiency has been achieved by increasing the temperature at the entrance of the turbine stage. A simple way to look at it is by assuming isentropic compression and expansion and constant specific heat; then the simple cycle thermal efficiency becomes:

$$\eta_{th,Brayton} = \frac{w_{out}}{q_{in}} = 1 - \frac{T_4}{T_3} \; (ideal)$$

If we switch our attention to the diagrams in Figure 1.1, T_3 is the temperature at the inlet of the turbine. Increasing its value will make the denominator larger and bring the thermal efficiency toward unity.

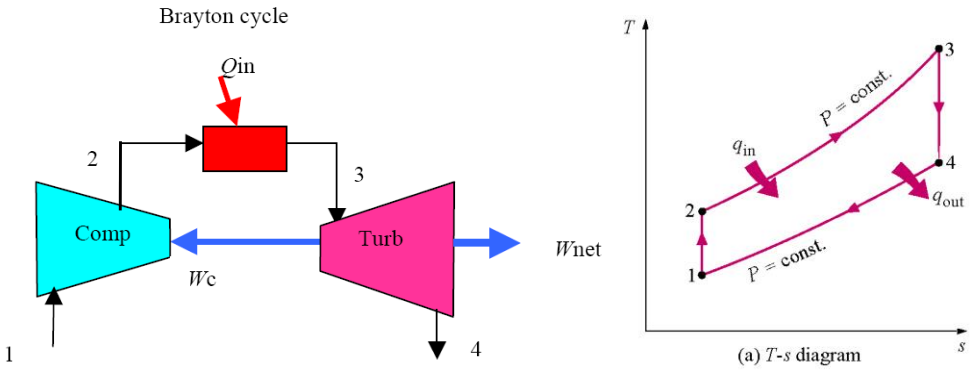

Figure 1.1 Simple cycle gas turbine (left) and its entropy-temperature diagram, Çengel and Boles, 2008

Since the 1950s, the implementation of cooling schemes to operate at higher temperatures has made it possible to reach higher efficiency. There are currently turbines that operate at simple-cycle efficiencies close to 40%, such as the Siemens SGT5-4000F, 292-MW plant. However, this comes at the cost of increased complexity, costly manufacturing processes and costly research.

Nowadays, the integration of a film cooling scheme is common practice in the gas turbine industry for combustor liners, turbine shrouds and blades, and other hot parts of the engine where thermal protection is necessary for operation. The coolant in this case is air which has been diverted from the compressor, before the combustor stage, and is guided through a system of ducts and internal channels to multiple cooling mechanisms and eventually to the main flow via the cooling holes. A fully implemented film cooling system can include thousands of cooling holes of various shapes and configurations. And while this may seem complex with the potential to be very costly, the operating conditions inside a turbine, right after the combustor, are so hostile that without such sophisticated cooling in place, parts would readily fail.

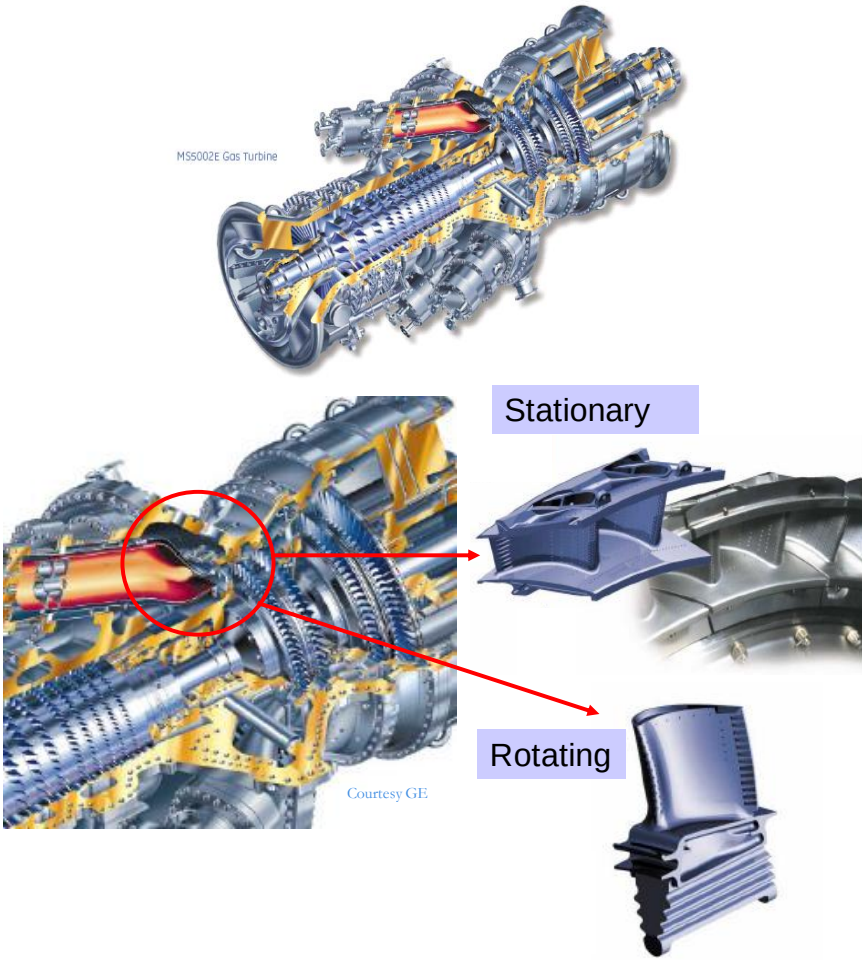

Figure 1.2 MS5002E gas turbine and first stage detail (Courtesy GE)

To illustrate typical engine conditions for the first turbine stage, where film cooling is most critical, combustion exhaust enters the turbine component at temperatures between 1500 and 2000 K, well above the melting point of the blade alloys. The centrifugal force acting on each blade as a result of rotation (12000–14000 rpm) is also on the order of several tons (Moustapha et al, 2003). The air at this point has been compressed by a factor between 10 and 28. So, it is easy to imagine an environment in which the first stage blades encounter unsteady, corrosive, thermally and structurally taxing conditions in which they must operate over extended periods of time. The blades and vanes in today's gas turbines for power generation are designed for a service life of 24 to 132 khr, 2500–5000 starts and 0–3 refurbishments (Kiesow and Kapat, 2008). Figure 1.2 shows a modern turbine with the transition duct and first turbine stage highlighted.

Dealing with the high thermal fluxes on the turbine-stage blades and vanes is a multi-pronged approach. Parts such as the shroud or the hub, which are not normal to the path of the hot gas, but are still subject to extreme temperatures, are cooled with a combination of jet impingement and sophisticated film hole patterns. Impingement is done in cavities that are designed to act as supply plenums for the film holes, illustrated in Figure 1.3. The impinged coolant makes its way out into the main flow through an array of cooling holes on the surface of the endwall.

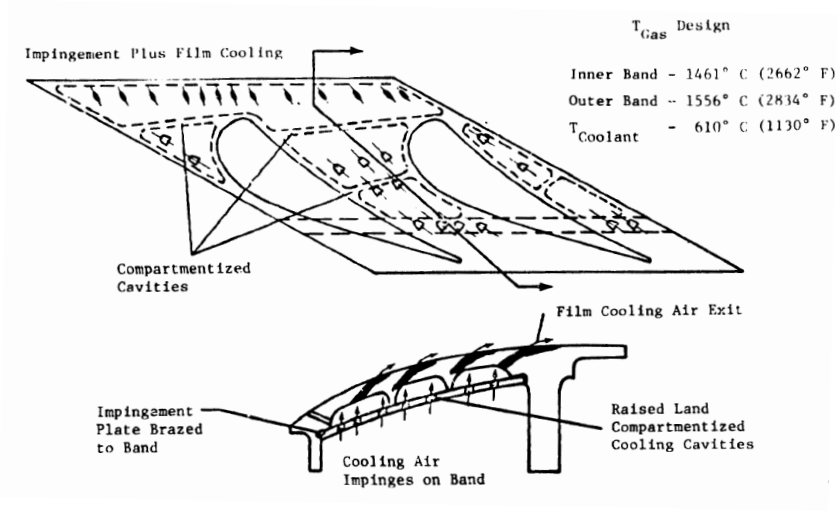

Figure 1.3 View of impingement system for endwall (Halila et al., 1982)

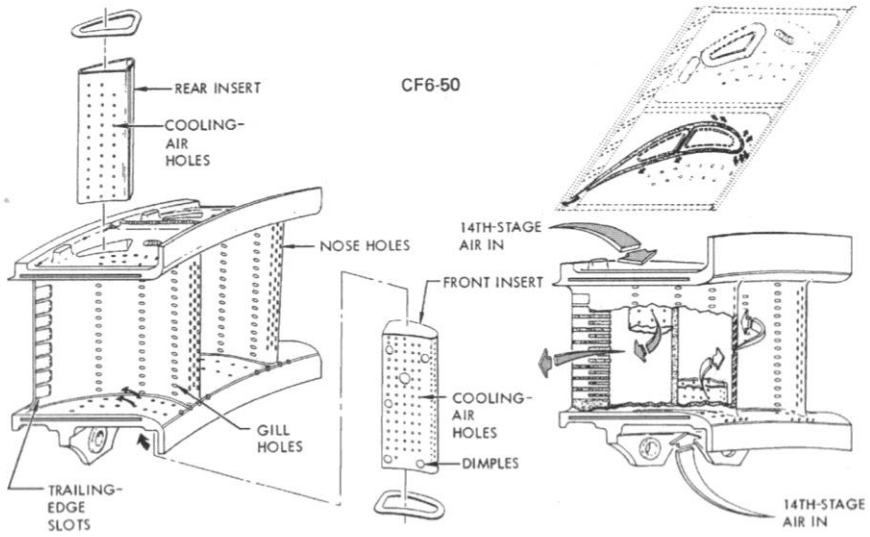

Figure 1.4 First stage turbine nozzle vanes for GE CF6 Engine (Adapted from Han et al., 2000)

First stage guide vanes, also called nozzle guide vanes (NGV), which bear the brunt of the combusted main flow and see the hottest temperatures outside the combustor, are also highly complex in construction. Pictured in Figure 1.4, the NGV features sets of inserts with arrays of holes that are designed to impinge coolant on the inner vane walls. The spent coolant then makes its way out through film holes on and over the surface of the airfoil for additional cooling. Han et al. (2000) point out that while these drawings are very detailed, they do not contain all of the state-of-the-art of cooling technology. In fact, these are highly guarded industry secrets, and they are not available in the open literature; even if they were, designs would vary widely by company and model.

Blades are built with serpentine passages, shown in Figure 1.5 through which coolant circulates. The removal of heat from the blade is enhanced by the inclusion of ribs and pin-fins in the path of the coolant. This coolant eventually makes its way out of the blade through a series of holes for film cooling.

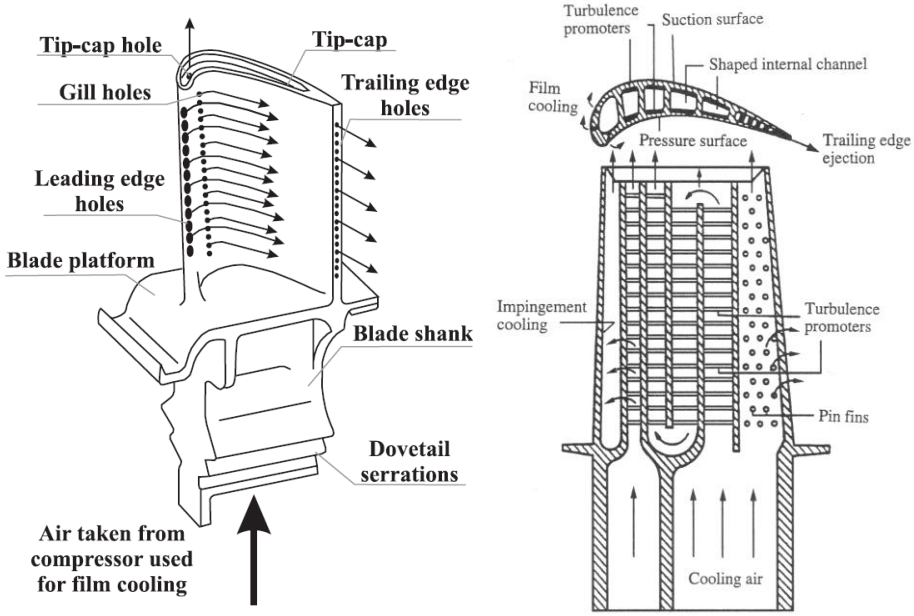

Figure 1.5 Modern blade cooling methods (Adapted from Han et al., 2000)

In all cases, the end result after internal coolant delivery is the creation of external jets on the surface of the part. Without a reliable cooling system, turbine technology—both industrial and military—would be seriously handicapped. What makes these jets work reliably and what parameters determine

that the end product will be useful? The behavior of jets in cross flow helps explain some of the underlying concepts of film cooling.

Film Cooling Basics

The aim of every film cooling design is to create a layer over a surface which adds an additional resistance to the flow of heat into the part. In the early stages of development, this was accomplished with slots. Slots are trench-like horizontal perforations attached to a coolant supply, from which the coolant is ejected in an even, uniformly distributed manner. The result of such setup is a blanket of coolant with a 2-dimensional profile that hugs the intended surface and protects it from direct contact with combusted air. Slots can inject the flow tangentially or at an angle, depending on the application, and their configurations can be numerous, as described in Goldstein's 1971 review on film cooling. The important parameters in this scenario are the slot height, the lip thickness and the flow conditions of the coolant and the main stream. Figure 1.6 is taken from Bunker (2005) and shows a tangential slot setup.

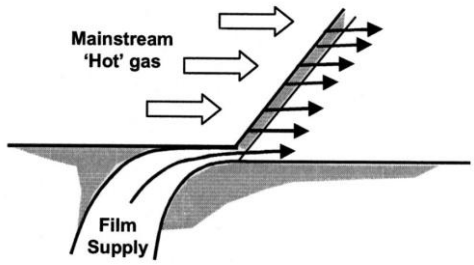

Figure 1.6 Tangential slot film cooling (Bunker, 2005)

But there are limitations to the use of slots. Inclusion of a slot on a rotor means having to subtract material, which in turn weakens the structure. Thermal demands on a robust modern cooling system would require a network of slots. But, since the blade is rotating at high rpm, facing a very high temperature main flow and experiencing large centrifugal forces, removing large portions of material will compromise its integrity and that of the entire engine. Thus, as the technology has become more

demanding on parts, the use of slots on blades and vanes has fallen out of favor and discrete film cooling took has taken its place.

Discrete film cooling consists of placing an array of small holes over a surface with the intention of somehow directing the flow to cover that surface and protecting it from the main flow. But discrete film cooling is not as straightforward as slot film cooling. Whereas slot cooling produced a directed blanket of coolant over the surface, discrete film cooling may actually cause coolant jets that do not even touch the surface. Thus it is more passive, and depends heavily on the geometry of the cooling holes, their arrangement on the component surface, the hole's supply and internal flow structure, as well as the conditions of the main flow. These parameters will determine the behavior of the coolant jet and how it behaves downstream as it interacts with the main flow.

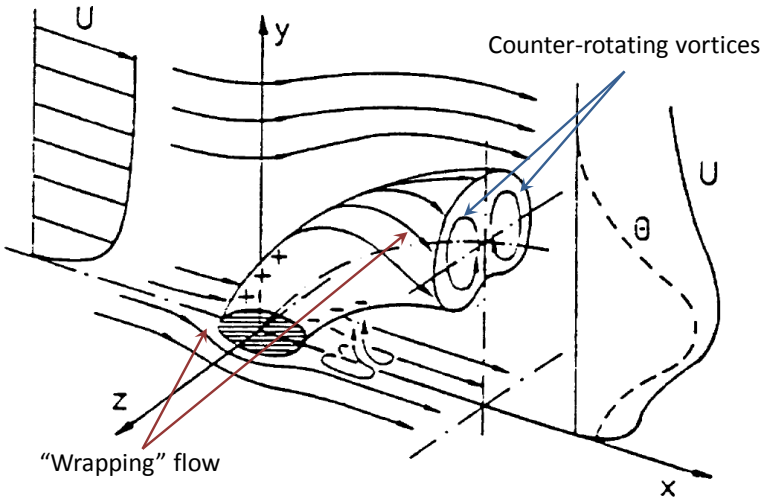

Figure 1.7 Jet in crossflow and the emerging vortex structures (Haas et al. 1991)

The salient features of the coolant jet in crossflow are the vortex structures that develop as a result of the interaction of the coolant and the main flow. As a jet emerges from the cooling hole, it encounters conditions that will eventually disintegrate it. Upon exiting the hole, the jet bends downward because of the pressure the main flow exerts on it. Because of the higher density and momentum of this jet shooting out, the main flow sees a sort of cylindrical structure in its path, and adjusts to go around it, from the sides and overhead. This continuous turning flow creates shearing on the "surface" of the

cylindrical jet, which begins to follow the circulating motion of the main flow. Since the jet is also moving downstream, because of its speed, the resulting structure of the jet is seen as two counter-rotating vortices, i.e. on either side of the jet, wrapping around it. Farther downstream, on the side near the wall, this vortex motion causes the jet to entrain hot gas as well as to lift off from the surface. As more coolant is injected into the main flow, the resulting effect is increased ingestion of the main flow, which leads to the liftoff of the jet. The main jet and vortex structures as described by Haas et al., 1991, are shown in Figure 1.7.

This is a simplified view of the jet-main-flow interaction. Other factors that contribute significantly to the final outcome are the length and inclination of the hole, the blowing ratio, the momentum flux ratio, the density ratio, the mainstream turbulence intensity and scale, the incoming boundary layer thickness, and the proximity to other jets. But before discussing these parameters, it is important to clarify in what context we are measuring this influence, after all, this must be related ultimately to turbine cooling.

Film Cooling Characterization

In the gas turbine industry, the performance of any film cooling scheme must be measured in a way as to ascertain how well it works. Film cooling is usually characterized by the non-dimensional adiabatic wall temperature (effectiveness) and heat transfer coefficient. Heat transfer in engines is driven by the temperature difference $T_{aw} - T_w$. However, it is more convenient to examine a dimensionless form of this temperature difference. This dimensionless parameter is defined as the adiabatic film cooling effectiveness, η, which is a ratio of the two temperature differences driving film cooling:

$$\eta = \frac{T_r - T_{aw}}{T_r - T_c}$$

The distribution of η is normally shown as a function of the distance downstream from the point of injection, x, normalized by the dimension D, the hole inlet diameter. x/D is equal to zero at the center of

the hole, or at the downstream lip. The main components of the effectiveness are shown in Figure 1.8. The value of η varies from 0 to 1. Zero means that the adiabatic wall temperature is equivalent to the recovery temperature, a worst-case scenario of no film protection. A value of unity means that the wall temperature is the same as the coolant temperature—a best-case scenario of ideal film protection.

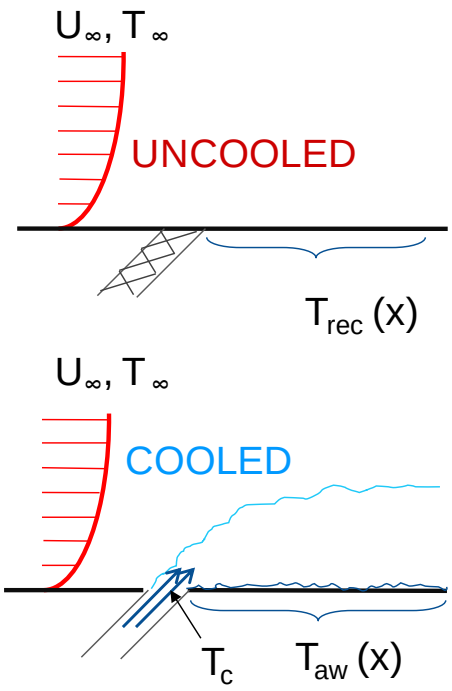

Figure 1.8 Temperature definitions for η calculations; top—no coolant; bottom—with cooling

In application, the value of the film cooling effectiveness is more useful as an average since it summarizes the results for a larger area of the cooled surface. For that reason, the distribution of η is averaged over one whole pitch, PI, the distance between two hole centerlines. This leads to the span-averaged film cooling effectiveness, η_{la}, whose maximum is under ideal conditions, the percent coverage. The percent coverage is a number that indicates what fraction of one pitch is occupied by the exit diameter of the hole, D_e at the point of injection. Thus, percent coverage can be defined as the ratio D_e/PI.

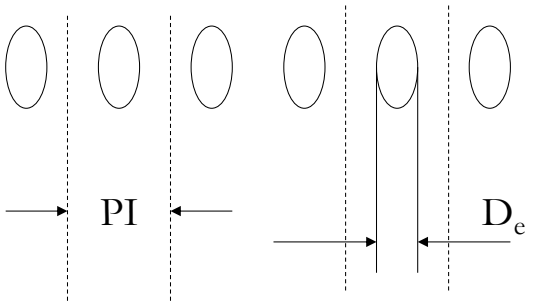

Figure 1.9 Definition of pitch and exit diameter

For cylindrical holes the near field (x/D < 20) effectiveness distribution, has a mountain-valley look because of the spaces between the holes. But as evident in Goldstein et al.'s (1974) results, shown in Figure 1.10, the widening of the jets downstream of the injection point allows the effectiveness value to reach a flatter value. Figure 1.10 shows a typical lateral distribution of the film cooling effectiveness at different planes downstream of cylindrical hole exits.

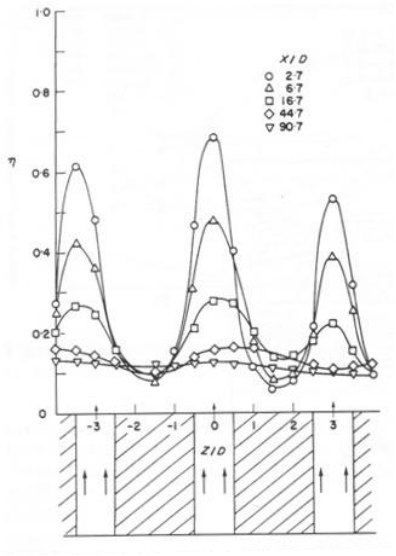

Figure 1.10 Local film cooling effectiveness at various x/D (Goldstein et al, 1974)

An early example of laterally-averaged film cooling effectiveness is given by Pedersen, Eckerd and Goldstein in 1979. In Figure 1.11, a set of curves is given that shows an average effectiveness value for a specific density ratio. What is important to notice is that while Figure 1.10 shows curves that contain local information near and around the holes, and cross sections downstream, every curve on Figure 1.11

gives a summary equivalent to that of Figure 1.10, but condensed into one line. While they are both valuable in analyzing the coolant's performance, industrial applications focus more on the general picture provided by the average curves of Figure 1.11.

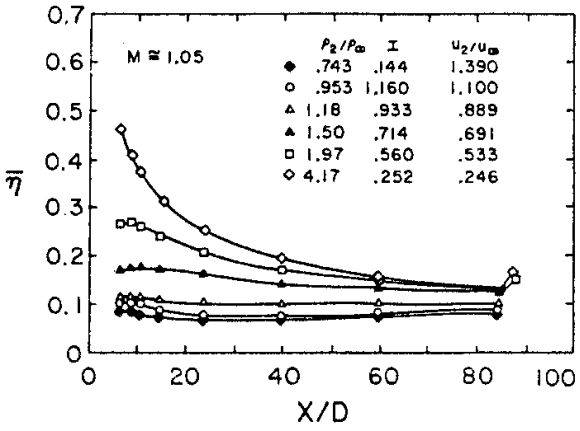

Figure 1.11 Laterally-averaged film cooling distribution (Pedersen et al., 1979)

While general curves for effectiveness of cylindrical geometry have been shown, the effects of the coolant and main flow properties, important geometry, momentum, and mass ratios will be discussed in depth in the literature review chapter. Some of the basic features of shaped holes are discussed next.

Shaped Holes

A review by Bunker in 2005 emphasized that the single major advancement in film cooling technology over the last 30 years has been the change from round film holes to shaped film holes. He calls them a "game-changing" technology. Shaped holes are those for which the exit expands, either laterally, toward the downstream edge of the hole, or evenly in all directions. Commonly, the inlet of these holes is cylindrical, with a length of at least 2 diameters, called the metering length, because it provides a reference on which to build the shaped part, at the same time it enables the flow to attach to the holes' walls. Bunker states that all shaped holes applied in practice have shaped diffuser exits with divergence angles between 10° and 15° on each side as well as on the side into the surface. Most of these holes are at inclination angles of 30°-35°, shown as α in Figure 1.12.

Shaped holes can be classified into four geometries, (A) standard shaped film holes that have both lateral expansion, fan-shape, and expansion into the downstream surface, or layback; (B) holes with pure lateral expansion, fans; (C) holes with only laidback expansion, and (D) conical holes expanding from inlet to exit uniformly around the centerline. These geometries are shown in Figure 1.12.

In industrial setups, geometry (A) is very common because of proven performance and ease in manufacturing, while (B) and (C) are not widely used as it is difficult to produce the pure single angle expansion direction in these cases. Geometry (D) is also rather difficult to manufacture precisely and there are very few studies in the open literature.

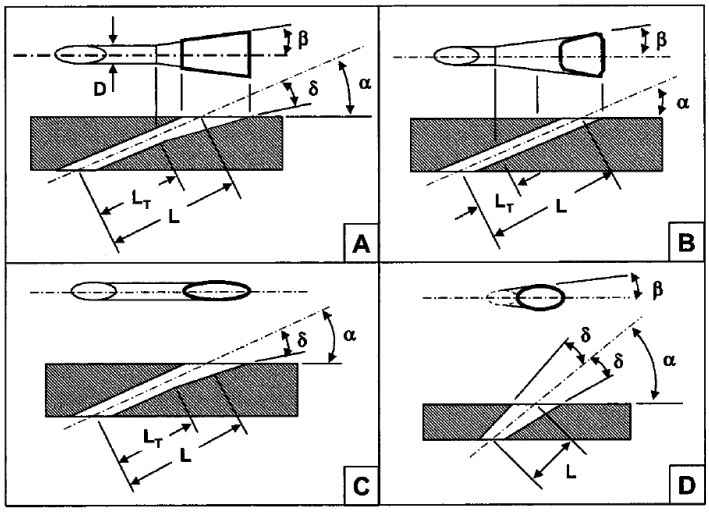

Figure 1.12 Four types of shaped holes (Bunker, 2005)

The success of the shaped geometry is due to the slowing effect it has on the velocity of the flow which is imparted by the expanding exit. Going from the cylindrical entry to the larger exit significantly reduces the momentum of the coolant, decreasing its penetration into the main flow, and also making it easy for the flow to hug the walls, e.g. the Coanda effect. The increased exit area, in most cases increases the coolant's coverage and helps a row of these holes approximate the slot 2-D flow more closely than that from the pure cylindrical geometry. At higher blowing ratios (M>1.0) (defined as $M = (\rho U)_c/(\rho U)_\infty$), the flow from shaped holes remains attached to the surface, and the film cooling effectiveness is no longer sensitive to blowing ratio, allowing them to operate at blowing ratios as high as

2.5. Cylindrical jets, on the other hand do detach above M>1, with some chance of reattachment downstream. At even higher M, cylindrical jets detach completely and do not reattach. Goldstein in 1974 conducted a study on flared holes and showed enhanced lateral spreading through the diffusion. He also concluded that the increase in the area at the exit allows higher injection rates before liftoff.

In addition to flaring of the holes, other technologies have been influential in increasing the efficiency of cooling schemes. These are thermal barrier coatings and hole manufacturing techniques.

Manufacturing Considerations

Film cooling holes are manufactured using a wide array of techniques suited to specific locations on the vanes, blades, and shroud. One of these techniques involves EDM, electrical discharge machining. EDM works by eroding material in the path of electrical discharges that form an arc between an electrode tool and a work piece. In die sinking, the EDM machine uses a machined graphite or copper electrode to erode the desired shape into the part or assembly; this is true for shaped holes. To create a potential difference between the work piece and the tool, sometimes the part is submerged in a dielectric fluid which is circulated to flush away debris. Another technique that has gained wide use is LASER drilling. High power industrial lasers such as Nd:YAG (neodymium yttrium-aluminum-garnet) drill holes very quickly and cost effectively. A combustor, for example, is made of several sheet-metal-formed parts with many thousands of holes with changing patterns, at multiple angles, and of different diameter (typically 0.4–0.8 mm). Percussion drilling, in which the laser beam pecks at the material, is one of the ways to work with such setup. Another technique used for drilling holes is abrasive waterjet. An abrasive material of controlled grading is embedded into the waterjet and is blasted through a nozzle to drill a hole. This technology is capable of producing shaped holes in hard to penetrate materials, including high strength alloys, ceramics or heat-sensitive laminates, yielding holes that are as small as 0.38 mm in diameter.

As diverse as they are, all manufacturing techniques have shortcomings in the form of deviations from the desired hole shape, more specifically, in maintaining the uniformity of the cylindrical shape they are designed to produce. For example, all the previously mentioned techniques generate residue during the manufacturing process that must be flushed out of the holes while drilling. In waterjet construction, it is easy to imagine that the jet would require some pressure adjustment as it drills deeper. In reality, the pressure is constantly adjusted during the process. Likewise, when using EDM to build holes, continuous use causes electrodes to wear out, requiring regular inspection and replacement.

Figure 1.13 A LASER drilling holes into a blade surface (Courtesy Primal/Laserdyne)

The imperfections that result range from diffusing shaped holes, when the intent is round; rough holes that may affect the flow field because the roughness is a significant percentage of the diameter; shaped holes that are formed in two-step processes in which the shaped area and the metering entrance are not properly aligned; and holes that are much larger than designed, leading to unnecessary coolant usage.

Along with manufacturing techniques and hole design, other advances in the field of materials have made possible the improvement of thermal protection and life extension of parts. They are driven by small improvements in the design of the blades themselves, optimization of cooling hole patterns, TBC coating formulations, and incremental advancements in the heat resistance of the blade alloys. This progress is slow and, as pointed out by Kiesow and Kapat (2008), despite the millions of dollars spent by industry in research and design, the curve of the uncooled allowable material temperature remains relatively flat. This is shown in Figure 1.13.

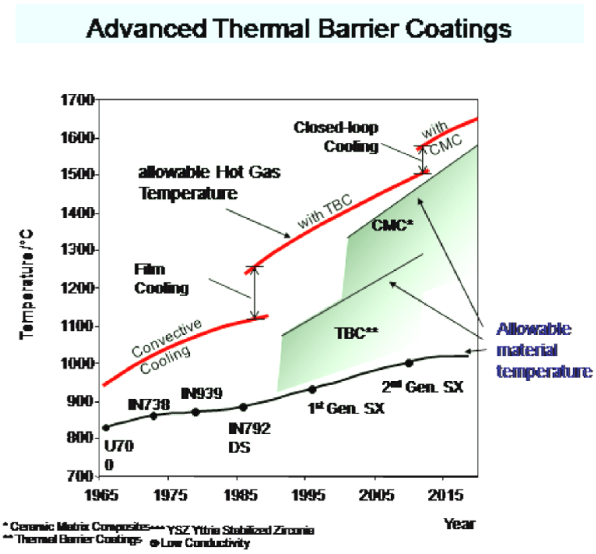

Figure 1.14 Turbine inlet operating temperature over the years (Kiesow and Kapat, 2008)

Thermal barrier coatings are ceramic-based low conductivity materials that significantly reduce the temperature at the surface of the metal substrate, be it airfoil surfaces or shrouds. Because of its low conductivity and high durability, the dominant material in TBC applications is YSZ (Yttria Stabilized Zirconia), Clark and Phillpot, 2005. TBCs are normally deposed on high temperature turbine components in the form of a film (usually from a refractory material) that adds an additional layer of resistance to the flow of heat into the metal components. In other words, these coats force a large temperature drop across the TBC, lowering the operating temperature of the metal.

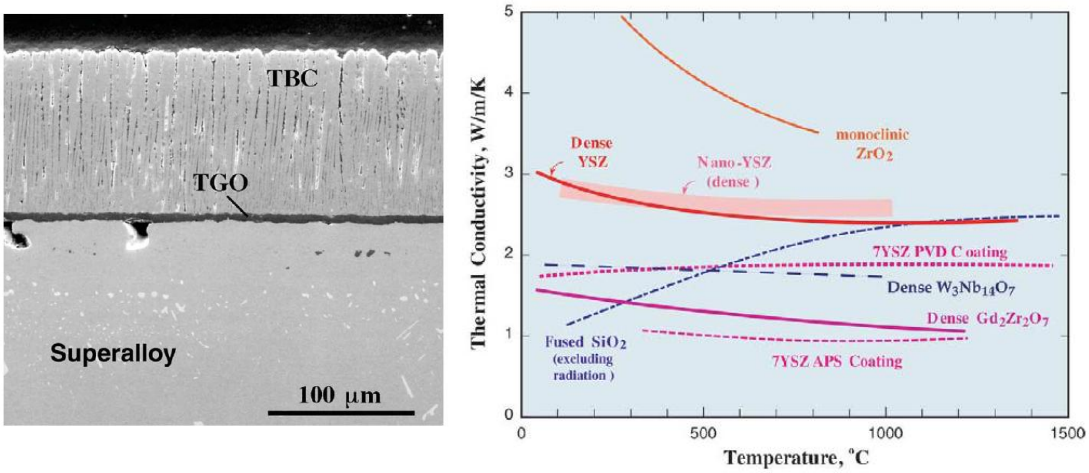

Figure 1.15 TBC deposed on alloy (left); typical values of k (right), Clark and Phillpot, 2005

The main source of cooling, compressed air is the mechanism of cooling. Even with the most effective TBC there is still the need to remove heat from the metal components; otherwise they will operate at the mainstream temperature resulting in failure. This is a concept that sometimes eludes engineers who think that better insulation will eliminate the need for coolant.

Film protection comes at a price. The source of the coolant is bleed-off air from the last stage of the compressor section. The bleed-off air, however, is removed from the core mass flow and subtracts from the engine's efficiency. Of course, the engine designer's aim is to minimize the amount of bleed-off diverted to for cooling. Therefore, improvements in technology are necessary in order to achieve higher turbine inlet temperatures and higher engine power output while reducing the amount of coolant and maintaining or improving the cooling system's performance. With this in mind, researches and designers have come up with creative approaches to enhance film cooling. The ideas which are further investigated in this study are discussed next.

Scope of the Present Study

This dissertation seeks to address multiple gaps in the literature pertaining to film cooling, especially with new concepts such as asymmetric diffusion and holes embedded in trenches. Another aim of this study is to just provide data for situations that are not addressed in the literature simply because they are not readily perceived as beneficial. For example, there are no published studies on the effect of trenching on the cooling performance of fan-shaped holes. While the author can readily predict that this effect will be negative, since the trench will be diffusing already-diffused flow, nothing on the matter has been published. This study will begin to quantify the effect in the form of a trend. Why is this important? Like round holes, fan shaped holes will likely undergo several refurbishing processes, which might leave the new fan holes inside a crater, or a trench, since TBC recoating does not rebuild the diffuser to its original shape. How will the new trench affect the performance of the fan? This will depend on the trench

depth. If the data are non-existing in the literature because they are not ground-breaking findings, the gap in knowledge will remain.

The investigations that will be performed are the following:

- study of the effect of increasing diffusion angle of conical holes; the geometries will vary from zero-diffusion to eight-degree diffusion; previous studies do not focus on trends, they only show one conical geometry to compare to other shaped holes
- the effect of adding an entry-length to a conical shaped hole
- study of the effect of pitch-to-diameter ratio on the film cooling effectiveness of cylindrical and fan-shaped holes embedded in trenches; PI/D will be varied up to 12, existing studies only go to 5.6 for round holes
- study of the effect of trench depth on the cooling performance of fan shaped holes embedded in trenches; this is a novel field
- study of the effect of asymmetric diffuser geometry on the film cooling effectiveness of fan shaped holes; only one study has addressed this subject as a side note (Gritsch et al., 2005); this is a novel field

The above mentioned studies will be performed on a variety of geometries and under a range of test conditions; the next subsection tabulates them.

Test Matrices

The first study focuses on purely conical holes. The effect of increasing angle of diffusion and its effect on film cooling effectiveness will be measured. The angles of diffusion studied will be 0, 1, 2, 3, 6, and 8 degrees. These holes will have an entrance diameter of 3.15 mm and a length-to-diameter ratio (L/D) of 3.5. In addition, two other plates will be studied that will have a larger L/D of 7.5. This will be accomplished by adding a cylindrical entry length to a conical section. The chosen conical angle will be 2

degrees, and the other plate will be a cylindrical plate. Both of these extra sets of holes will have metering diameters of 2 mm. These configurations are summarized in Table 1.1.

Table 1.1 Test matrix for study of conical diffuser configurations

TEST PLATE	D	M	PI/D
DA0(L/D=3.5) DA1 DA2 DA3 DA6 DA8	3.15 mm	0.5, 0.75, 1.0, 1.5	3
DA0(L/D=7.5) DA2(L/D=7.5)	2 mm		

For the study on the effect of pitch-to diameter-ratio, sixteen different configurations will be tested. The focus will be the trends that result in the film cooling effectiveness when the distances between the holes are increased. The plates CYL, and FAN are non-trenched baselines. The others are trenched geometries. Each configuration, listed in Table 1.2, will be tested at five different blowing ratios. More descriptive coupon names will be fleshed out in the experimental setup chapter.

Table 1.2 Test matrix for PI/D variation in trenches

TEST PLATE	PI/D	M
CYL CYL TRENCH FAN FAN TRENCH	4, 8, 12	0.5, 0.75, 1.0, 1.5, 2.0

Continuing with trenches, the next part of the study will be the evaluation of the effect of trench depth on fan holes. h/D stands for trench-depth-to-diameter ratio. This study begins with the baseline plate FAN.00, which has no trench. Then the holes are embedded in trenches that are 0.2 diameters deep, then 0.4, 0.6 and to a final depth of 0.75 diameters. The matrix for these tests is shown in Table 1.3; again, five blowing ratios will be tested.

Table 1.3 Test matrix for study of effect of trench depth on fan shaped hole effectiveness

TEST PLATE	S/D	M	PI/D
FAN.00	0	0.5, 0.75, 1.0, 1.5, 2.0	4
FAN.20	0.2		
FAN.40	0.4		
FAN.60	0.6		
FAN.75	0.75		

Switching focus to fan geometries, the next aspect is to study the effect of diffuser asymmetry on film cooling effectiveness. For this, five fan shaped configurations will be tested. All fans will have two lateral angles of diffusion, shown as α_L and α_R , and one laidback, λ. The right lateral diffusion angle will be gradually increased from 5 to 13 degrees. The pitch for these holes will be 4 diameters, a very common parameter. Five blowing ratios will be tested. These are summarized in Table 1.4.

Table 1.4 Tests matrix for fan shaped holes asymmetric diffusion study

TEST PLATE	α_L	α_R	λ	PI/D	M
5-7-11 FAN	7°	5°	11°	4	0.5, 0.75, 1.0, 1.5, 2.0
7-7-11 FAN		7°			
9-7-11 FAN		9°			
11-7-11 FAN		11°			
13-7-11 FAN		13°			

The above studies, driven by geometric effects were decided after careful examination of the literature and discussing what would be the trends that should further be explored. In one of the subjects, trench cooling with cylindrical holes, the literature has moved rather fast because of the revolutionary and potentially game-changing increases in cooling performance. However, the other fields, conical holes and asymmetrical holes suffer from a lack of publications. Although there exist recent patents in the case of conical holes, there are not enough public domain studies to give a clear idea about their performance. Chapter Three summarizes the literature available for all the proposed studies.

CHAPTER TWO: LITERATURE REVIEW

Film cooling is a subject of great interest to the power generation industry and academia. Over the last five decades, an estimated 3500 papers have been written on all subjects related to film cooling. This chapter will highlight important studies that will serve as the backbone on which to start a discussion on film cooling. Once this is in place, the newer ideas, which are the focus of this dissertation, will be presented. However, some topics are not at all established in the open literature, but the ideas behind them as well as their usefulness in industrial applications will be presented.

This review of the literature comprises four areas:

- studies on basic film cooling
- holes with conical diffuser exits
- cylindrical and fanshaped holes embedded in trenches: trench cooling
- fan-shaped holes with asymmetric exits

The first topic explains the important parameters that affect film cooling and will have direct bearing on all results from this study.

Film Cooling

In the late sixties, Goldstein, Eckert and Ramsey (1968), published a study on film cooling effectiveness with discrete cooling holes. At the time, discrete film cooling was a novelty, at least in the open literature, and the complex interaction of the discrete jets with the mainstream, and between adjacent jets was not well understood, yet from their observations they made far reaching conclusions which apply even today. Goldstein et al. showed some of the effects of Reynolds number on film cooling effectiveness, as well as the effect of inclination angle of the cooling holes. One of their major conclusions was that at low blowing ratios, the spreading of the jets is almost the same, and that an

increase in the mass flow rate through the holes leads to an increase in the centerline effectiveness downstream of the holes.

In 1977, Pedersen et al. studied the effects of the density ratio on the film cooling effectiveness of cylindrical holes at an inclination angle of 35 degrees, with a pitch-to-diameter (PI/D) ratio of 3, and holes of length-to-diameter ratio (L/D) of 40. The richness of data produced in this study would become a staple in the literature and a standard source for comparisons. Some of their results are included in the current study for comparison purposes.

Following their example, Sinha et al. in 1991, expanded on the Pedersen paper and studied the effect of varying the coolant-to-mainstream density ratio (DR) over a range from 1.2 to 2.0. They used holes with 1.27 cm diameter, PI/D of 3, and L/D of 1.75. The large amount of data in their study allowed them to make some generalizations on the behavior of the jet interaction with the mainstream, mainly quantifying the momentum flux ratio, I, at which jet detachment occurs, as well as generalizations about the conditions for jet reattachment or complete detachment. I is defined as $I = (\rho U^2)_c/(\rho U^2)_m$. They were also able to provide laterally averaged effectiveness values for their different blowing ratios. They concluded that increasing the mass flow rate causes the effectiveness values to fall off at a slower rate for attached jets. They also showed that detachment occurs at values of I greater than 0.3, but that the jets reattach quickly. However, as I is increased, the location of reattachment occurs further downstream, and that values of I greater than 0.7 lead to complete detachment. Figure 2.1 illustrates the concept of detachment. For cylindrical plates, the values of I correspond to ranges of the blowing ratio, M.

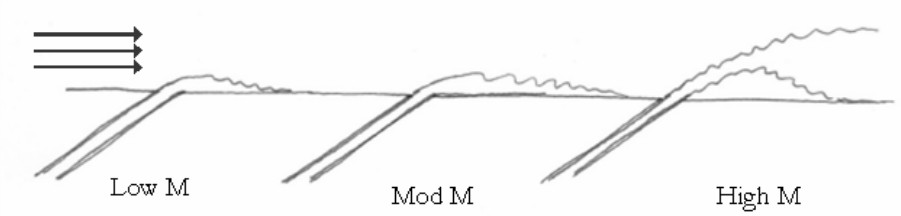

Figure 2.1 Jet and film behavior at different blowing ratios

Sinha et al. (1991) also concluded that laterally averaged effectiveness is strongly dependent on the lateral spreading of the jets, a fact that would explain the quick rise in the use of fan-shaped cooling holes in the 1990's.

Lutum and Johnson, in 1999 noticed that although data were reported at similar blowing ratios or momentum flux ratios, there were always discrepancies and disagreements between studies when reporting values of film cooling effectiveness (η), especially laterally averaged η. They pointed out that early, high impact studies like Goldstein et al., (1968), Pedersen et al., (1977), and Sinha et al., (1991), show a wide range of hole length-to-diameter ratios (L/D), from 1.75 to 40. They theorized that L/D plays a significant role in the value of η, since L/D directly impacts the internal development of the flow inside the coolant holes. Up to this point, film cooling studies had concentrated on coolant flow ratios and gas path characteristics. So, they ran a study on 4-mm holes with L/D values of 1.75, 3.5, 5, 7, and 18. Unfortunately, their PI/D was 2.86, and not 3 like all the previous studies (this would cause their laterally averaged η to be slightly higher due to increased lateral coverage and jet interaction). Their blowing ratios went from 0.5 to 1.56. Their findings suggest that after an L/D of 5 and up, L/D does not greatly impact the value of η. The biggest changes in the value of laterally averaged effectiveness were noticed between L/D of 1.75, 3.5 and 5, in which η_{la} increases 20 to 25% from L/D of 1.75 to 3.5. The increases are larger from L/D of 3.5 to 5 for low blowing ratios. At the mid and high blowing ratios, holes with L/D of 1.75 and 3.5 behave similarly, but less effectively when compared to holes with L/D of 5 and higher. Although their study was ambitiously designed to tie in very important previous findings, their data did not compare well versus that of Sinha et al., 1991.

A major advancement in film cooling technology has been the change from round film holes to shaped film holes. The review by Bunker in 2005, points out the four distinct shaped geometries and discusses important characteristics of shaped holes explaining their increased performance.

The effects that have been identified as causing fanshaped holes to remain attached are three (Haven and Kurosaka., 1997). One is the physical separation or distancing that the sidewise diffusion

imparts on the counter-rotating vortex pair, forcing both vortices to effectively lose contact. Two, is that in addition to this separation, another pair of vortices emerges (a smaller doublet) called the anti-kidney vortex pair. The name comes from the fact that these vortices are situated between the larger pair and actually rotate in a contrary sense to the original pair (hence, anti-KVP). This new pair of vortices counteracts the motion of the larger pair, effectively reducing the rate of ingestion of the main flow by the coolant. The third effect is the fact that the lateral diffusion caused by the geometry of the fan holes themselves, forces the jets to be wider and interact more quickly. Normally in application, the coverage of the fan holes is much higher that 50%, commonly approaching 70%. So as suggested by Baldauf et al, 1999, "adjacent jets of a row of holes interact to form a thickened, closed film" at higher blowing ratios. The thick layer slows the ingestion of hot gases and has a high thermal capacity, preventing early film degradation.

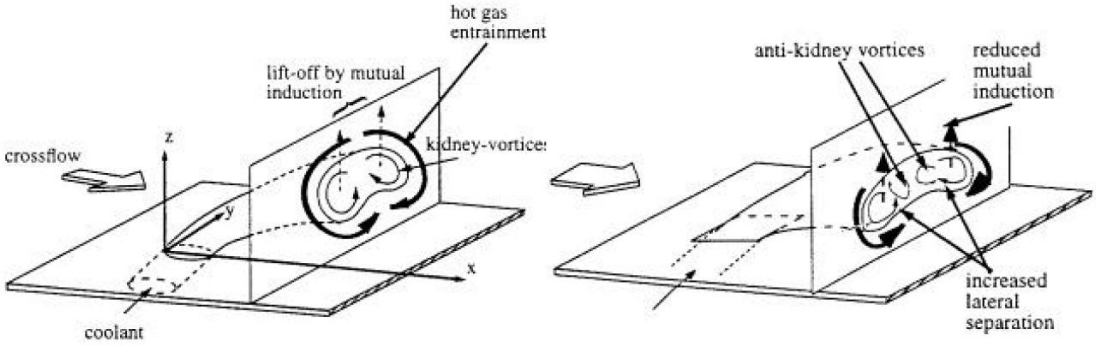

Figure 2.2 Vortex structures from cylindrical and shaped holes, Haven and Kurosaka, 1997

Investigations reported in a lower compressible flow range by Thole et al. in 1998 on a single hole test set-up indicated that by expanding the exit of the cooling holes, both penetration of the cooling jet and the intense shear regions are significantly reduced relative to that of a round hole. They observed that the peak turbulence for the fan-shaped holes was located at the exit of the cooling hole resulting from the expansion angle being too large, while for the round hole it was located downstream of the hole exit where velocity gradients were very large. Gritsch et al. also in 1998, using the same set-up, presented the

adiabatic effectiveness distribution at Mach numbers of 0.3, 0.6 and 1.2 and the coolant passage Mach numbers of 0 and 0.6. They also observed higher effectiveness values for holes with expanded exits.

In 2002, Yu et al. attempted to reduce the momentum of the injected flow while still trying to cool far downstream. Their idea involved a cylindrical hole at a 30 degree inclination, with L/D of 10. They compared it to two other shaped geometries: downstream flared (laidback) and laidback with lateral flare. The flares occurred very close to the hole exit (L/D = 0.8). Their results suggest that the lateral expansion is a more effective mechanism to increase η.

That same year also produced a very ambitious study by Baldauf et al, 2002. In their paper, they provide a correlation for film cooling η based on an extensive systematic study into the effects of blowing ratio, density ratio, mainstream turbulence intensity, inclination angle of the coolant holes, pitch to diameter ratio, and L/D on the value of η, conducted with infrared thermography, in conjunction with CFD analysis. While their study does not provide conical hole data, many of the parameters they isolated and investigated are important to the present study. Their discussion of the effect of the blowing rate on η is very insightful. In addition, the extensive amount of data generated in their publication provides many opportunities to compare results with the present study.

In 2003, Dittmar et al. assessed the performance of various cooling hole shapes, including compound angle fan shape. They reported that at low blowing ratios all the hole configurations showed similar film-cooling effectiveness, while at higher blowing ratios the fan-shaped holes out-performed the others. By the end of the 1990's, the momentum reduction of the coolant was well understood and the use of shaped holes to achieve this was well established in industry. Not surprisingly, a major study by Goldstein et al. back in 1974 had shown that with flared holes, the lateral spreading of jets over blade surfaces was enhanced, and concluded that slowing down the jets through diffusion in the flares, allows higher injection rates before jet liftoff occurs.

Saumweber el al. in 2003, studied the effects of turbulence on film cooling with shaped holes and found that cylindrical and shaped holes show different behavior under turbulent conditions. Moreover,

they found that increased turbulence is detrimental to the performance of shaped holes. They also mentioned cases in which turbulence in the areas between the holes, downstream of the exits, increases effectiveness between 50% and 100% solely because of the accelerated spanwise diffusion. Their findings showed that low levels of turbulence allowed shaped hole jets to remain attached, even at higher blowing ratios; and that for shaped holes that are close together, increased levels of turbulence actually reduce the effectiveness, since at the exit, the jets begin to interact immediately, and that high turbulence only does not help, at the very least.

In 2005, Gritsch et al. conducted a study on shaped holes in order to determine the effect of isolated geometric parameters such as area ratio (AR), coverage/pitch (C/PI), PI/D, L/D, and compound angle. The wealth of data provided by their paper provides a great source of parameters for comparison in the present study. Their findings however, suggested that varying the above mentioned parameters did not yield significant changes in film cooling effectiveness. For example, they changed AR from 3.5 to 4.2 to 4.7, without noticing any significant changes; they cautioned, though, that maybe within the range studied, the variation has little effect.

Holes with Conical Diffuser Exits

Conical hole studies are very sparse in the literature. One of the reasons for this is that the entrance to these holes is difficult to control making it difficult to build these holes in a fast and reliable way (Bunker, 2005). Although the open literature does not offer much in the number of studies on film cooling performance of conical holes, there are patents that imply their use as viable in existing designs.

However, some conical hole studies have become available in the last two decades, including a limited study by Camci and Arts (1990), as well as a study by Hay and Lampard (1995) investigating the discharge coefficient of two flared hole configurations with a cylindrical starting length. The importance of the latter study is that, at the time, there was not much literature focusing solely on conical geometry.

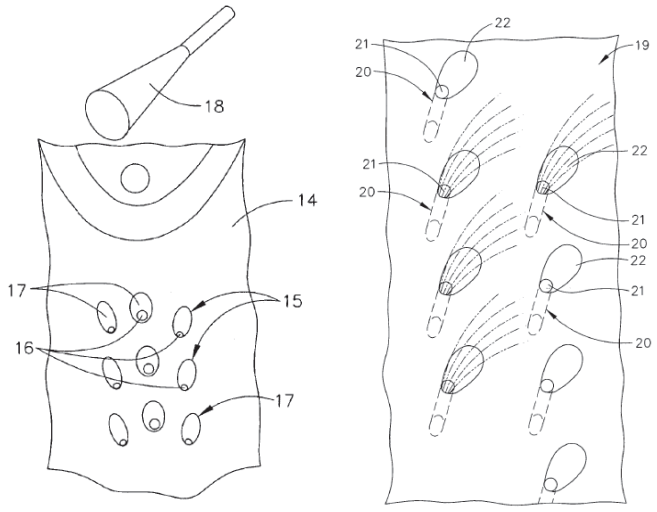

Figure 2.3 Conical holes on an airfoil section, cited U.S. Patent 7,246,992 (Abdel-Messeh et al. 2007)

Hay and Lampard arrived at a number of conclusions including that the C_D of flared holes is higher than that for cylindrical holes. This would offer the advantage of a smaller pressure drop requirement for a given flow rate, at the same time helping to reduce the momentum of the jet at the exit, which in turn would improve film cooling performance. This improvement in C_D is most visible at lower pressure ratios. The study also concluded that the cylindrical entry length "should be at least 2 diameters long and preferably 4 diameters. This allows flow to reattach to the walls of the hole before entering the flare, thereby improving the diffusing effect of the flare." The conclusions reached in their study were of particular pertinence to the design of the test geometry for the present study, since it provides guidelines for entry length geometry, as well as expectations for the values of C_D.

Another case of conical diffusion research is the flow visualization study presented by Haven et al. in 1997 on fan-shaped and conical holes for a blowing ratio of 1.0. It was observed that the so-called anti-kidney flow structure with vortices was developing in the opposite sense for diffusing holes to those associated with cylindrical holes. It was also observed that kidney vortices tend to separate the cooling fluid layer, potentially leading to lower film effectiveness downstream.

In 2001, Cho et al. studied two geometric configurations involving conical holes with entry lengths, following guidelines set by Hay and Lampard in 1995. The study involved a purely conical hole

with diffusion angle of 4 and L/D of 8.1, half of which was the cylindrical entry. Although their findings are not specifically of use to the present study, since they concentrated on near-hole local effectiveness and heat transfer coefficient, they did conclude that the "penetration of the jet is reduced and higher cooling performance is obtained even at relatively high blowing rates because the increased hole exit area reduces hole exit velocity."

One of the most recent studies involving conical holes was performed by Taslim and Ugarte in 2004. They studied C_D for a 7 degree diffusing conical hole at various inclination angles for a very large range of pressure ratios, from 1 to 5. They showed that at higher pressure ratios, conical holes have higher C_D than cylindrical holes and that lower inclination angles lead to decreases in C_D.

Trench Cooling

In the last seven years, trench cooling has emerged as a very promising configuration because of its potential to make round hole film cooling deliver protection that is on par with that of fan shaped geometry. Trench cooling is an innovative technique that imparts some of the benefits of slot film cooling onto cylindrical holes and has been shown to improve dramatically their performance over all blowing ratios. The idea is simple, embed the cylindrical holes inside a two-dimensional slot and force the flow to exit uniformly. The observed remarkable increase is due largely to the diffusion of momentum and forced jet interaction that the trench imposes, while protecting the jets from the oncoming main flow. This particular geometry is linked to thermal barrier coatings and the refurbishing process of engine parts. The TBC refurbishing process allows engine components to be repaired, rather than replaced, cutting down costs and downtime. The repair process involves removal of the TBC layers, masking the holes and recoating to the desired specifications. Once the coating is done the holes are unmasked. Depending on the region of application, the holes end up inside either craters or slots, which may not be perfectly shaped, meaning they can be rough, and at angles since the process is messy, Bunker 2002. One researcher, Bunker, wondered how the presence of this particular geometry affects film cooling and thus

emerged the idea of trench cooling. The idea of the craters and trenches and their formation in the refurbishing process are shown in Figure 2.4.

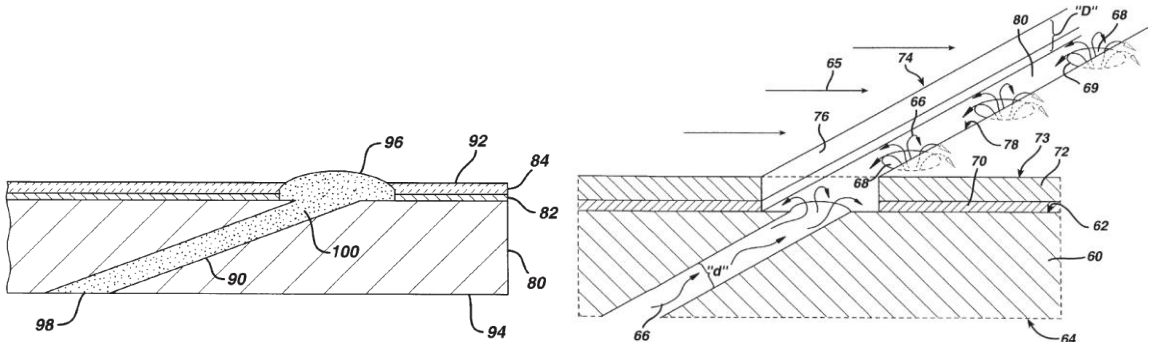

Figure 2.4 Crater formation (left) and trench (right) from U.S. patents 6,234,755 and 6,383,602

Credited in the literature as the earliest study to suggest putting discrete holes inside a slot in order to improve film cooling, Wang et al., (2002) reported on what goes on inside such arrangement in terms of mixing and its consequent benefit to film cooling applications. They studied multiple parameters, such as width and depth and axial versus radial holes, in order to determine how to transform discrete hole cooling into a 2-D phenomenon. They found an ideal slot depth range of 2 to 2.8 diameters and recommended compound angle arrangements, as opposed to pure axial holes.

Bunker, who shares patents for the discovery of "trench" cooling found that it is best to have a shallower trench as opposed to a deep one. He did so in his 2002 study, in which he tested two trenched geometries with holes embedded in them. He tested two sets of radial holes (holes that do not flow with the main flow, but at an angle) with the intent to fill up the trench with coolant. The trenches were three diameters deep and had different widths. The PI/D of the holes was 3.57 and the L/D was 5.7. The density ratio was 1.8, and the main flow was increasing from Ma = 0.33 to 0.8 to simulate airfoil surface conditions. The results did not yield the increase in effectiveness that was expected; although he only measured centerline data. The conclusion was that while the deep trenches studied by Wang are meant to mix the flow and make it more even, they do not provide enough protection downstream to be practical.

Bunker then tested a shallow trench with pure axial holes. He also reported an improvement in film cooling effectiveness between 50 to 70% higher for x/D <40, for the shallow trenches and that the geometry is insensitive to changes in blowing ratio. The setup and the effectiveness data are shown in Figure 2.5. He concluded that the shallow trench was more promising than the deep trench and that the shallow trench was much easier to manufacture since its depth was comparable to the thickness of TBC, and its inclusion on an airfoil would not compromise the metallic component of the part.

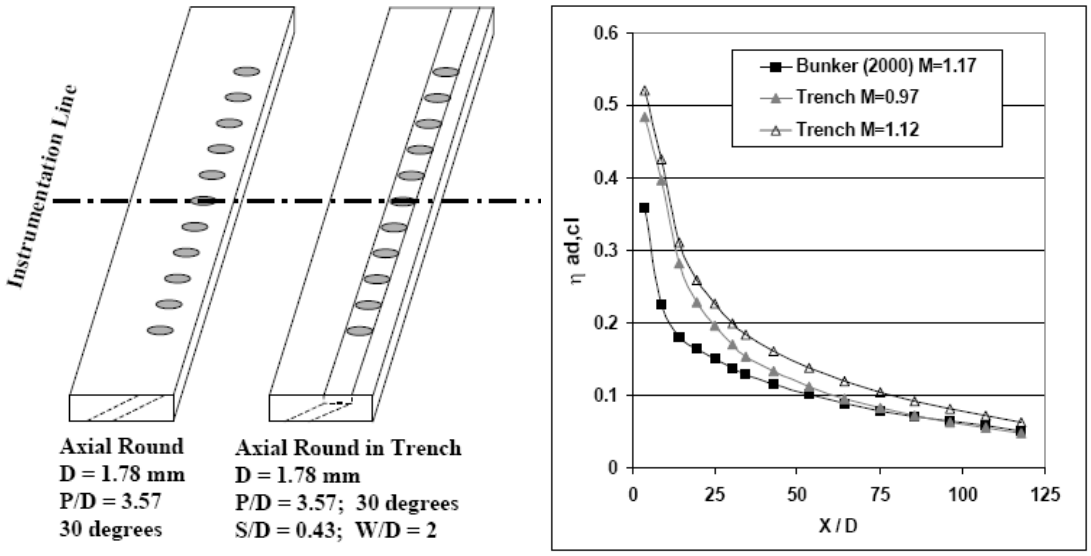

Figure 2.5 Axial holes inside trench (left) with results (right) from Bunker, 2002

In 2005, Lu et al. presented a semi-parametric study of trench wall placement for a set of cylindrical holes, shown in Figure 2.6. They studied a set of trenches of four different arrangements, one with a upstream and downstream gap (case 1), one with an upstream gap and no gap upstream (case 2), one with no upstream gap, but with downstream gap (case 3), another one with upstream gap and a downstream angled lip (case4), and case 5 being a baseline cylindrical hole.

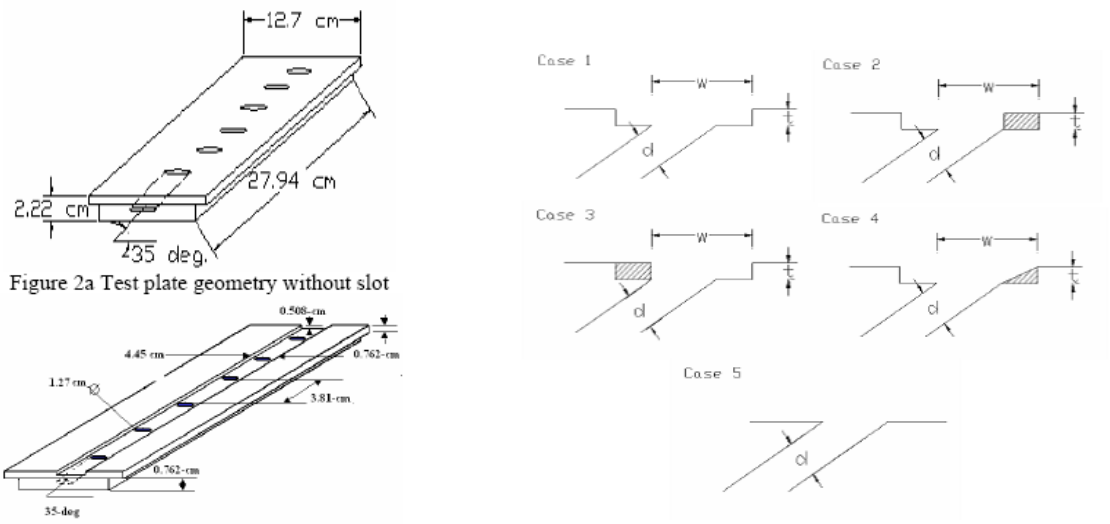

Figure 2.6 Test coupons (left) and case configurations (right) from Lu et al., 2005

Their study was aimed at evaluating more in depth the performance of trenches. They knew that trenched holes showed enhancements, but did not know which way to place the slot best. They found that the geometry of the slot greatly affects the film cooling performance downstream of the slot. They measured film effectiveness and HTC for three blowing ratios using a transient infrared thermography technique in an open tunnel. Their density ratio was kept at 1.22. Their most significant results are shown below, summarizing the performance of every configuration. Curiously, they thought that case 4, which has a lip similar to that of a shaped hole, was the best performing slot at the lower blowing ratios. They did point out that case 2 did perform best at the highest blowing ratio, as seen in Figure 2.7.

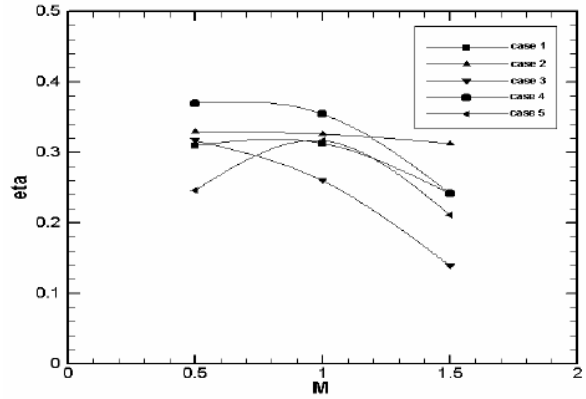

Figure 2.7 Spatially averaged film effectiveness for all cases from Lu et al., 2005

In 2006, Waye and Bogard presented an ambitious study of trench cooling. They measured film cooling effectiveness on a vane surface at various blowing ratios, density ratios and turbulence intensities. They tested nine trench configurations plus one baseline as shown in Figure 2.8.

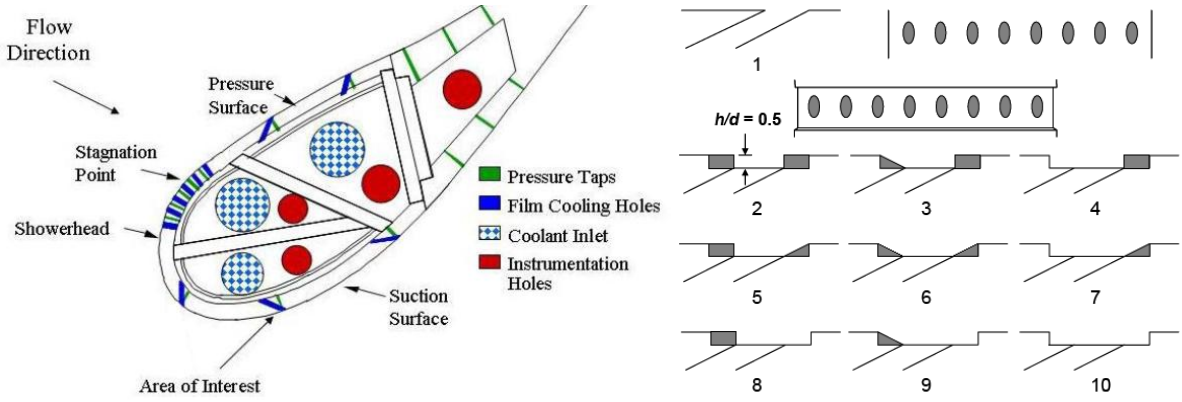

Figure 2.8 Test surface (left) and trench cases (right) for Waye and Bogard, 2006

Their test rig simulated a three-vane linear cascade. The flow was accelerating from 5.8 m/s at the inlet up to 32 m/s at the exit. The Reynolds number at the test plane was 1.06x10 with a turbulent intensity of 3.9% and 1.0% for the high and low cases. The baseline cylindrical holes had L/D of 6.7; 5.7 with the trench. PI/D was 2.78, and h/D was kept at 0.5, with w/D at 4 max. These parameters describe all cases in Figure 2.8 (above).

From the beginning, Waye and Bogard noticed that there was one particular type of trench that outperformed all others, that with the trench wall at the edge of the hole exit. It clearly outperformed the other configurations, by far, as seen in Figure 2.9. In their study, they also disputed the results found by Lu eat al. in 2005 and showed them to be inconsistent with the literature. They also shifted the focus of their study to the narrow configurations since they seemed the most promising and ran a thorough study of the narrow configuration, as seen in Figure 2.10.

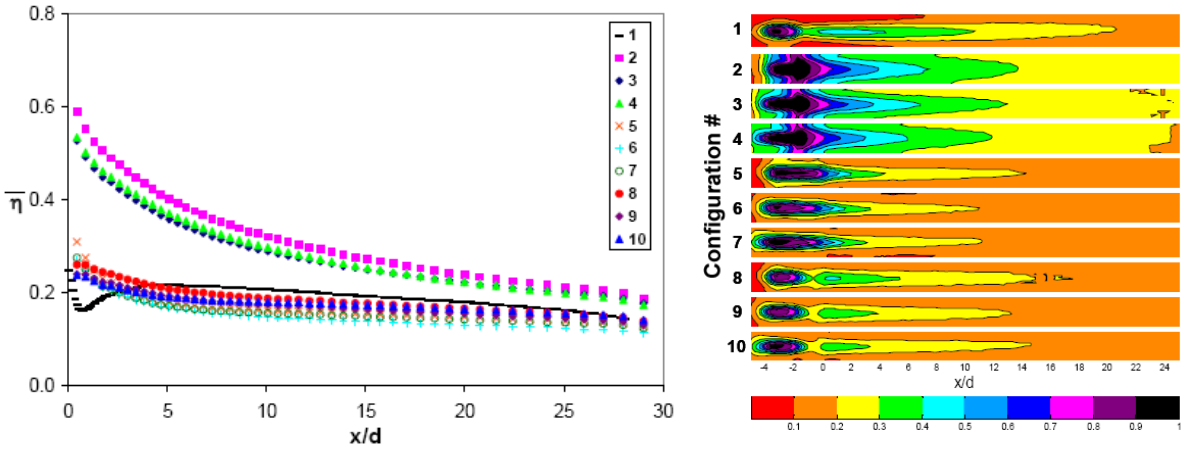

Figure 2.9 M = 1.0: averaged effectiveness (left) and local (right) values from Waye and Bogard, 2006

Waye and Bogard attributed the higher performance of the narrow trench to the idea that the wall immediately at the exit of the hole forced some of the coolant to spread laterally before coming out of the trench. This, in turn prevented the coolant from entraining hot gas from the main flow, thus leading to increased film performance over all x/D. They noted that the narrow trench configuration increases effectiveness by 300% at M = 1.4 compared to the baseline, while the wide trench increased performance by 65%.

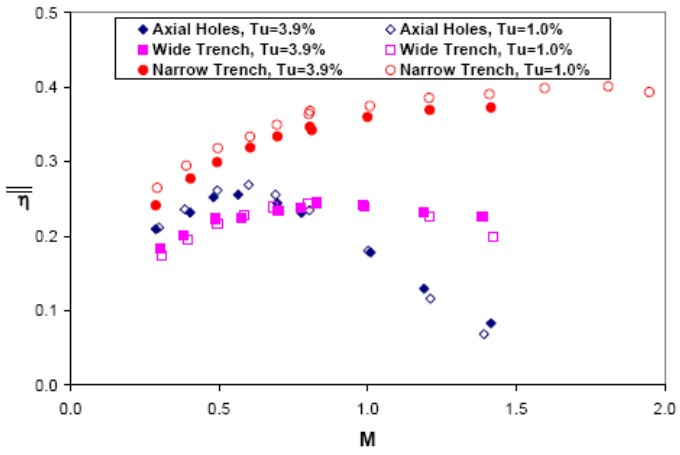

Figure 2.10 Area-averaged effectiveness for baseline, narrow and wide trenches; Waye and Bogard 2006

In their study, Waye and Bogard also compared their results with data from the literature on fans, as seen in Figure 2.11. They found that the spatially averaged effectiveness of the narrow trench

compared in performance to the results of the different configurations studied by Saumweber et al. in 2003.

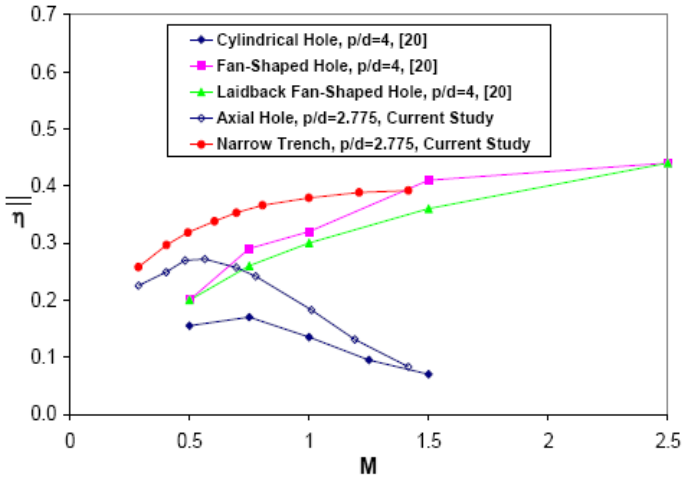

Figure 2.11 Waye and Bogard's (2006) comparison against fan shaped holes in the literature

All in all, Waye and Bogard established that the narrow trench was the best performing trench geometry in the set and that it performed as well as fan holes. This was a significant study since it singled out the narrow trench and the perpendicular wall effect from all the candidates, something other studies had failed to do up to then.

Lu et al. presented another study in 2007 in which they tested trenched holes at three different values of h/D (0.5, 0.75, and 1.0) and two trench widths (w/D of 2 and 3). They performed HTC and film effectiveness measurements with infrared thermography at three different blowing ratios, M = 0.5, 1.0, 1.5, and 2.0. They also conducted a CFD study of their most significant findings to explain the measured observations. The test section was an open tunnel and the main flow air was heated with a high response mesh. The density ratio of the coolant to main flow was 1.07. The main flow velocity was kept at 13.8 m/s, and had a turbulence intensity of 2%. The diameter of the test holes was 1.27 cm and their L/D was estimated at 3. The angle of the holes was 30°. The cases run in the study are shown in Figure 2.12. There was also a shaped hole geometry which appears to have 100% coverage. The authors do not give any details on angle or L/D, so these values are estimates.

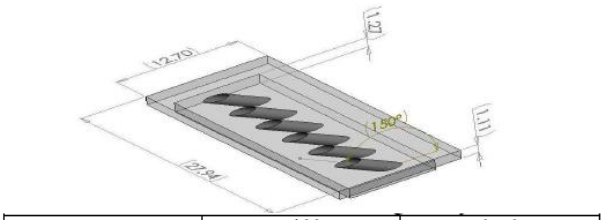

	width	depth
Case 1 (Fig. 4b)	2D	0.5D
Case 2 (Fig. 4c)	3D	0.5D
Case 3 (Fig. 4d)	2D	0.75D
Case 4 (Fig. 4e)	3D	0.75D
Case 5 (Fig. 4f)	2D	1.0D
Case 6 (Fig. 4g)	3D	1.0D

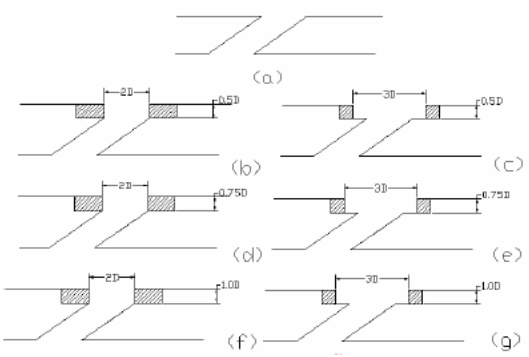

Figure 2.12 Test coupon and cases run by Lu et al., 2007

Lu et al.'s 2007 results show that cases three and four, the two trenches with the h/D of 0.75, provide the best film effectiveness among the trench cases, indicating that 0.75D is the optimum depth for the trenches. They also show that the narrow trench is also the best performing, compared to the wider case 4, implying that the added space before the hole exit does indeed hurt performance.

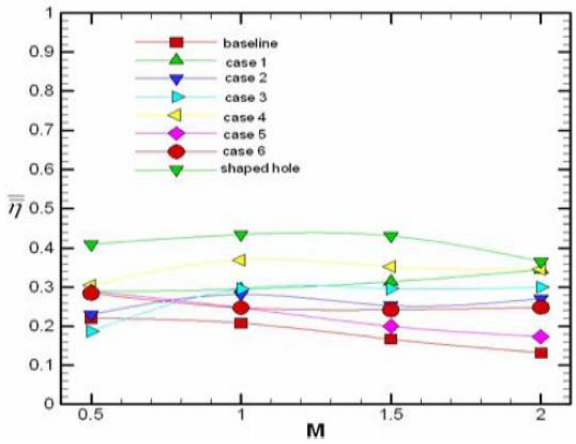

Figure 2.13 Spatially-averaged effectiveness for all case, from Lu et al., 2007

Lu et al.'s results are summarized in Figure 2.13. They show that the fan holes perform better than all configurations, even though the shape of the holes seems arbitrary, providing no basis for the comparison. However, all shapes do outperform the baseline cylindrical holes, with cases three and four being the best trench cases. In addition, the trench performance seems unaffected by the increase in blowing ratio. The explanation given by the authors for this enhancement is that the trench decreases the average exit velocity. For the wide case, the decrease is 20%, for the narrow case it is 30%. The decrease

in momentum allows the coolant to hug the walls and remain attached. They found that their computational results agreed with observed experimental data.

Also in 2007, Dorrington et al. presented an experimental study on trenches and craters of great scope. They showed values and trends of spatially-averaged film effectiveness for twenty configurations. They tested the geometries in a closed loop cascade. Each configuration was tested on the suction side of a vane, as seen in the Figure below. The technique was infrared thermography and the vane material was low conductivity foam.

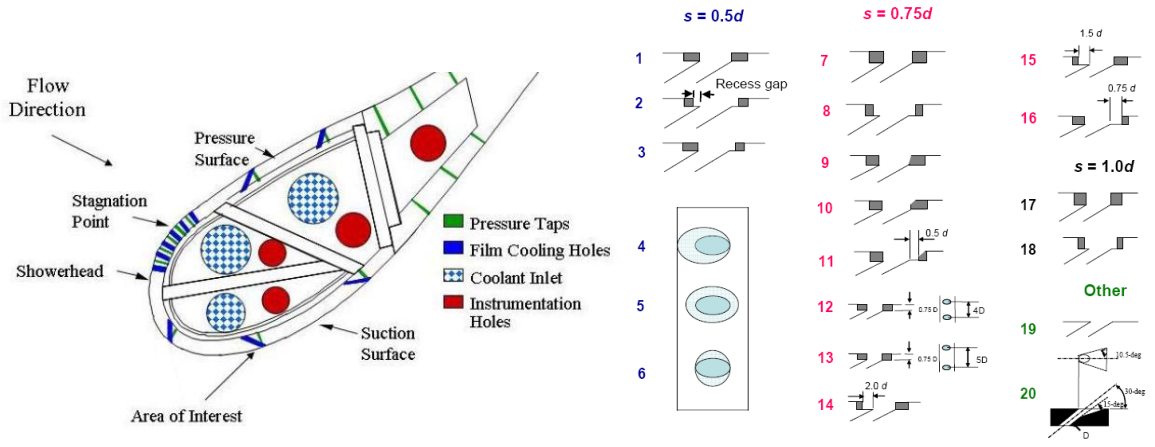

Figure 2.14 Test section (left) and test hole configurations (right) from Dorrington et al. (2007)

Results were reported as spatially-averaged film effectiveness from $0 \leq x/D \leq 22$. Where x = 0 is defined as one diameter downstream of the projected hole centerline onto the cooled surface. For their narrow trench (configuration 7), this meant one diameter away from the lip of the trench.

Their results indicated that the narrow trench configuration, in which the edges of the holes are flush with the trench wall perform the best. From that subset, they tested at three different trench depths (h) and found h = 0.75D to be optimal (configuration 7); beyond that, the deeper trench provided no added benefit. For reference, a row of cylindrical holes, configuration 19, was added. Shown in Figure 2.15, they showed that as h/d changes from 0.5 to 0.75, there is an increase of up to 40% in the spatially averaged film effectiveness for the largest blowing ratios (1.6). Compared to the baseline cylinder, the

improvement is in the 300% range. They concluded that the trench appears to reduce jet separation and that as the depth increases, the trench fills up providing almost uniform distribution of film for h/D = 1.

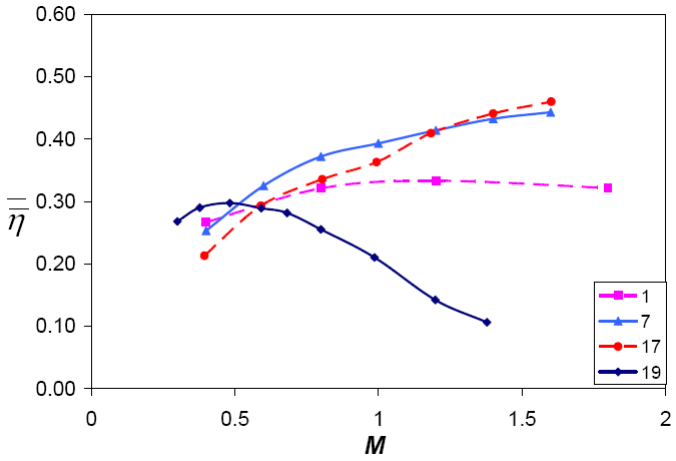

Figure 2.15 Film effectiveness for narrow trenches from Dorrington et al. 2007

The 2007 study of Dorrington et al. also analyzed the effect of trench width, downstream gap width, upstream gap width and a downstream angled trench lip. For a shallow, wide trench (configurations 2 and 3), the film effectiveness is poor compared to a deeper trench of the same width (h/D = 0.75 or 1). For deeper trenches, the width is unimportant. However, the effect of the downstream gap between the hole exit and the trench wall is important because it reduces film effectiveness by as much as 50% compared to the narrow configurations. The presence of an upstream gap, however, is not as severe in its degradation of film performance. The addition of an angled downstream trench wall also decreases film performance by as much as 40% for the two configurations tested compared to the top-performing trench.

Another aspect of the Dorrington et al. study was the variation of the pitch between holes. The original configuration had a PI/D of 2.78; they also studied PI/D of 4 and 5. What they found was that if they used the effectiveness results for the PI/D of 4 and 5 and used them to predict the value of film effectiveness for the PI/D = 2.78, their results were lower by 10%, indicating an enhancing effect that was missing in both higher-PI/D plates. Another suggestion by Dorrington et al. is that in the higher PI/D

trenches, there is no interaction between the jets. The authors show a contour plot of effectiveness for the trenches as seen in Figure 2.16.

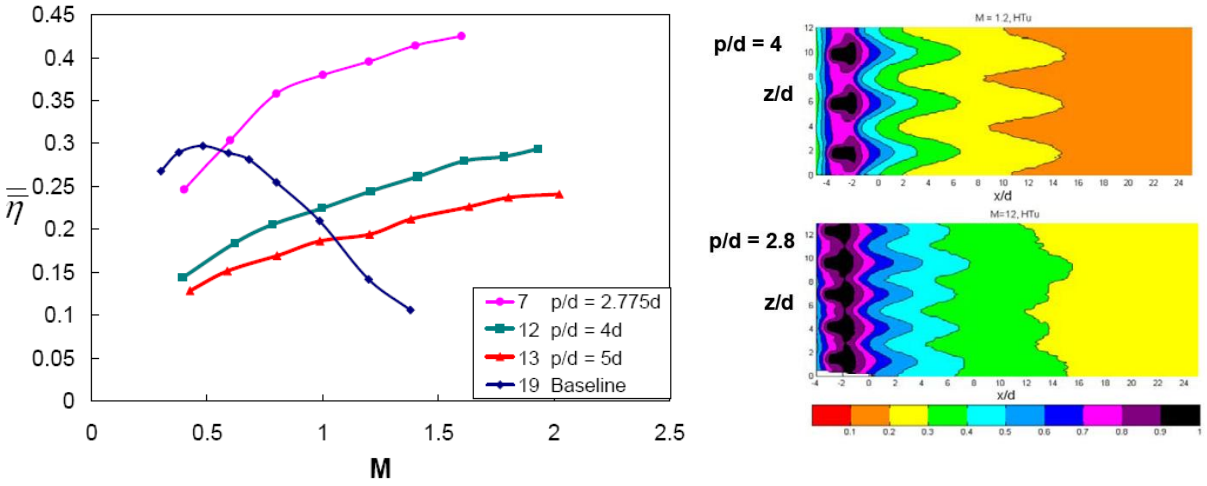

Figure 2.16 Effectiveness plots (left) and contours (right) for PI/D study, from Dorrington et al., 2007

In addition to the cylindrical baseline, the study of Dorrington et al., also included a fan hole baseline. They used a 10.5-10.5-15 configuration to compare its performance to that of the trenches. They found the trench film effectiveness on par to that of the fan hole, as shown in Figure 2.17. This brings up a similar conclusion to that of the studies by Waye and Bogard, 2006, in which they suggest that using trenches can provide performance similar to the more expensive fan holes, but at a lower cost, since fan holes are rather laborious to build, compared to cylindrical holes. Their study concludes with the inclusion of craters, which improve cooling performance significantly compared the baseline, but not as dramatically as the trench holes. The impact of their study is their systematic measurement of so many parameters and the quantification of the parameters important to trench and crater cooling. Their work verifies and encompasses the findings of other trench studies.

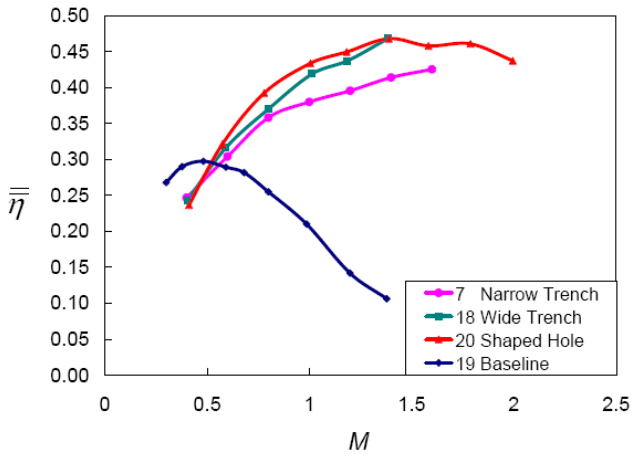

Figure 2.17 Film effectiveness for trenches, fan and baseline from Dorrington et al., 2007

Harrison and Bogard (2007) conducted a computational study to try to see if CFD could be used to predict the trench behavior observed in the Waye and Bogard study of 2006. They used a realizable k-ε model in FLUENT which yielded moderate success. They knew before starting that CFD has been found in previous studies to under-predict the laterally-averaged values of film effectiveness and over-predict centerline values of the film cooling effectiveness. They simulated three geometries: one baseline, one narrow trench and one wide trench, seen in Figure 2.18.

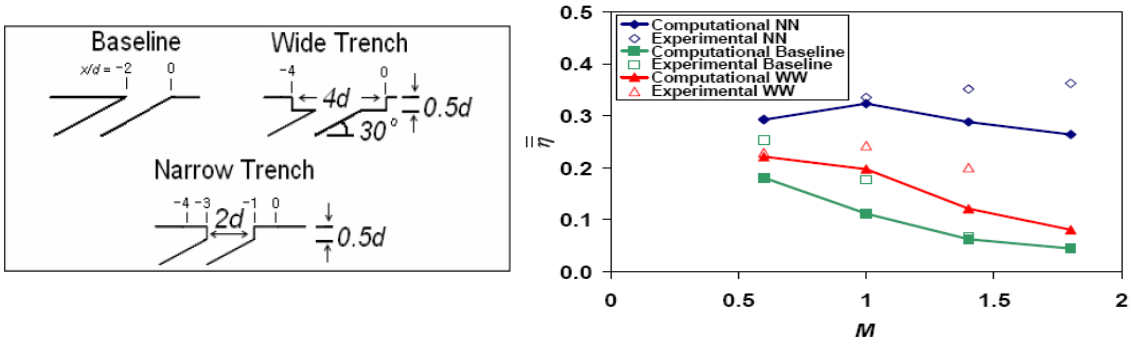

Figure 2.18 Cases studied (left) by Harrison and Bogard, 2007, and summarized results (right)

The general trends observed from the simulation were in agreement with the experimental trends. Although the aim of the study was to see if CFD could be useful in predicting the effectiveness of novel geometries, its lack of accuracy could become an issue if designers were to base important decisions on unverified CFD results.

The studies discussed thus far have only dealt with cylindrical holes in trenches and their comparisons to shaped holes. But none have addressed shaped holes inside trenched. The only study to be found on this subject is that of Baheri et al., 2007. They simulated a cylindrical hole, a cylindrical hole in a trench, a forward-diffused shaped hole, and a forward-diffused shaped hole inside a trench. They found the shaped hole to outperform all other configurations in laterally-averaged effectiveness.

Fan-shaped Holes with Asymmetric Exits

Although it has been suggested that a non-symmetric lateral diffusion could mitigate the ill effects of having a compound angle by Gritsch et al., 2005, little has been written on the effect this non-symmetry has on film cooling effectiveness. Figure 2.19 shows the only comparison between a symmetric and asymmetric shaped hole found by the author in the open literature. The geometries J and P correspond to 4-4-8 shaped holes at 45° compound angles. The geometry P is asymmetric, having 4-0-8 diffusion and at 45° compound angles. The side of the hole having zero diffusion for configuration P, is the side facing the main flow.

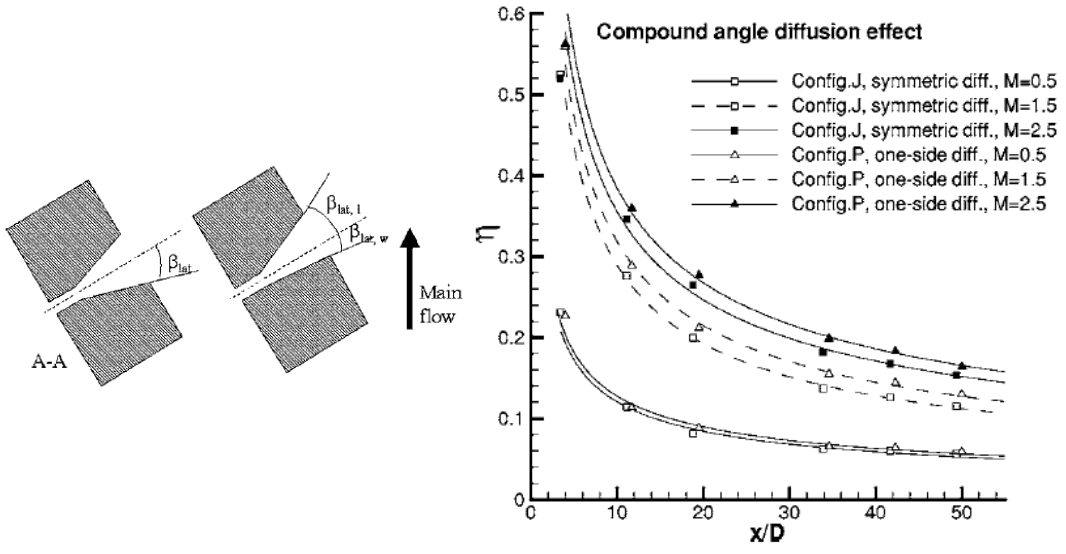

Figure 2.19 Symmetric and asymmetric shaped holes (left); Effectiveness plots (right), Gritsch et al. 2005

One can notice there is only a slight difference in the performance of the two different arrangements. While the study does not shed much information on the subject of the sensitivity to the diffusion angle, the authors suggest there may be a benefit from making holes asymmetric, especially since compounding has been shown in other studies to be detrimental to the performance of fans.

The present paper attempts to study the effect of asymmetric lateral diffusion on film cooling effectiveness by systematically varying one side of the fan shaped hole from 5 to 13 degrees. Results, in the form of laterally averaged effectiveness plots, are presented for a single row of fan shaped holes with a pitch-to-diameter ratio of 4 and blowing ratios ranging from 0.5 to 2.0.

CHAPTER THREE: EXPERIMENTAL SETUP

Test Conditions

Tests were conducted in the Basic Film Cooling (BFC) rig in the Engineering Field Lab facilities located on the main campus of the University of Central Florida. The rig operates at a temperature of 68 ± 1°C and a Mach number of 0.14 at the test section. The operating temperature is mainly dictated by the blower, which does work on the air mass, thus heating it up. The freestream turbulence intensity is less than 1% at the test section. Having a tunnel that is closed loop led to the choice of nitrogen for coolant; as a result, during tests, the coolant-to-mainstream density ratio is maintained at 1.26. More details on the wind tunnel are discussed in the following sections.

The Basic Film Cooling Rig

The Basic Film Cooling rig is shown in Figure 3.1. The wind tunnel is a closed loop system capable of operating around the clock.

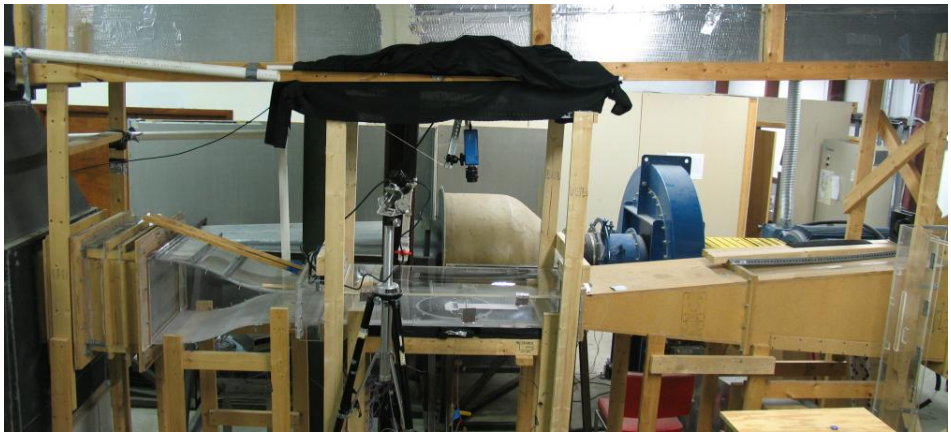

Figure 3.1 Photograph of BFC rig (foreground)

The BFC rig can be divided into five sections: 1) the blower, 2) flow conditioning, 3) test section, 4) the grommet and plenum, and 5) the recirculating ductwork. Figure 3.2 shows a schematic of the main components of the BFC rig.

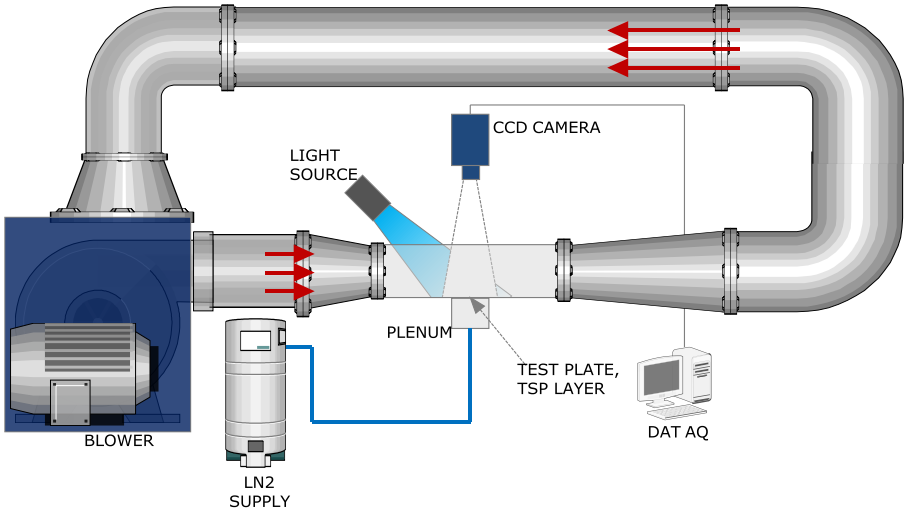

Figure 3.2 BFC rig schematic

The freestream air inside the rig begins at room temperature. It is recirculated and slowly heated by a 15-kW blower. This blower is capable of supplying air at a rate of 4.7 m^3/s and at a velocity of 52 m/s at the test-section. It normally takes about three hours for the freestream air to heat up to 68°C. However, to ensure that the tunnel wall temperature is close to the freestream air temperature, the tunnel is allowed to warm up an extra hour. The difference in temperature between the tunnel walls and the main flow is monitored with a thermocouple encrusted in the floor of the test section, close to the surface exposed to the mainstream. After the four-hour period, the difference in temperature is less than 1.5 °C and does not change by more than 0.1°C in 10 minutes; the tunnel is considered to have reached steady state.

Immediately downstream of the blower is the flow conditioning section, which consists of a honeycomb and three screens. Figure 3.3 shows the setup of the screens and the nozzle. The tunnel, at this point, has a cross-section 44.5 cm high by 53 cm wide. The honeycomb screen is 12.7 mm thick and is followed by the three remaining fine wire screens, spaced at 8.9-cm intervals. Following the screens is

the start of the 2-dimensional Plexiglas nozzle. This nozzle contracts from a cross-section height of 44.5 cm to 16.5 cm, over a length of 73.7 cm, while keeping the cross-sectional width constant.

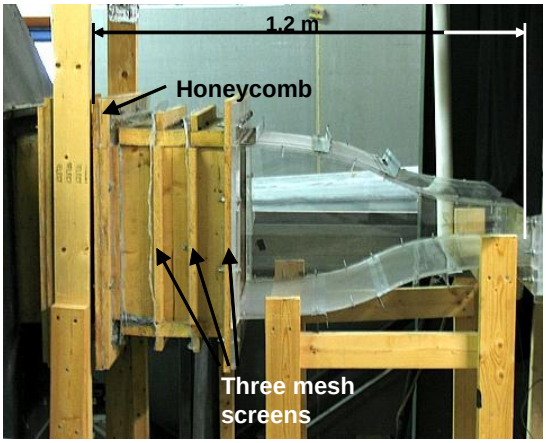

Figure 3.3 Flow conditioning screens and nozzle

The exit of the nozzle leads to the test section, which is made up of 12.7-mm thick transparent Plexiglas panes. It has a length of 1.2 m, 53-cm width, and 15.4-cm height. The top Plexiglas pane is removable for easy access and cleanup during preparation for the test, and is sealed with weather-stripping and clamped before every test. At the bottom surface of the test section, in the center, there is a 2.54-cm by 8.9-cm slot for the test coupons. Figure 3.4 shows in detail the internal components of the test section, as well as the outside insulation.

In order to provide stability and rigidity to the test section, a second pane of Plexiglas was installed underneath the original bottom pane. It has the same dimensions as the original pane (called upper pane), and provides a layer of sealing in order to prevent leakage of outside air into the test section while this runs at sub-atmospheric pressure. The major difference between the lower and upper floor panes is that the lower pane has a 40.6-cm disk cutout in the center. This disk cutout has been replaced with a stainless steel disk. The stainless disk has a built in support system of tabs in order to hold the test plates rigidly and prevent warping during tests. The purpose of the disk, besides holding the coupons in place, is to provide rigidity to the upper acrylic plane. In order to accomplish this, a pattern of holes was drilled into the upper pane and through the metal disk to press both tightly. The stainless steel in the disk

has also been kept separate from the upper Plexiglas® pane by an air gap and weather-stripping, assuring that there are no large conduction effects influencing the upper pane of the test section bottom. Additional measures were taken in order to prevent thermal leakage, such as installation of two layers of 25-mm thick insulation along the bottom of the test section and around the plenum.

Before running a test, the test coupons are inserted from under the test section into the slot, and are supported by the grommet. The layer of temperature sensitive paint, TSP, discussed later, lies downstream of the coupon slot.

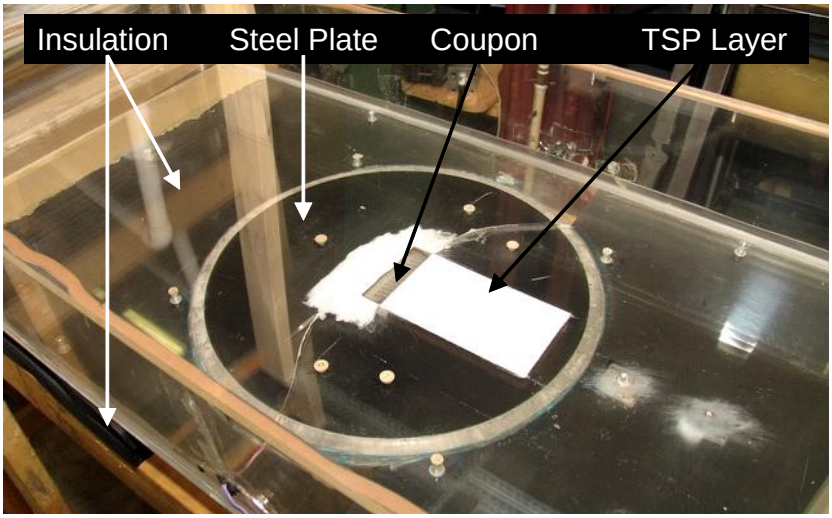

Figure 3.4 Detail of test section as seen from above

Under the test-section, directly in the center are located the plenum and grommet. These two components are integral parts of the support and sealing of the test subjects. The plenum is discussed once the basic design of the plates is described. The grommet is an aluminum sleeve whose primary function is to press the coupon tightly against the bottom of the stainless steel disk, and hold them in place through the slot in the test section floor. The grommet's shape can be best described as a hollow prism 10.16-cm long, 3.8-cm wide, and 2.54-cm high, with walls 6.35-mm thick. It is hollow along the long and wide dimensions, with a tab at the bottom extending 2.54-cm outward along the perimeter. This tab had six holes drilled for the purpose of screwing the grommet to the metal plate while holding up the test coupon,

in other words, the coupon is sandwiched between the grommet and the metal plate and has only its top surface inside the actual test section. For a more descriptive representation, please refer to Figure 3.5.

In order to avoid contact between the grommet and the test coupon, a layer of weather-stripping 2-mm thick is applied to the lip of the grommet and also over the tabs. This weather-stripping also assures that there is no leakage of coolant between the grommet and the test coupon. The inner surfaces of the grommet are also lined with 12.7-mm thick Rohacell, a rigid, rough porous material that provides insulation for the coolant as it flows through the inner part of the grommet, and prevents it from heating up as it approaches the coolant holes.

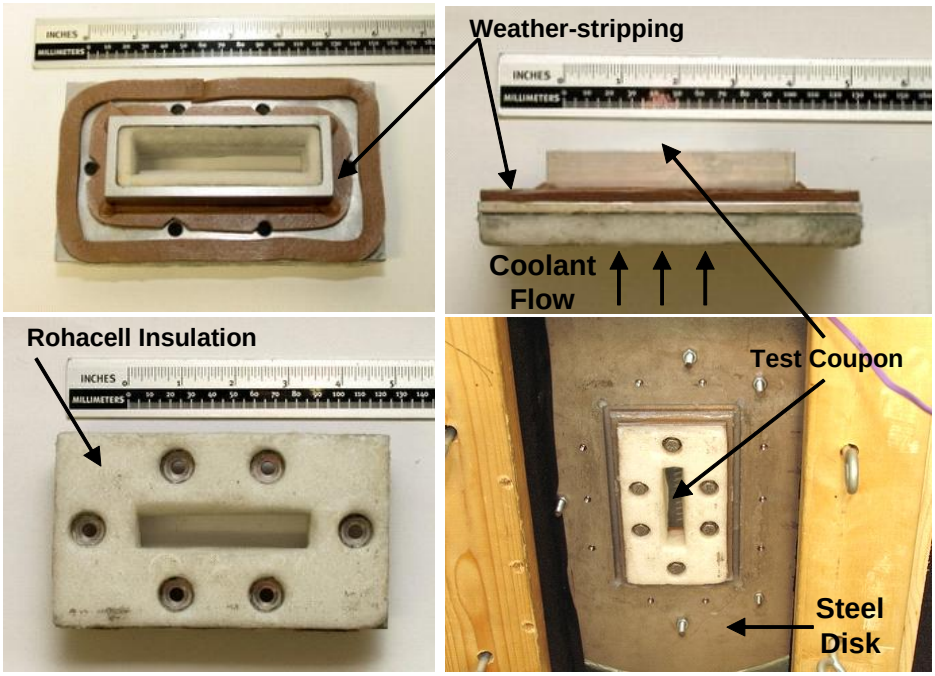

Figure 3.5 The grommet

The volume of air inside the grommet, immediately before the test coupon hole inlet, is considered a smaller supply plenum. This smaller plenum is 17-mm long (in the direction of the main flow), 67.5-mm wide and 31-mm tall. The bottom surface of the grommet is also insulated with 2.54-mm thick Rohacell®, (k = 0.02 W/m·K) since allowing the coolant to come into direct contact with this area, which does warm up during testing, would contribute to heat leakage into the coolant.

Once the flow has made it through the test section, it goes through a diffuser. The diffuser is a wooden 2-dimensional-flow structure which allows the flow to recover pressure. This diffuser is 2.22-m long and with an area ratio of 3.5. The exit of the diffuser leads to an elbow in the tunnel, which begins the recirculation process. After this bend, the flow continues through a duct with a 0.4-m2 square cross-section and a length of 4.6 m. At the end of the square duct lies another bend. This is a 90° bend redirects the flow back into the blower. Figure 3.6 shows the diffuser and the structures used to turn the flow.

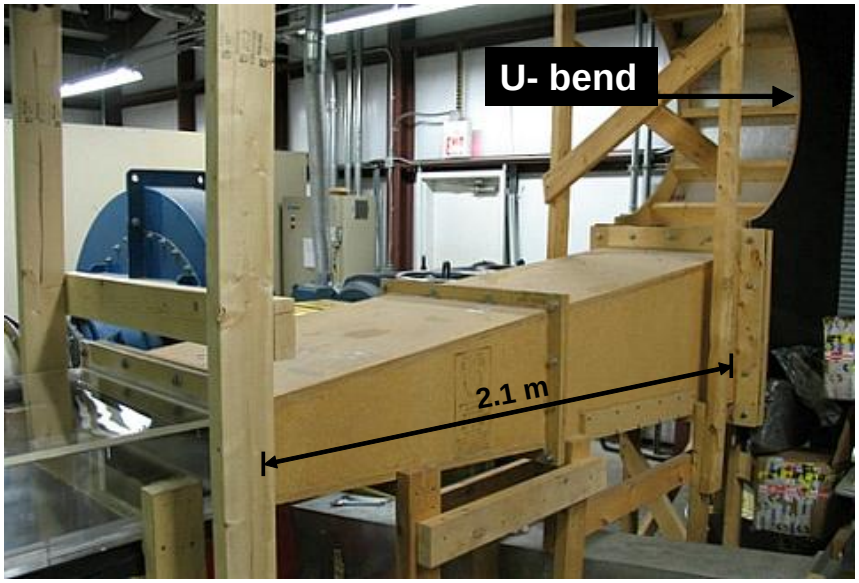

Figure 3.6 Diffuser and flow recirculation detail

Before reaching the blower, there is a slot on the side of the tunnel that allows for the insertion of filters or other obstructions for the purpose of "tuning" the speed of the flow. For the present study, there are six small wooden pieces that keep the speed of the flow at about 52 m/s.

Test Coupons and Cooling System

Test Coupon Design

The test subjects in this investigation are acrylic coupons with different hole geometry configurations. All coupons have the same size and shape and are designed to fit snugly in the test section slot.

The test section was designed for specific objectives in mind by other researchers and its structure was not meant to be easily changed. This meant that basic dimensions such as the coupon's length and thickness had restrictions which could not be changed without major changes to the rig.

In the first part of the study the focus is on two configurations: Coupons with pure conical holes of increasing diffusion angle, and coupons with conical holes with a cylindrical entry length. Many parameters had to be considered in designing the acrylic coupons, but there was also the need to compare the results to published data. To this effect, considered when designing the holes were: test section setup geometric restrictions, hole inclination angle, diameter (D), length-to-diameter ratio (L/D), pitch-to-diameter ratio (PI/D), and coolant system capacity.

It was found that the most important parameter when starting the design of the coupons is the inclination of the holes with respect to the direction of the flow. Common angles used in the literature are 30, 35 and 45 degrees. Careful analysis of literature testing conditions, and blowing ratios led to the choice of the 35° geometry. The next things to consider were the geometric constraints of the rig itself. For example, holes of 1.27 cm diameter and an L/D of 1.75 were used in Sinha et al.'s paper, and while the coupons can accommodate the L/D of this test, they cannot have holes of that diameter, they are simply too big. It was decided to keep the L/D of 3.5 as in the study by Lutum and Johnson in 1999. From then on, the thinking process for deciding the rest of the parameters is as follows: the test coupons have a thickness of 6.35 mm, which implies that at an angle of 35°, the length of the holes would be 11.11 mm, this means the diameter of said holes would have to be 3.175 mm to keep an L/D of 3.5. These

dimensions were deemed appropriate. Next for consideration was the pitch-to-diameter ratio (PI/D). Pitch is the distance between the centerlines of the holes, which is commonly measured in terms of multiples of the diameter. Figure 3.7 illustrates the concept of PI/D for cylindrical holes, in which the exit diameter is the same that for the inlet. A common value for PI/D is 3, that is, the pitch is 3 diameters long. Thus, picking an angle of 35° helped in deciding most of the dimensions of the coupon holes. The number of holes per coupon was chosen so as to have the most holes in a row, without compromising the structural integrity of the coupon itself, which yielded a number of 8 holes per coupon. Having 8 holes also meant having a larger amount of area from which to collect information.

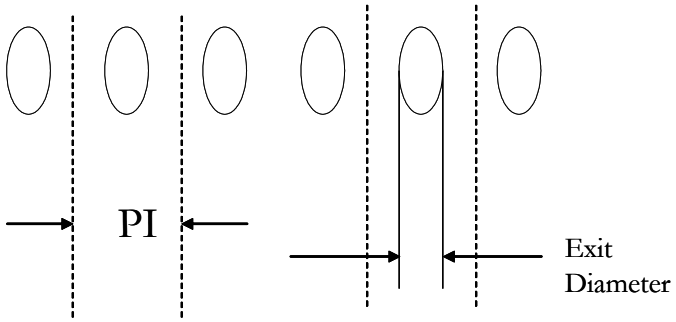

Figure 3.7 Pitch-to-Diameter ratio, PI/D

The next step was deciding the conical angles of the holes. The concept of the conical holes and studying trends as the angles changed had been suggested long before this work by a colleague. Discussions with the author's advisor led, at first, to choosing angles of 1°, 2°, and 3°, and also a reference angle from the literature. In this case, the most convenient would be a coupon with perfectly cylindrical holes, i.e. a coupon with 0° diffusion. Having decided, these plates were manufactured and studied. A decision was later made to continue the observed trends and to build plates with 4°, 6° and 8° conical holes. Since the original configuration was purely conical, meaning it has a diffusing shape from the beginning of the hole to the exit, it was also decided to test a configuration in which the conical hole begins after a certain cylindrical "entry length." The study by Hay, and Lampard (1995) suggested that the shortest entry length used should be no less than 4 diameters long in order to make sure the flow is attached to the walls of the cooling hole. Following their suggestion, the new holes were designed to

have a cylindrical entry length of 4 diameters, followed by a conical diffuser of 3.5 diameters. The diameter value would have to be changed in order to keep the plate dimensions the same. The overall L/D of these holes was now 7.5, so keeping the same plate thickness would lead to a hole diameter of 1.476 mm. Due to difficulties mentioned by machinists for manufacturing the 1.476-mm holes, it was decided that the diameter would be kept at 2 mm. Adjustments were made and the thickness of the test coupon was changed to 8.6 mm, without compromising the seal of the test section. The smaller hole configuration led to a smaller pitch, but same PI/D. With the smaller pitch, the number of holes was changed to 12. It was then decided that only a specific geometry should be studied to see if the entry length would have a big effect on the results. The 3° (DA3) configuration was chosen, a choice in the middle of the range of the conical set. This coupon's holes were to have a 2-mm diameter, a cylindrical section of 4 diameters length, followed by a conical diffusing section, 3.5 diameters long, at a diffusion angle of 3°. Also, in order to have some reference with which to compare these results, a coupon with purely cylindrical holes of 2-mm diameter was designed. These two coupons were also manufactured and studied for the present work. The following Figures summarize the dimensions of the test coupon configurations and show their manufactured counterparts.

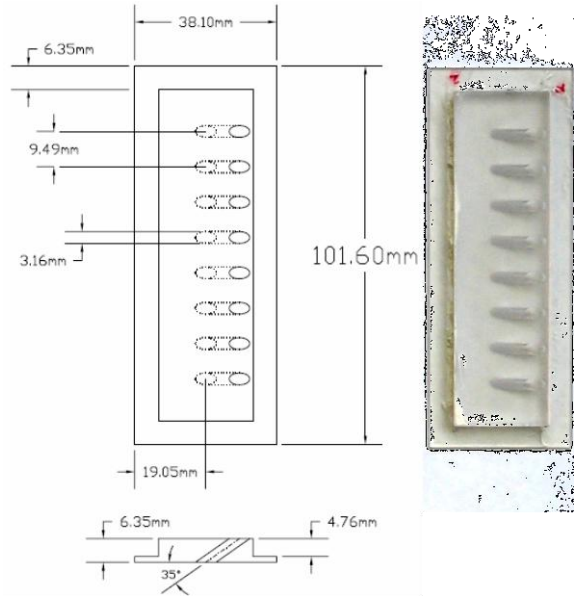

Figure 3.8 Nominal cylindrical hole coupon (DA0) design vs. manufactured piece

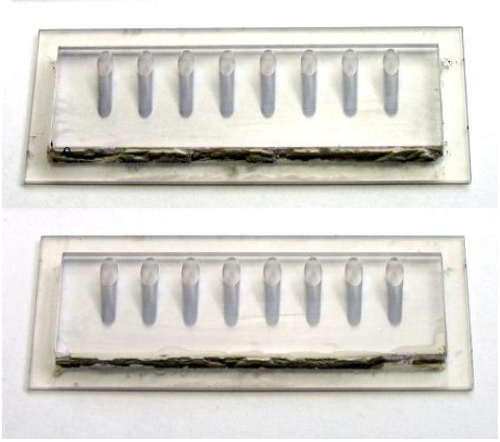

Figure 3.9 Comparison of DA1 (top) and DA2 manufactured coupons

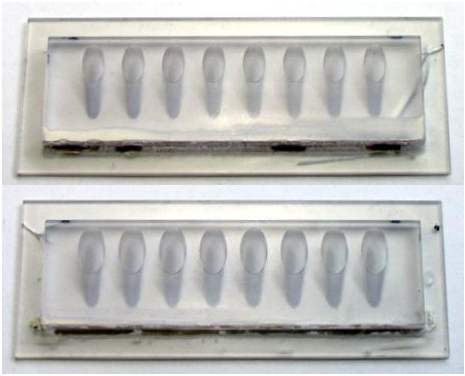

Figure 3.10 Comparison of DA6 (top) and DA8 coupons

The second part of the conical hole study, meant to test the effect of the entry length, two coupons were manufactured: one with pure cylindrical holes and one with conical holes with a cylindrical entry length. In order to accommodate the entry length, the diameter of the holes was reduced, while the conical diffuser part was kept at the same L/D. This meant that the new L/D was 7.5, 3.5 for the diffuser part and 4 for the entry length. In order to fit the new specifications in the coupons, the diameter was reduced to 2 mm. The angle of diffusion of chosen for the second part was 2°. All other ratios were kept as before.

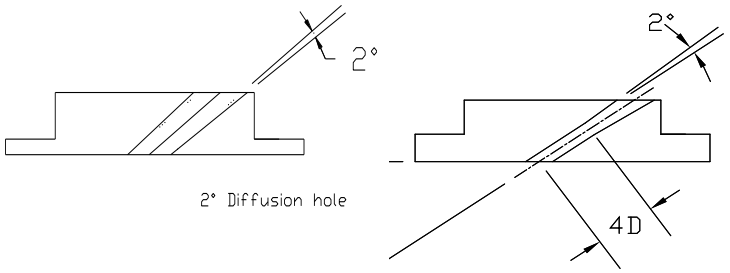

Figure 3.11 Comparison of DA2 (left) and DA2(L/D=7.5) coupon (right)

For the second study, the plates were manufactured in a rapid prototyping laboratory. The material used was a photopolymer. The basic dimensions of the test plates remained the same. The diameter was kept at 2 mm. The fan holes were designed similar to the entry-length conical holes.

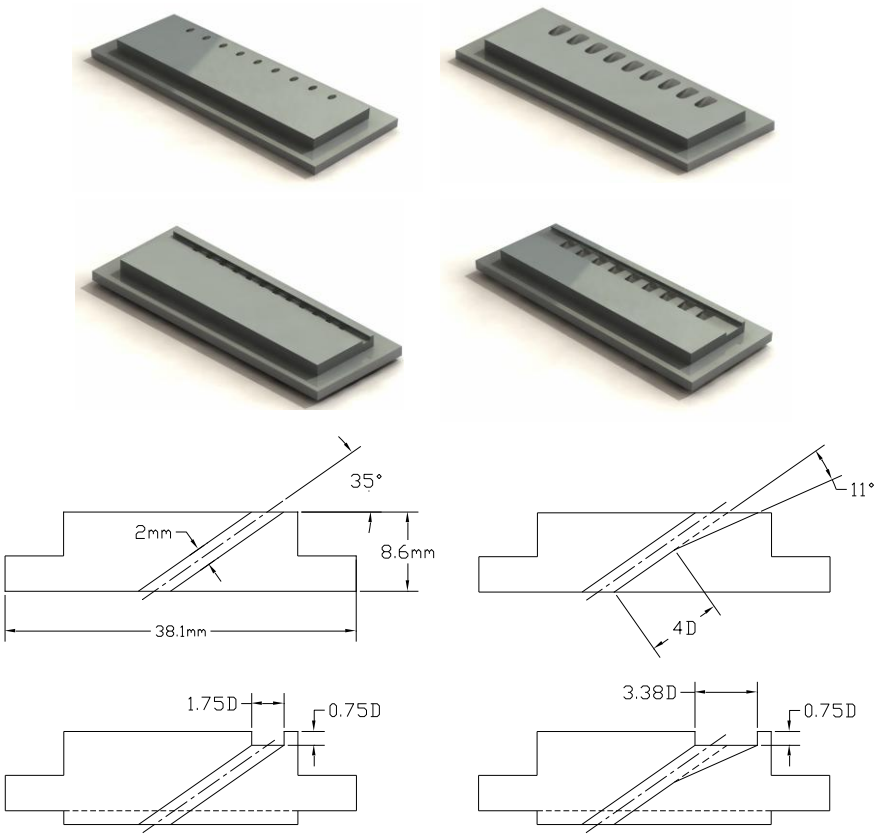

Figure 3.12 Renderings of the solid models of the coupons (top) and basic dimensions of holes (bottom)

The fan geometry was chosen to resemble that of Gritsch et al. (2005); more specifically geometry C, with L/D of 7.5, and lateral diffusion of 7° and forward diffusion of 11° (both lateral

diffusion angles are part of the name, hence 7-7-11). The baseline PI/D was 4 and it varied from 4 to 8 to 12. For the trench plates, the L/D was also 7.5 and all baseline parameters were replicated. The depth of the trench was compensated with extra material at the bottom of the plates. The 0.75D depth of the trench was chosen from the literature since it was found to be the optimal depth by Waye and Bogard (2007) and Lu et al. (2007).

For the last study, the coupons were also made out of photopolymer resin and had the basic dimensions of those in the previous studies. The fan-shaped holes had an entry length of 4D and the flared holes had a 7-7-11 configuration as baseline. As shown in Figure 3.13, the baseline holes have symmetric diffusion angle α_R and α_L. The angle α_R was varied from 5° to 7° to 9°, 11°, and 13°, with the 5° holes yielding a narrower fan than the baseline.

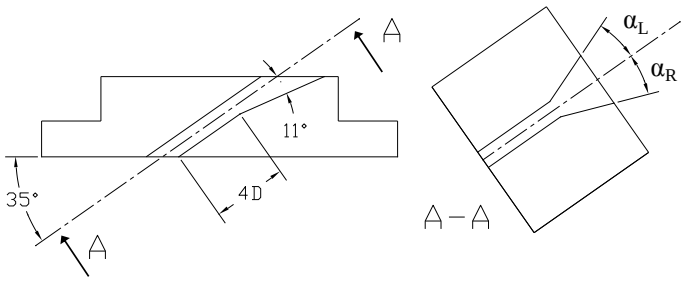

Figure 3.13 Baseline design of the asymmetric fan-shaped holes

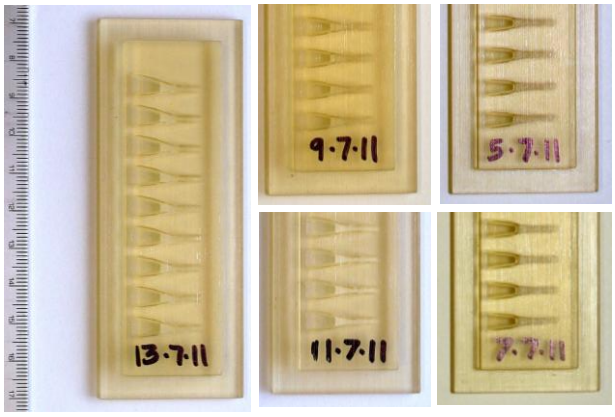

Figure 3.14 Coupons for the asymmetrical fan study

The Plenum

A plenum is an enclosure in which a fluid is kept at a pressure different from the ambient. In the context of fluids experiments, a plenum should also homogenize the flow's properties, such as pressure, velocity distribution and temperature. This is done in order to avoid impingement on the test coupon, or bringing in other sources of error. For our current test, the plenum's functions are multiple: it guides and stabilizes the coolant before it goes into the coupons and ultimately into the test section, it regulates the supply pressure and homogenizes the flow, all while providing housing to the instruments used during testing. The plenum, shown in Figure 3.14, is shaped as an open box, with walls 12.7-mm thick. It is made of Plexiglas, which is also an insulator, and works to keep the coolant from picking up heat as it makes its way out of the cooling circuit. The dimensions of the plenum box are: 17.75-cm wide, by 10.16-cm long, by 16.5-cm high. At the main opening, the plenum has 6.4-mm thick short tabs which match the grooves in the stainless disk. These grooves are filled with silicon for extra sealing when the plenum is put in place for testing. For support of the plenum, there are four acrylic tabs extending outward at the top. These tabs, much like the grommet's tabs, have screws which hold the plenum up firmly against the stainless plate.

Inside the plenum, at half the depth, there is an acrylic plate across the entire cross-section, held in place with epoxy. This acrylic plate is 12.7-mm thick and divides the plenum in two. The acrylic plate has an array of 5-mm diameter "pinholes" which act to straighten the coolant flow. Coolant is supplied though a 12.7-mm opening at the bottom wall of the plenum box. But, before going through the pinhole plate, the flow must go through a small acrylic box which has pinholes only through the side walls, located at the bottom of the plenum. This pinhole box forces the coolant to go only sideways. Allowing the coolant to shoot straight up through the plenum undisrupted, would make the flow impinge on the test coupon, giving uneven flow from the cooling holes. Once the flow comes out of the pinhole box, it must flow vertically through the pinhole acrylic plate, straighten up and finally pass into the smaller plenum

between the walls of the grommet, and out the cooling holes. The instrumentation housed by the plenum is critical for the current work and is discussed in the next section.

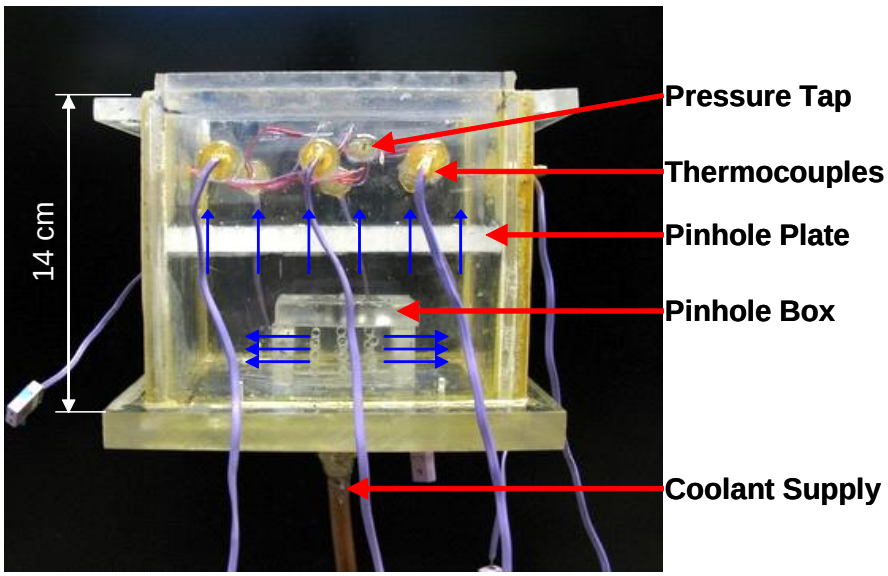

Figure 3.15 Supply plenum (blue arrows indicate coolant flow)

The plenum is supplied with either air or nitrogen during testing. Both gases are supplied from different sources, but share some of the same circuitry leading them to the plenum.

For the discharge coefficient tests, the coolant used is air. Air is supplied to an 8.5-m3 tank by a compressor, equipped with a dryer and filter. The air is also circulated through a ZEKS condenser, which further eliminates humidity from the tank. The air is then circulated through 21 meters of 8.5-cm pipe in order to bring it to the BFC rig. Once the 8.5-cm pipe reaches the rig, it is reduced to a 1.27-cm copper pipe, which is connected to a flowmeter and then the plenum. There are a total of five valves in the air's path before reaching the plenum.

For the film cooling effectiveness tests, the coolant used was nitrogen gas. Nitrogen gas is obtained from the boil off of liquid nitrogen contained in dewars (large storage, vacuum-insulated tanks) commonly at 1.62 MPa. Using a system of valves, and liquid nitrogen's thermal instability, gas flow is obtained at controllable rates. The temperature at which the gas exits the vessel depends on the mass flow rate of the gas; the larger the amount being released, the colder the gas' temperature. If a large enough

amount of gas is released continuously, the resulting outflow will be liquid. Therefore, while running a test, in order to achieve nitrogen gas flow at a desired temperature, the mass flow rate must be monitored.

Nitrogen gas exits the tank through a main-flow control valve and into an insulated 1.27 cm diameter copper pipe. The copper pipe runs an approximate length of 7 meters before reaching a t-junction. The t-junction allows the diversion of excess nitrogen into the ambient. For example, if the plenum is to be kept at 1.723 kPa-gage, but the nitrogen gas is flowing out of the tank at a rate that would keep the plenum at 3.45 kPa-gage, then the excess gas must be diverted, or the flow from the tank should be reduced. Reducing the amount of flow from the tank, would warm the flow of the nitrogen gas, therefore this is not an acceptable option. Thus, at the T-junction there is a valve to allow for the release of excess gas, while keeping the plenum at the desired conditions of pressure and temperature. Two meters after the t-junction, the nitrogen flows through the plenum valve and into the plenum.

Instrumentation

In order to capture the conditions in the BFC rig as well as those of the coolant in the plenum and the temperature distribution downstream of the film cooling holes, the following instruments were used:

Thermocouples

Type E thermocouples were placed in multiple locations of the BFC rig and the plenum in order to capture the temperature of the mainstream and the coolant while the rig warmed up, and while TSP images were being captured. Figure 3.16 shows the location of the thermocouples.

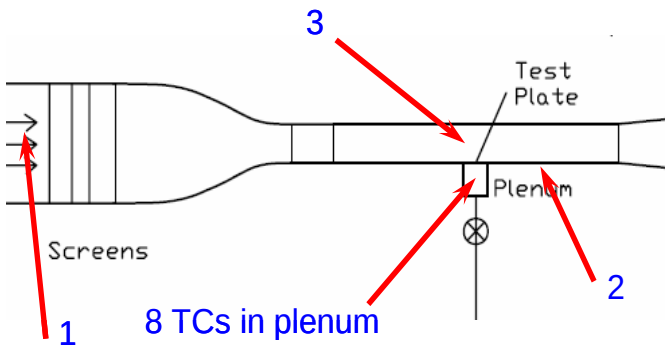

Figure 3.16 Location of thermocouples in BFC rig

The thermocouple in location 1 was used primarily to measure the mainstream temperature. This temperature started at about 25 ºC and could reach up to 69 ºC in 2.5 hours. The thermocouple in location 3 was also used to monitor the temperature of the mainstream, but it always registered the same temperature of location 1, so it was seldom used. The thermocouple in location 2 was used to monitor the recovery temperature of the test section floor. While the mainstream could warm up in as little as two hours to 62ºC, location 2 took longer to catch up to the mainstream temperature, and this was by design. A hole was drilled through the metal disk and the acrylic in the test section floor, and the thermocouple was inserted. Care was taken to place the thermocouple just inside the surface of the acrylic. The material in which it is embedded is putty. The temperature reading takes approximately three and a half hours to stabilize since the rig heats up very slowly. When steady state is reached in the rig, the difference between the temperature registered on the floor of the test section and that of the mainstream becomes about 1.5 ºC and remains quite steady throughout the test. The uncertainty in measurements with these thermocouples is 1.0ºC.

Temperature Sensitive Paint

Uni-coat Temperature Sensitive Paint, TSP, formulated by ISSI, is used in this study. The effective temperature range is 0–100 ºC, beyond which the temperature sensitivity of TSP becomes weaker. It is packaged in aerosol cans and can be applied easily with a spray. After it is heat treated

above 100 ºC for 20 minutes the temperature sensitivity of the paint is about 0.93ºC, (Liu, 2006). The TSP painted surface is smooth. The emission spectrum of TSP is shown in Figure 3.17. An optical 590-nm long pass filter is also used on the camera to separate the excitation light and emission light from the paint.

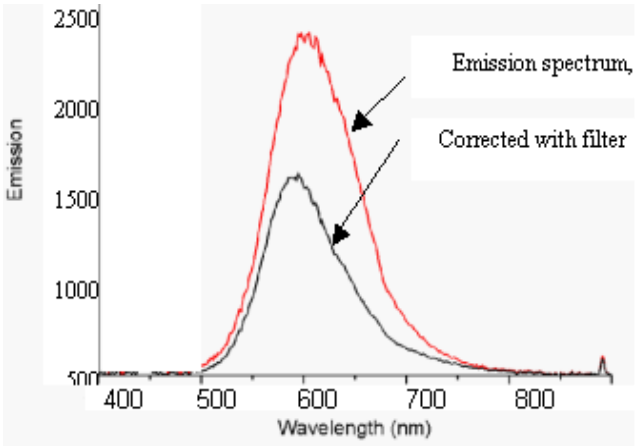

Figure 3.17 Emission spectra of TSP (Liu, 2006)

TSP incorporates luminescent molecules in paint together with a transparent polymer binder. Light of the proper wavelength is directed at the painted model to excite the luminescent molecules. The sensor molecules become excited electronically to an elevated energy state. The molecules undergo transition back to the ground state by several mechanisms, predominantly radiative decay (luminescence). Sensor molecules emit luminescent light of a longer wavelength than that of the excitation light. The appropriate filters can separate excitation light and luminescent emission light, and the intensity of the luminescent light can be determined using a photodetector. The excited energy state can also be deactivated by quenching processes. Through two important photo-physical processes known as thermal- and oxygen-quenching, the luminescent intensity of the paint emission is inversely proportional to local temperature.

In principle, a full spatial distribution of the surface temperature can be obtained by using the TSP technique. Figure 3.18 shows a typical TSP set up.

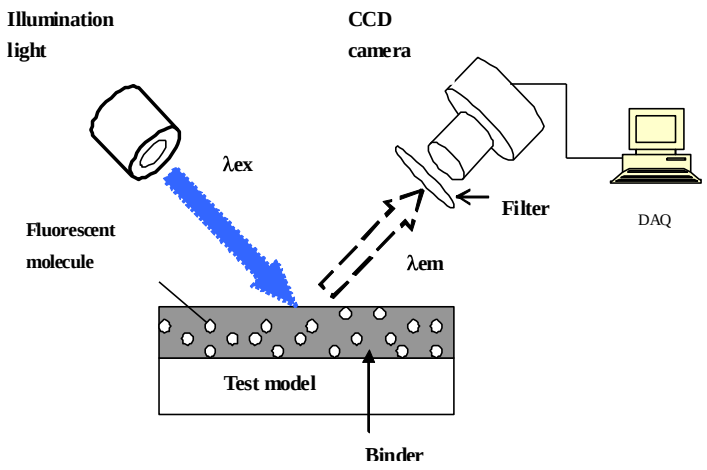

Figure 3.18 Typical TSP setup and instrumentation (Liu, 2006)

For a more thorough description and theoretical explanation of the properties of TSP, refer to the study by Liu et al., 2003, as well as Liu, 2006.

CCD Camera

A high resolution 14-bit CCD (Charged Couple Device) camera was utilized for this study. It is a PCO-1600 CCD camera, shown in Figure 3.19, provided by the Cooke Corporation with spatial resolution of 1200 by 1600 pixels. The image data is transferred via an IEEE 1394 ("firewire") cable and firewire PCI card to a data collection PC. "CamWare" software provided by Cooke Corp. is used in the Windows operating system to control initialization, exposure time and image acquisition. The acquired image data are processed using MATLAB. The camera is thermo-electrically cooled and has high quantum efficiency at the paint emission wavelengths. The choice and quality of the scientific-grade camera dictate the measurement accuracy.

Figure 3.19 CCD camera and light source, courtesy Cooke Corporation

Light Source

LED-based illumination source (peak wavelength at 464 nm) was selected as the excitation light for the TSP. The stability of the light source provided by ISSI is within 1% after 10 minute warm up. The excitation spectrum of LED is shown in Figure 3.20.

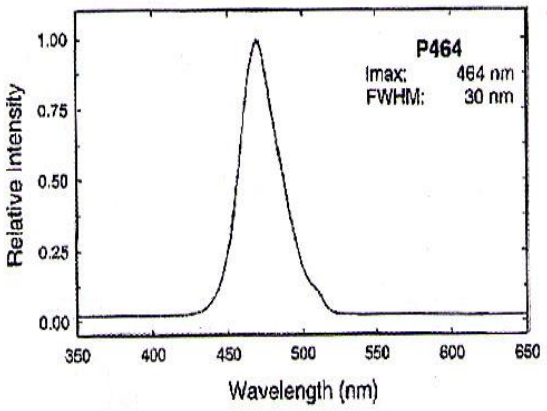

Figure 3.20 Spectrum of LED source (Liu, 2006)

Pressure Transducer

Pressure measurements were made with pressure taps connected to a Scanivalve pressure transducer. The range of the transducer is from -34.5 kPa to 34.5 kPa, and has a sensitivity of 6.9 Pa

(0.001 psi). It is connected to the plenum through a pressure tap located on the side of the plenum, and was used to monitor coolant static pressure. Other measurements involved the static pressure of the test section, performed regularly to assure tunnel stability. Figure 3.21 shows the NIST-certified calibration of the Scanivalve.

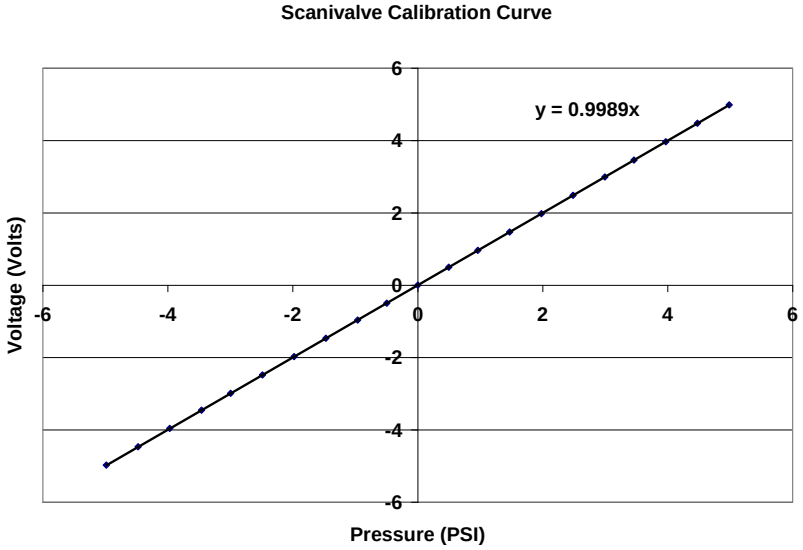

Figure 3.21 Scanivalve calibration curve from certificates

Mass Flow Meters

Flow measurements were made with two different thermal mass flow meters, high range and low range to cover the entire range of testing, and keep the accuracy as high as possible. The high range meter was a SIERRA 730 Series Accu-Mass thermal flow meter with a range of 0-1100 L/min, a response time of 200 ms, and an accuracy of 1% of full scale. The low range flow meter used was a McMillan 50K-14C, with a range of 0-500 SCFH, also with an accuracy of 1% of full scale. Figure 3.22 shows both flow meters.

During testing, it was ensured that the company-recommended tubing schemes were followed. Tests were performed first with the low flow rate, for the lower pressure ratios, and then with the high flow meter to cover the high pressure ratios.

Figure 3.22 Flow meters, McMillan

Testing Procedure

Testing was performed in two steps. First, each plate had its discharge coefficient measured as a function of pressure. Once those data were processed, the pressure ratios were calculated for each desired blowing ratio needed for the effectiveness tests, but this time properties were adjusted for N_2 as the coolant. Two types of tests were conducted in this study: flow tests, C_D, and film cooling tests. The procedures for both types of tests are explained as follows:

Flow Tests

The discharge coefficient is calculated from the results of the flow tests. The main objective of this test is to measure the amount of mass flow through a given coupon at increasing pressure ratios. The first step is to insert the coupon into the slot at the bottom of the test section and press it in to place with the grommet, making sure that the grommet has all the necessary weather-stripping layers. Once the grommet is in place, the grooves in the steel plate on the outside of the test section are filled with silicone. The plenum is inspected for cleanliness to make sure that no debris is present inside. Thermocouples are aligned to make sure they will not be touching any walls or each other. Once the plenum is ready, a layer of silicone is applied to the uppermost edges that will be inserted into the steel disk grooves. The layer of silicone ensures that the plenum will be sealed.

Going back to the test section, any gaps between the coupon and the floor of the test section must be sealed with a putty or wood filler, which must then be allowed to dry before sanding for smoothness. The exit holes of the coupon are then covered with metal adhesive tape. The plenum is then connected to the pipe that provides compressed air. All valves are sealed. A pressure tap connects the plenum to the Scanivalve pressure transducer. The flow meter is turned on and allowed to stabilize. The valves are opened and the plenum is slowly allowed to pressurize up to 20 kPa. Once the plenum is at a constant pressure, the mass flow rate is observed, and if it changes by less than 3 SCFH, then the plenum is considered to be sealed and the test can proceed. All the tape is removed, the test section is sealed and the tunnel is started.

Once the tunnel has warmed up to 65ºC, the pressure in the plenum is increased at very small intervals and the mass flow rate is taken for each pressure. The temperature of the coolant air must be allowed to stabilize, since the plenum warms up while the tunnel warms up. So, a certain amount of air must be allowed to flow to bring the plenum to the same temperature as the coolant. Once the coolant temperature is constant, the test can proceed. Coolant temperature, static pressure and mainstream temperature are the main data taken for this test. Once the highest pressure has been recorded, the tunnel can be stopped. Pressure and mass flow rate biases are averaged between the beginning of the test and the end. The reduction procedure for this data is explained in the analysis chapter.

Film Cooling Tests

The procedure for the film cooling tests starts the same as that for the flow tests. The coupon is inserted and the plenum is sealed as in the discharge coefficient tests. However, in this case, the desired data is not a flow rate, but the temperature distribution downstream of the cooling holes. As explained in earlier, the main means of obtaining a temperature distribution downstream of the cooling holes is through utilization of TSP and a CCD camera. The CCD camera obtains pictures containing intensity distributions, I(x,y), which must then converted to temperature. A layer of TSP is applied to a rectangular

section of the test-section, downstream of the cooling holes. Once it is dry, it is cured to a temperature above the range needed for the experiments. The LED light source is suspended at a location above the test section, which will allow it to irradiate the TSP layer without obstruction. The CCD camera is also suspended perpendicular to the TSP layer, aligned with the test coupon. The experiment in now ready to begin.

At the start of the test, conditions in the room must be known, especially the TSP temperature. A set of pictures of the TSP radiated with the light source is taken. A set is normally four images. These are called the reference pictures. The tunnel is started and the plenum valves are closed so no air or leakage of any sort flows through the coolant holes into the test section. Once the four hour warm up period passes, a set of pictures is taken of the TSP layer. These images are analyzed in situ to avoid the introduction of erroneous temperature distributions, and make sure that the temperature distribution on the TSP is uniform. If that is the case, then this set of images is called the BR0 set. BR0 stands for blowing ratio of zero, and once processed these images yield the recovery temperature distribution on the TSP, Tr. Once this set of images is obtained, cooling can begin. Cold nitrogen gas is allowed to flow through the plenum, at the desired temperatures and pressure ratios. Once a pressure ratio has been held for a period of approximately 10 minutes, then a set of pictures can be taken. This is called a "run." After all the runs are finished, the tunnel and cooling are stopped, and the test has ended. All images are saved and the equipment is turned off. The next step is to process the data to obtain the results.

CHAPTER FOUR: ANALYSIS OF DATA

Discharge Coefficient

Viscous effects, paired with the effects of geometry, give rise to deviations from ideal conditions on the flow entering a cooling hole. These deviations can be identified and quantified, since there are equations that predict ideal behavior. A prime example of such deviation is the vena contracta, a contraction in the flow area which forms as fluids turn sharp corners into orifices. Thus, as a fluid enters an orifice, friction in the orifice entrance reduces the actual area through which it can flow. And while theory for compressible flow may predict a certain amount of fluid passing through the cooling hole, based on inviscid flow assumptions, in reality only a fraction does flow through. The discharge coefficient, C_D, is a ratio that compares the observed amount of flow going through a hole, or number of holes, to the predicted flow, based on the compressible flow equation for a given physical area. The equation used for the discharge coefficient is:

$$C_D = \frac{\dot{m}/N_h}{\frac{\pi}{4} D^2 \cdot P_c \cdot \left(\frac{P_{stat,\infty}}{P_c}\right)^{\frac{\kappa+1}{2\kappa}} \cdot \sqrt{\frac{2\kappa}{\kappa-1} \cdot \frac{1}{R \cdot T_c}\left[\left(\frac{P_{stat,\infty}}{P_c}\right)^{\frac{\kappa+1}{2\kappa}} - 1\right]}}$$

The numerator terms are the main measurand, while the denominator (which also contains measured quantities) predicts ideal amount of compressible flow through the cooling hole. Thus, if flow behaved ideally—with no viscous effects—both numerator and denominator would be equal, yielding a discharge coefficient of unity.

C_D tests were performed with air as the coolant as explained in chapter 3. During these tests, the measured variables were: the volumetric flow rate, which was then multiplied by the density to yield the mass flow rate, $\dot{m}$; T_c, the temperature of the coolant inside the plenum; P_c, the static pressure of the coolant inside the plenum; and $P_{stat,\infty}$ the main flow static pressure at the coolant injection plane. The

remaining terms, N_h, κ, R, and D were known constants, or obtained from tables. The data were reduced with the aid of a MathCAD® sheet. As will be explained further in the section on Flow Tests, the C_D curves are used because it is not possible to measure the mass flow rate at very low coolant temperatures.

Cooling Hole Dimensions and Related Parameters

Of all the terms in the C_D equation, the one that presented difficulties in quantifying was the diameter term, D. The diameter term used in this study is the minor axis of the ellipse formed by the intersection of the cylindrical hole and the inlet plane of any cooling hole. For cylindrical holes, the minor axis of the ellipse at the inlet is the diameter of the cylindrical hole. Following this same logic, the previous definition was also applied to the inlet of the conical holes. However, under close inspection, the cooling holes had deviations from their design, mainly in their diameter, D. Since the diameter is such a crucial parameter in this investigation, a thorough study of the geometries of the holes was performed in order to quantify deviations from the design, as well as to measure other important parameters influential in the computation of the blowing ratios, coverage area, and uncertainty.

The test coupons were taken to CREOL and had their inlets photographed, hole by hole, under a microscope. A 1/100th-inch (0.254-mm) scale was used to measure their minor axis. The images were later analyzed and their diameter calculated.

Table 4.1 Cooling hole data for conical hole analysis

Plate	Diam. (mm)	Exit Area (sq.mm)	Area Ratio	Coverage (%)	L/D
DA0	3.152	7.80	1.01	33.3	3.5-cone
DA1	3.312	11.33	1.31	39.9	3.5-cone
DA2	3.411	13.50	1.48	43.5	3.5-cone
DA3	3.624	17.53	1.70	49.6	3.5-cone
DA6	3.445	22.35	2.40	56.0	3.5-cone
DA8	3.774	31.67	2.83	66.7	3.5-cone
DA0(2mm)	1.947	2.98	1.03	33.3	4-cyl+3.5-cone
DA2(2mm)	1.95	4.57	1.53	40.2	4-cyl+3.5-cone

It can be observed that most of the DA holes do not have uniform diameter. In theory, they all should. The dimensions obtained in this section will be used throughout the rest of the study.

For the rest of the studies, since the resin pieces were made with a high resolution SLA polymer, per manufacturer's guidelines, the expected deviation from the designed diameter is on the order of 0.005 inches. Thus, it was deemed appropriate to not measure the resin plates' hole inlets and assume that the inlet diameter was 2 mm, as designed.

Determination of Blowing Ratio and Momentum Flux Ratio

The blowing ratio, also called the mass flux ratio, is a dimensionless number used in film cooling to quantify the ratio of the mass flow rate per unit area of the coolant to that of the mainstream. When all simplifications are done, what is left is the density ratio multiplied by the velocity ratio of the coolant to the mainstream. For the current test set up, M is calculated using the following equation:

$$M = \frac{(\rho U)_c}{(\rho U)_\infty}$$

The blowing ratio is also very convenient to use because in the current setup, it is a function of the pressure ratio. However, some issues come up when calculating the mass flow rate of the coolant in the effectiveness tests. For the C_D tests, the coolant used is air at about ambient conditions, while in the effectiveness measurements, the coolant used is nitrogen gas, at about -15°C. The subzero temperatures of the nitrogen prevent the measurement of its flow rate with the current flow meters. However, it is possible to back-calculate the flow rate using the C_D curve, adjusting ρ and κ of the nitrogen for the cooler temperatures.

Keeping in mind that PR, the coolant-to-mainstream static pressure ratio is controllable, one must back-calculate the blowing ratio prior to running the effectiveness tests. The procedure used to determine the blowing ratio using nitrogen is as follows:

1) decide a coolant pressure, P_c, since $P_{stat,\infty}$ is known, find PR
2) rearrange the C_D equation, solving for $\dot{m}$
3) from the C_D curve for that particular hole, find C_D for the current (cold) PR and insert into the new $\dot{m}$ equation, this yields the value of $\dot{m}$
4) with $\dot{m}$ of coolant, use equation (4-6) and obtain M; it is important to note that this is an iterative process that must be done to find the pressure ratios for the desired blowing ratios at which to keep plenum conditions when measuring effectiveness.

The momentum flux ratio, I, is defined similarly to the blowing ratio. While the blowing ratio is based on the velocity of the coolant, the momentum flux ratio is more closely related to the kinetic energy of the coolant. It compares the kinetic energy of the coolant (per unit volume) versus that of the mainstream. The momentum flux ratio is classically defined as:

$$I = \frac{(\rho U^2)_c}{(\rho U^2)_\infty} = \frac{M^2}{DR}$$

Since the density ratio, DR, is kept nearly constant at 1.26, the momentum flux ratio can be obtained by squaring the blowing ratio, and dividing by DR, given by $\frac{\rho_c}{\rho_\infty}$.

Cooling Effectiveness Calculation

Film cooling effectiveness (η) measurement is one of the primary goals in this study. However, obtaining the final plots of η requires a significant amount of data reduction. As mentioned before, η has been commonly defined as follows:

$$\eta = \frac{T_\infty - T_{aw}}{T_\infty - T_c}$$

Notice that this definition involves the mainstream temperature, which is sensitive to the injection of coolant. Said definition applies only if there are no conduction effects on the test section as a result of cooling, heat leakage, or other sources of thermal noise that would cause a temperature difference

between the mainstream and the TSP surface, or render the conditions downstream of the cooling holes non-adiabatic. An additional consideration is the fact that the test section is exposed to a significantly high velocity flow (>52 m/s), which means there will also be a recovery temperature due to viscous dissipation. Since the actual data collection occurs at the floor of the test section, under steady, un-cooled conditions, this floor's temperature is the recovery temperature, Tr. To reflect this concept the following adjustment has been made to the definition of η:

$$\eta = \frac{T_r - T_{aw}}{T_r - T_c}$$

For the conical hole studies, the recovery temperature is measured once the tunnel has reached steady state conditions without any cooling. Steady state is defined as having the temperature of the mainstream not change by 0.1°C in 10 minutes. This condition leads to the temperature difference between thermocouples A and B to be no more than 1.5°C. During experiments, it has been shown on the BFC rig that after the experiments have started, the T_r changes little, even under cooling conditions. It takes the bottom of the section less than ten minutes after cooling has stopped to go back to its original recovery temperature.

For the experiments involving trench cooling and asymmetric fans, the recovery temperature is obtained differently. It is obtained at the same time the adiabatic wall temperature is obtained. The process and the reason for this change are explained in the next section.

Reduction of Temperature Data

To calculate film cooling effectiveness, three temperatures must be known: Tc – the coolant temperature, Taw – the adiabatic wall temperature distribution downstream of the cooling holes, and Tr – the recovery temperature of the test section. To analyze the TSP pictures, matrix handling software such as MATLAB is used. The images are read into a matrix containing the intensity information over every pixel of the TSP.

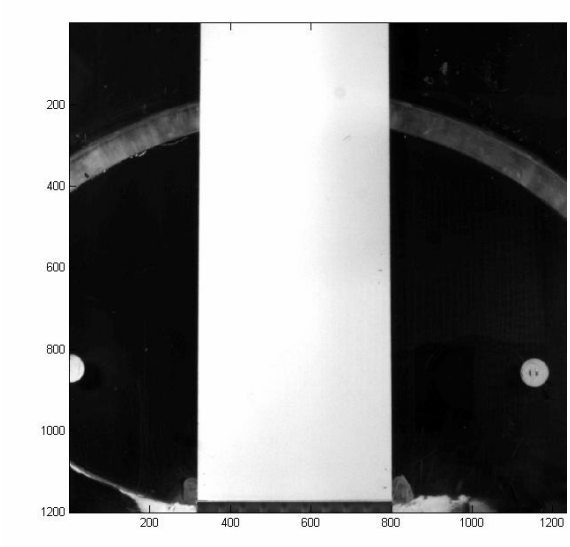

Figure 4.1 TSP layer in ambient lighting

Figure 4.1 shows an image of the TSP downstream of the coolant holes (bottom). This image was taken under non-test conditions, without any LED lighting, and is used mainly for locating the holes with respect to the edges of the paint layer. The coolant holes are very difficult to see under testing conditions because they reflect back very little light.

Figure 4.2 shows the same image, but this time under LED lighting. If the TSP is at room conditions, and testing is ready to begin, then this image becomes the reference image, and the intensity from any pixel becomes I(TR). The LED light is kept on throughout the duration of the test. Neither the camera nor the LED light may be moved, or the usage of the reference image will not be valid due to changes in lighting conditions. Precautions must be taken to ensure that the data will not be polluted due to outside lighting condition changes. For all tests and blowing ratios, images are taken in sets of four, which are then averaged to filter out any fluctuations. For the reference image, the temperature must be uniform, and known. Typical reference temperatures are around 25 ºC, or room temperature.

As mentioned in the film cooling test procedure, section 3.6.2, the tunnel is allowed to warm up for over four hours. At that point another set of pictures is picture is taken. The images look just like the reference image, but the intensity is lower due to the higher temperature. TSP intensity is inversely

proportional to temperature. These images, called Tr, are be processed in the same way all flow images are processed, and whose procedure is explained next.

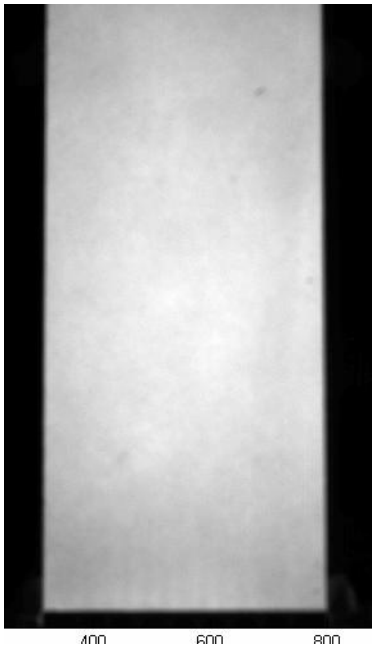

Figure 4.2 Reference Image

To obtain a flow image, first the plenum must be kept at a constant pressure and temperature for approximately 8-10 minutes to achieve the desired blowing ratio, and thus film cooling conditions over the paint. Once these conditions are met, the set of images can be taken. Figure 4.3 shows TSP under cooling conditions. The darker sections of the paint indicate higher temperatures, the lighter sections, cooler paint. Hence, the cooling jets can be observed as light colored. One must keep in mind that the "lighter and darker" sections are relative to the reference images, not compared to other sections of the TSP. Following this concept, the Tr image would look uniformly darker than the reference.

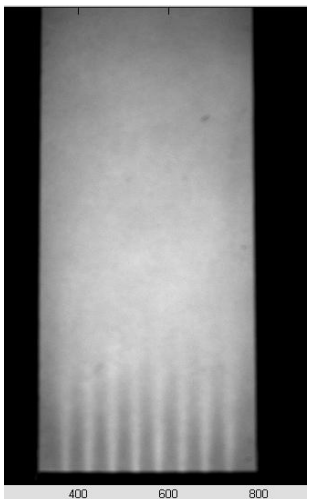

Figure 4.3 Image of TSP showing coolant flow

The process of taking images continues until all the blowing ratios are taken. Once this has occurred, the testing ends and the images can be processed.

During testing, the camera may shift slightly, appearing on the images as movement on the order of a couple of pixels, so the images must be cropped to only study the area of interest. This is usually the TSP area only. The new cropped images contain only the TSP, from left edge to right edge, from upper edge to the holes. This cropping must be done carefully, making sure that any feature on the paint has the same pixel position value in all cropped images. In other words, when looking at the cropped image of run 1, it must be identical in size and position as the reference images and all the other runs. Supposing there is a dot on the TSP, on all cropped images, that dot should be at exactly the same position. This is important in the processing of all images because temperature is obtained as follows: the ratio of emission intensity I(T) at any temperature T to the emission intensity I(TR) at an unspecified reference temperature TR is

$$IR = \frac{I(T)}{I(T_R)} = f(T, T_R)$$

In terms of images, this means, we divide each pixel intensity value for Figure 4.3 by that of Figure 4.2 to obtain Figure 4.4. The intensity ratio IR is also called the relative intensity. Figure 4.4 illustrates the ratio of intensity of 4.3 and 4.4.

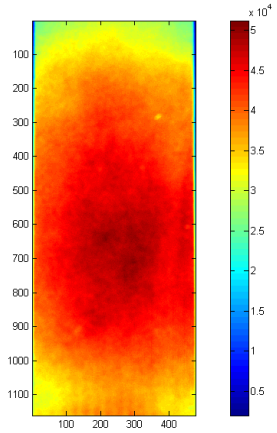

Figure 4.4 Relative intensity ratio, IR

The effects of lighting and paint thickness are, in principle, eliminated by taking the ratio IR (Liu, 2006). The next step is to convert these local ratios into temperature values. This is accomplished with the use of the calibration curve of the paint. Figure 4.5 shows a typical calibration curve for TSP.

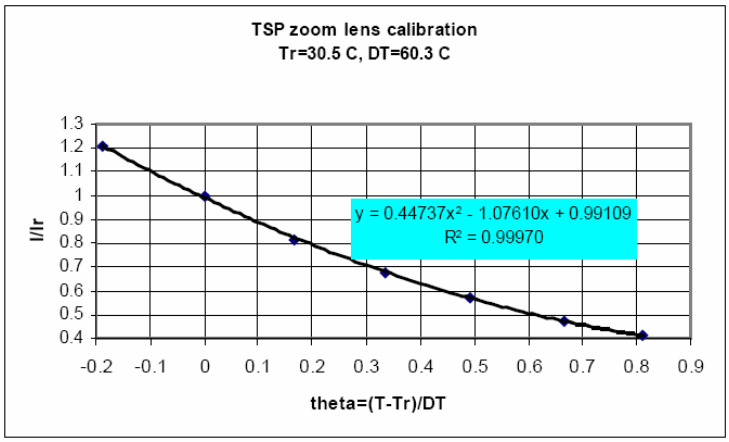

Figure 4.5 TSP calibration curve, from Liu, 2005

The function theta can be determined by fitting non-dimensionalized calibration data with a polynomial. The polynomial is then used to back-calculate the temperature from the intensity ratios. From the value of theta, T can be solved since Tr and DT are known quantities established during

calibration. The manipulation is done with software on a per-pixel level. Once the processing is done, the intensity information yields temperatures. This is how the recovery temperature and the adiabatic wall temperature distributions are obtained. Please refer to Appendix B for the MATLAB codes used to process the intensity images.

Figure 4.6 shows the final result from processing. In that Figure, the jets are clearly discernible. The reduction process is explained in the following subsection.

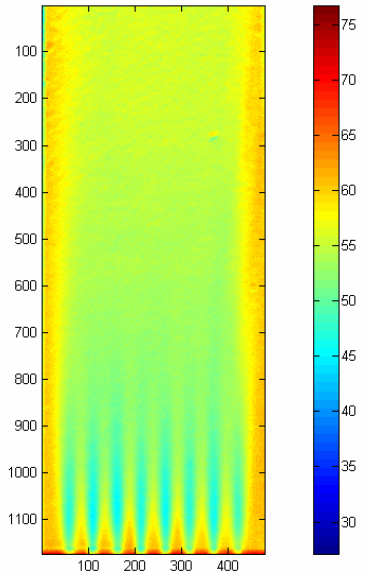

Figure 4.6 Raw temperature image from TSP

Conversion of Temperature Data to Film Cooling Effectiveness

To calculate the span-wise-averaged cooling effectiveness, several physical factors are considered such as edge effects, the number of cooling holes and the diameter of the holes. To discount edge effects from influencing the temperature data, only holes close to the middle of the coupon center are included in the averaging step. Since the conical coupons have only eight cooling holes, the holes used are the middle four. This means that temperature averaging occurs from the line exactly between the second and third hole, to the line between the sixth and seventh holes, for the all the coupons with L/D of 3.5. For the compound coupons, since there are twelve holes in this arrangement, the holes considered are the middle

six holes. This assures that flow passing through the part of the test section that is not cooled, and which may interact with the cooling process by entrainment, will not affect the temperature data in the averaging process.

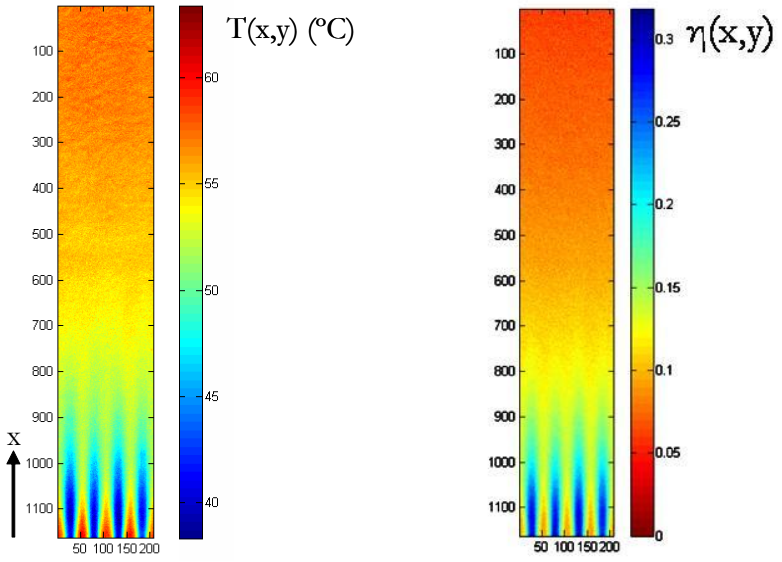

Figure 4.7 Temperature plot cropped for processing (left); processed for effectiveness (right)

Figure 4.7 shows the temperatures downstream of the cooling holes considered for the calculation of the effectiveness. In that Figure, another important parameter shown is x. x is the distance downstream of the holes. In Figure 4.7, x is reported from the downstream edge of the paint in pixels. This is corrected during processing using a pixel-per-millimeter ratio and dividing the resulting millimeter values by the diameter of the holes, to reflect the distance downstream from the exit of the holes. This yields X in terms of the parameter x/D, a dimensionless distance commonly used for cooling effectiveness comparisons of holes of any size.

Once the intensity data has been reduced to pixel temperature data, the second part of the processing focuses on finding the film cooling effectiveness over the TSP surface. This step can be done with MATLAB: Figure 4.6is subtracted from the Tr obtained after the tunnel warmed up, before cooling. This difference is divided, pixel-by-pixel, by the difference between Tr and Tc, which is known from testing. This yields an effectiveness distribution, like the one shown in Figure 4.7. It must be stated, that

the resolution of η obtained with this method is too low to show local or centerline effectiveness. In other words, it is not recommendable to use centerline values from these images because the local values are themselves fuzzy "averages" due to the lack of resolution. Once the effectiveness distribution is obtained, it is averaged spanwise and collapsed into a two column matrix. The first column contains the value of x/D, the second contains the value of ηla. The result of this process is shown in Figure 4.8.

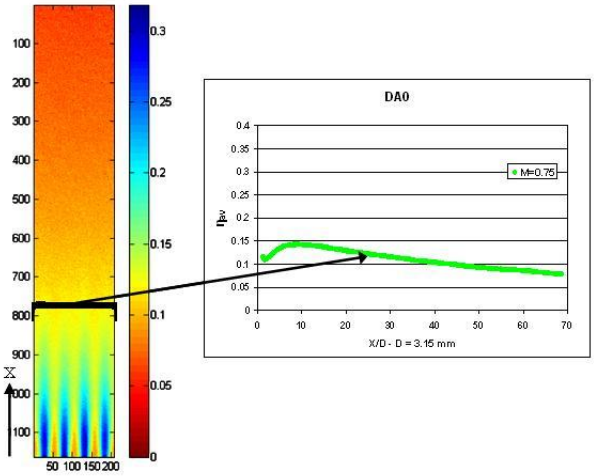

Figure 4.8 Results of averaging η; arrow indicates collapse into one point

The MATLAB code then saves the information to a "results" file, which is used to continue the post-processing. The data file output by MATLAB is easily opened in a spreadsheet program, in this case EXCEL. Thus, film cooling effectiveness is obtained on a pixel-by-pixel basis downstream of the cooling holes. All effectiveness results for this thesis were obtained in this fashion and are reported in Chapter 5.

Measurement Uncertainty

The The uncertainties reported were estimated taking into consideration the approaches described by Kline and McClintock (1953), Moffat (1988), Holman (1994) and Wheeler and Ganji (2004). The effectiveness as defined as a non-dimensional temperature difference is used to find the derivatives in the uncertainty equation:

$$U_\eta = \sqrt{\left(\frac{\partial \eta}{\partial T_c} U_{Tc}\right)^2 + \left(\frac{\partial \eta}{\partial T_{rec}} U_{Trec}\right)^2 + \left(\frac{\partial \eta}{\partial T_{aw}} U_{Taw}\right)^2}$$

In this case U_{Tr} and U_{Taw}, the uncertainties in the recovery and adiabatic wall temperatures are equal since both are obtained with TSP, which was calibrated with a thermocouple whose. Their value is ±0.8ºC (Liu, 2006). U_{Tc} is 1.0ºC, which is the uncertainty in the coolant temperature, as measured with the plenum thermocouple set up. The values of U_η are evaluated at every point on the η_{la} curve, and give the uncertainty band shown in Figure 4.9. Please refer to Appendix for a more detailed derivation of Figure 4.9.

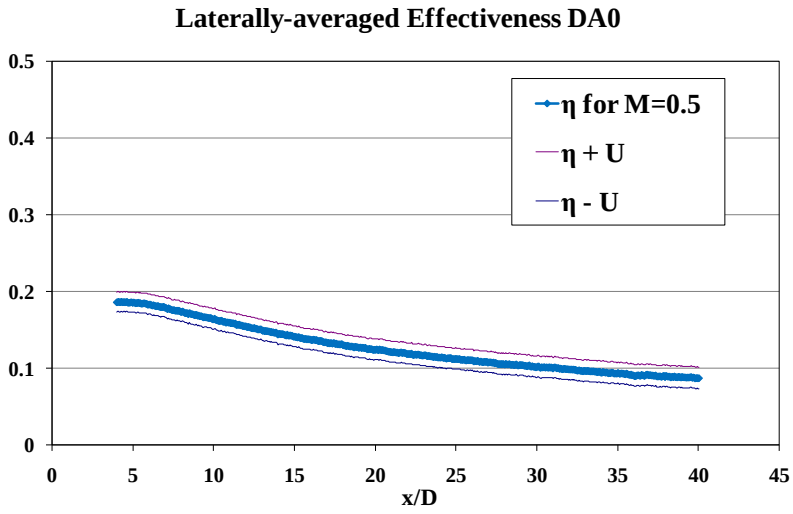

Figure 4.9 Baseline effectiveness with uncertainty bands

The uncertainty in the discharge coefficient has been calculated similarly, with the following equation

$$U = \sqrt{\frac{\partial CD}{\partial m} U_m + \frac{\partial CD}{\partial Pc} U_{Pc} + \frac{\partial CD}{\partial Pstat} U_{Pstat} + \frac{\partial CD}{\partial Tc} U_{Tc} + \frac{\partial CD}{\partial D} U_D}$$

This equation yields results that suggest the uncertainty at the lower pressure ratios is on the order of ± 9%, and ± 1% at the higher pressure ratios. The results at four pressure ratios are shown in Figure 4.10.

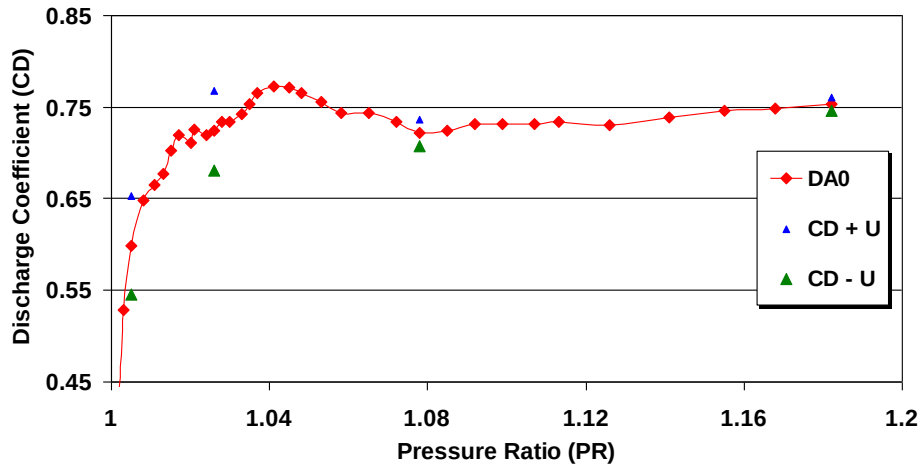

Figure 4.10 C_D measurements for DA0 with uncertainty points

With these error bands in mind, we are now able to look at Chapter 5, which gives the full set of results for all tests.

CHAPTER FIVE: RESULTS

Results of the film cooling tests for all test matrices are presented in this section. Before delving into the data, their validity is assessed by comparing results obtained in sample tests against those found in open literature. For this purpose, the studies used were: Sinha et al. (1991), Pedersen et al. (1977), and Baldauf et al. (2004). These studies were chosen because of their inclusion of a variety of test cases for simple cylindrical holes and their validation with other studies in the open literature.

Validation of Results

According to Goldstein et al. (1968), it is appropriate to compare effectiveness data at very low blowing ratios, even if the geometry is different. Their study showed this in a dramatic fashion since they presented data for holes at inclination angles (α) of 90º versus 35º with satisfactory results. Data from one important study conducted by Lutum and Johnson in 1999, and with which this study is most compatible geometrically, were not presented for M of 0.25. Data are available, however for other blowing ratios. Figure 5.1 shows η_{la} for DA0 and data from several studies, both recent and from several decades ago. Testing conditions for these tests are summarized in Table 5.1.

Table 5.1 Summary of parameters of tests in Figure 5.1

Study	M	L/D	Diameter	α	Tu (%)
Sinha	0.25	1.75	1.27 cm	35º	0.2
Pedersen	0.213	40	1.17 cm	35º	~0.35
Baldauf	0.2	6	6 mm	30º	1.5
Present DA0	0.3	3.5	3.15 mm	35º	0.6

Figure 5.1 shows the spanwise-averaged film cooling effectiveness (η_{la}) for DA0 at a blowing ratio of 0.3. It is possible to see that the data match quite well; even the trend downstream at x/D > 10 holds very well. Considering the differences across testing rigs, geometry of the test plates or holes, and the differences in testing techniques, the agreement is quite satisfactory.

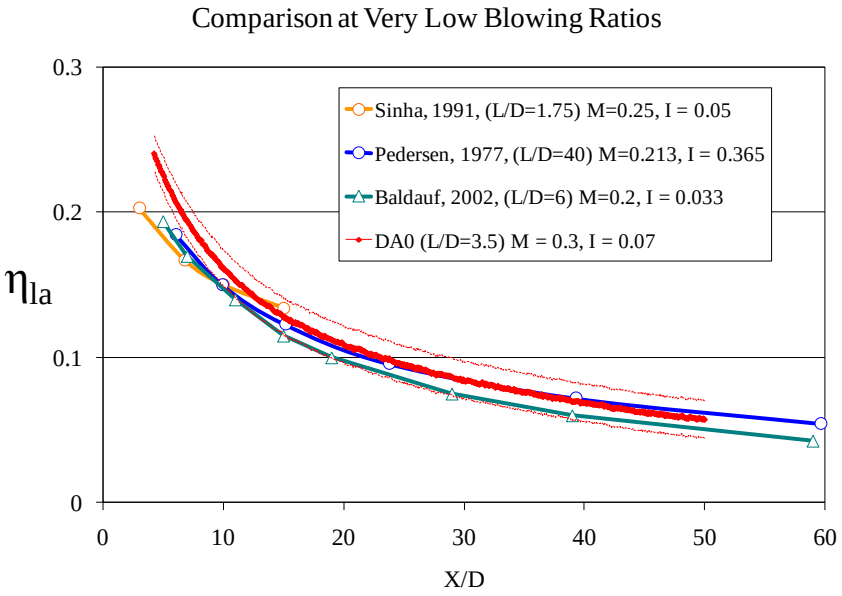

Figure 5.1 Comparison of results against previous studies for low M

For this study, the blowing ratio M = 0.3 was run on the baseline cylindrical plate, DA0, only for comparison purposes, since the such low blowing ratio is not used in turbine applications.

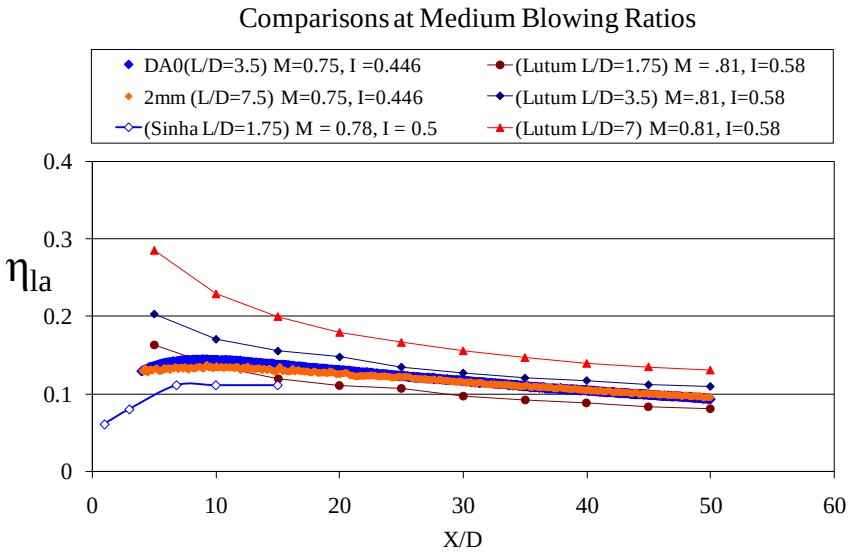

Figure 5.2 Comparison of η_{la} versus literature at M = 0.75

Looking at Figure 5.2, it is possible to notice that the results begin to diverge when compared to open literature especially in the near hole region, x/D<15. Since the blowing ratio is moderate at 0.75, it

is safe to say that at this point the peculiarities of the rig, as well as operating conditions need to be examined more closely. The geometry used by Lutum and Johnson (1991), as discussed in Chapter 2, has a PI/D of 2.86, meaning that the holes are relatively closer together than in the present study, naturally yielding higher η_{la} values. This is in addition to increases in effectiveness at the exit due to a main flow turbulence intensity of 3.5%, compared to the present study's Tu_{∞} = 0.6%. The enhanced turbulence can lead to higher effectiveness values, especially in the near-exit region, at x/D < 20. Given these differences, it the effectiveness values are actually in good agreement. At larger distances downstream of the holes (x/D >25) the curves exhibit similar values; the exit geometry does not matter at this point.

Since the present study is also conducted at higher values of M, it is necessary to compare sample results against those in the literature. To that aim, Figure 5.3 is presented.

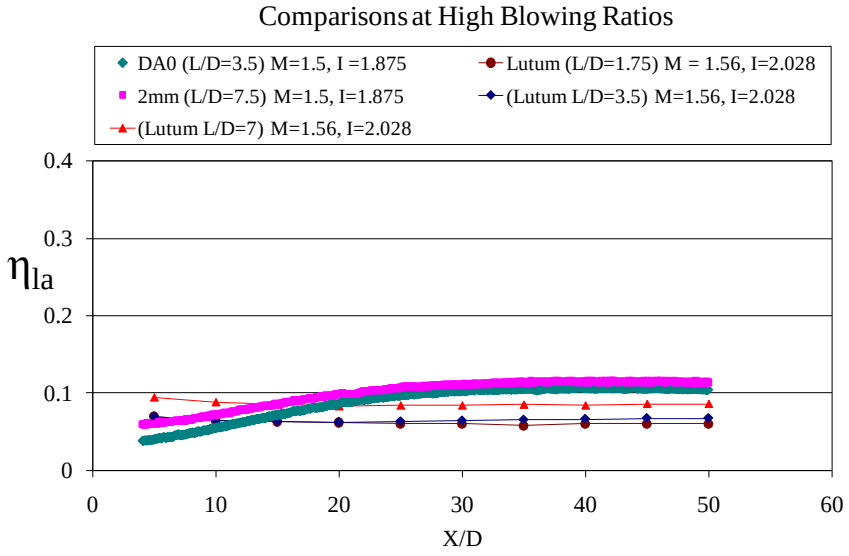

Figure 5.3 Comparison of η_{la} at M = 1.5 vs. Lutum and Johnson, 1999

The values of η_{la} observed in Figure 5.3 for DA0(L/D=3.5) and DA0(L/D=7.5) are again satisfactory, and agree with the Lutum and Johnson data. What sets apart both sets of data is the difference in mainstream conditions. While in the present study, the turbulence intensity level is at 0.6%, with a boundary layer thickness of 4.85 cm [15.4 diameters for DA0(L/D=3.5), and 24.9D for DA0(L/D=7.5)], Lutum's tests were run at Tu = 3.5%, with a boundary layer thickness of 4mm (1

diameter). The resulting effect is that even though the jets lift off in the present study (the η values dip), the low turbulence level does not completely dissipate the structure of the jets, and allows them to reattach (at about x/D =20) and continue offering protection downstream. The lower turbulence levels allow the DA0 jets to maintain some integrity and thus reattach later downstream. In Lutum's case, the high turbulence, combined with the very thin boundary layer, present a setup in which the jets are battered by the mainstream right from the hole exits, and do not have a chance to reattach. The resulting flow downstream has no structure; it is just the mass flow what keeps the η_{la} at 0.08 and lower. For Lutum's study, the increased L/D effect is what allows the coolant for the L/D=7 holes to remain closer to the surface and thus provide slightly higher η_{la}.

All in all, it is this author's belief that the presented sample data agree very well with the data in the literature. When studying film cooling, it is quite difficult to replicate other groups' results exactly. Given the level of agreement between results in the current study and those found in other published data, the quality of the data is deemed adequate.

Part of the reliability of data is the ability to reproduce it. The experiments for this study were conducted over a period of approximately 15 months. During that time, there were opportunities to repeat several tests, and choose the results for which the data yielded seemed to have better resolution, or to have a longer range. Such is the case presented in Figure 5.4, in which the test labeled Test 1, showed results within acceptable uncertainty, but there had been questions about the cleanliness of the data, as well as the extent of the range over which it was presented. Thus, the test was repeated months later, over a longer stretch of TSP for the current study. Two weeks later, the test was repeated again and the data is shown for a blowing ratio of 0.75. For that case, a completely new layer of TSP was used, and the results were identical. For a given set of data, multiplying the maximum x/D by the diameter of the hole yields the maximum distance downstream of the exit; the shorter the value, the older the test. When observing the plots in the next section, the age of the tests does not seem to affect the trends, only the range.

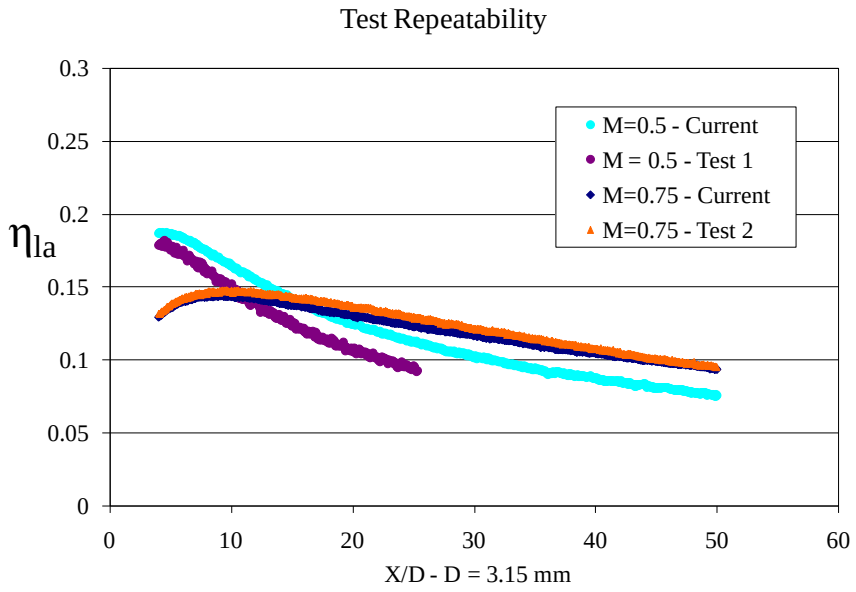

Figure 5.4 Data from current study vs. repeats and older tests

It has been shown in this section that the results obtained for the configurations DA0(L/D=3.5) and DA0(L/D=7.5) compare satisfactorily against previous studies by showing acceptable η_{la} values and consistently following expected trends. It is then, with this in mind that the results for the investigated geometries are presented next.

Shaped Holes with Conical Diffusion

Results for the laterally-averaged film cooling effectiveness are shown first grouped by blowing ratio, and then grouped by geometry.

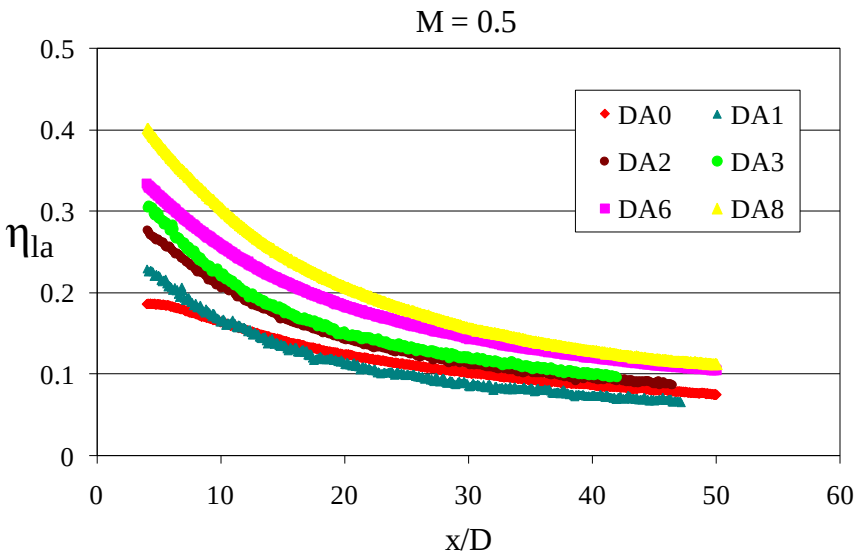

Figure 5.5 Laterally averaged effectiveness for M = 0.5 for conical holes

Figure 5.5 shows that DA8 offers the highest η_{la} of all the configurations at M=0.5, with DA0 and DA1 offering the least protection. DA1 does not fit perfectly in the trend, but the difference between its η_{la} values and those for DA0 are within uncertainty. The increased effectiveness values provided by the wider conical angles continue at distances downstream greater than 20 x/D.

It is important to keep in mind when looking at this data that the coverage values of all the holes are different. While coverage for DA0 is 33%, it is 65% for DA8. This means that the highest value of DA8 at the exit of the holes should be toward η_{la} =0.65, while only 0.33 for DA0. The implications of this will be discussed later in this section. For now, only general trends will be discussed, in the context of the parameters M and I as defined in literature.

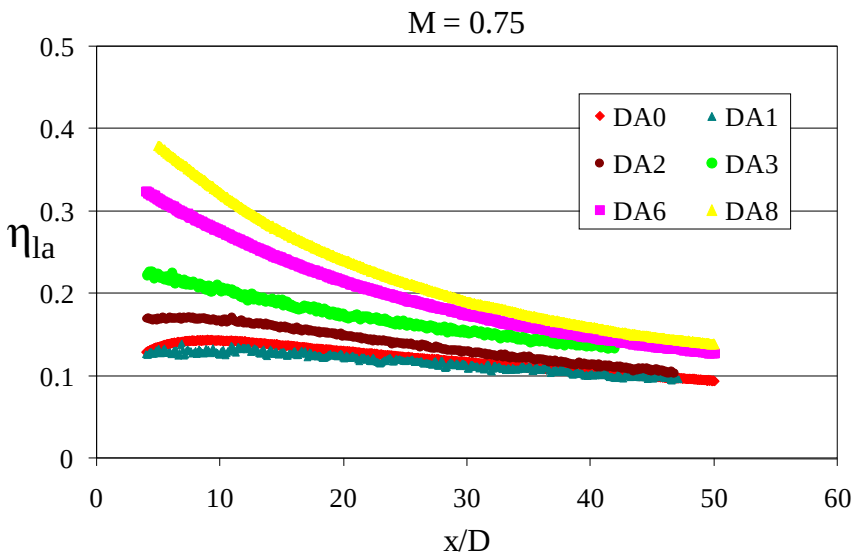

Figure 5.6 Laterally averaged effectiveness for M = 0.75 for conical holes

Increasing the blowing ratio to 0.75 brings changes in the performance of the coupons. The general shape of the curves in Figure 5.6 is flatter, meaning the non-dimensional spanwise-averaged temperature is more uniform, a trait more pronounced in the DA0 and DA1 configurations. Even though the higher diffusion angled plates show lower η_{la}, at low x/D, close inspection reveals that at x/D = 20 all coupons have higher values than in the previous = 0.5. At x/D = 40, the same observation applies. The trend continues for all remaining values of x/D.

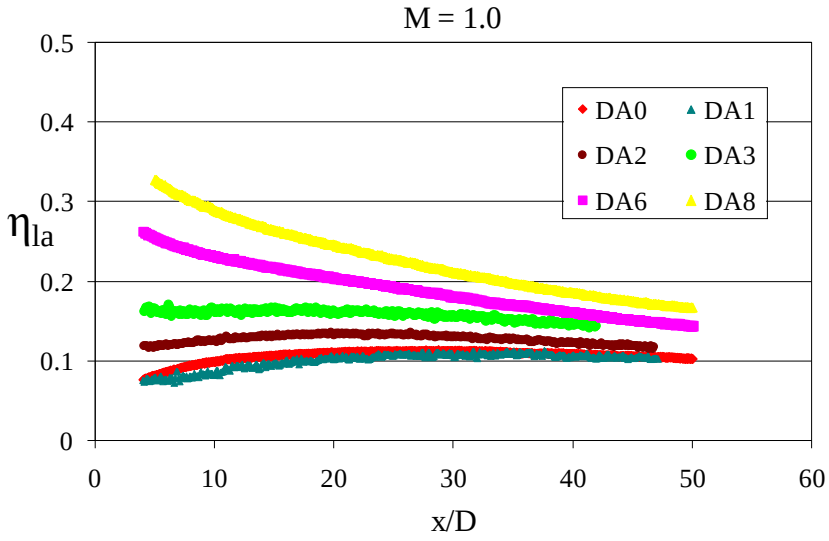

Figure 5.7 Laterally averaged effectiveness for M = 1.0 for conical holes

At blowing a ratio of 1.0, seen in Figure 5.7, DA0, DA1 and DA2 start to lift off. This is evident in the "dip" of the curves at low x/D, and the subsequent rise and preservation of the η_{la} value of 0.1. DA3 also flattens out, while DA6 and DA8 show very similar values of η_{la} at x/D =20 as in M=0.75. However, the performance of these two plates, DA6 and DA8 improves for values of x/D > 30 when compared to M=0.75. As discussed extensively by Baldauf et al. in their 2004 study, it can be seen that while the laterally averaged effectiveness of these coupons is not higher than that for values of M of 0.5 and 0.75 close to the holes, if these jets (mainly for DA3, DA6 and DA8) are not detaching, then the increased flow must have another effect. The effect on the curves is a sort of shift toward the higher x/D values, compared to the previous M values. What this indicates is that the jets coming out of the holes have higher momentum and travel downstream more quickly; as they travel, they spread, eventually widening enough to the point that they start to interact with each other. Baldauf et al., 2004, say that the effect of this interaction is the creation of a new massive "thickened closed film" whose thermal capacity prevents intense hot gas entrainment and cooling film degradation. This idea will become more evident observing the individual effectiveness curves for each configuration later on.

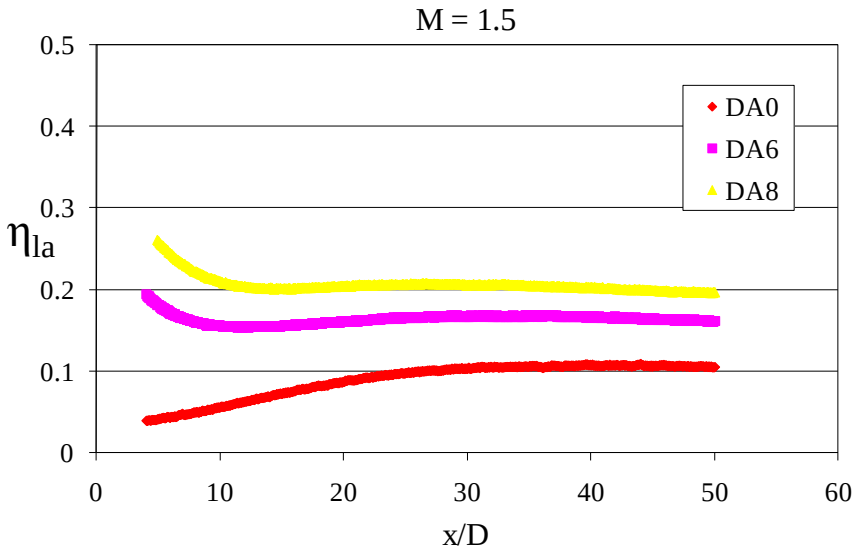

Figure 5.8 Laterally averaged effectiveness for M = 1.5 for conical holes

Figure 5.8 shows the DA) curve as detached. This is expected for such high blowing ratio, and is consistent with the literature. DA6 and DA8 are still attached. DA0 seems to reattach after an x/D of 30. At x/D of 10, the value of η_{la} for DA8 falls by 25%, while after x/D of 32, the trend is reversed, and the values of η_{la} actually increase, and are preserved, further suggesting that jet interaction does help keep effectiveness values at 0.2 after sixty diameters downstream. For DA6, the same happens, but since the amount of mass flow for this coupon is less, 27% less, increase in effectiveness as a result of reattachment occurs and starts to fade over a shorter length than that for DA8. A closer look at the second "peaks" of the curves, which happen close to x/D =36, η_{la} = 0.17, for DA6, and at x/D = 27, with η_{la} = 0.20 for DA8, shows that there is less than 20% difference in effectiveness between them. It is important to point out that the protection levels at blowing ratios of 1.5 are significant. For a line located 50D downstream of the point of injection to see a level of effectiveness as 0.2, it is impressive and compares to protection offered by fan-shaped holes. This will be discussed further when all data is averaged spatially.

Now that all conical coupons have been compared against each other, it is appropriate to look at them individually. For this purpose, laterally-averaged film cooling effectiveness curves are presented for each coupon for all blowing ratios. Data for the compound holes DA0(2mm) and DA2(2mm) are also shown. For the sake of brevity, instead of presenting them one at a time, the coupons are shown in three groups. First, DA0 through DA3 are shown together as the low diffusion angle plates in Figure 5.9. DA6 and DA8 are shown as the large diffusion angle plates in Figure 5.10, and DA0(2mm) and DA2(2mm) are shown together as the compound hole group, Figure 5.11.

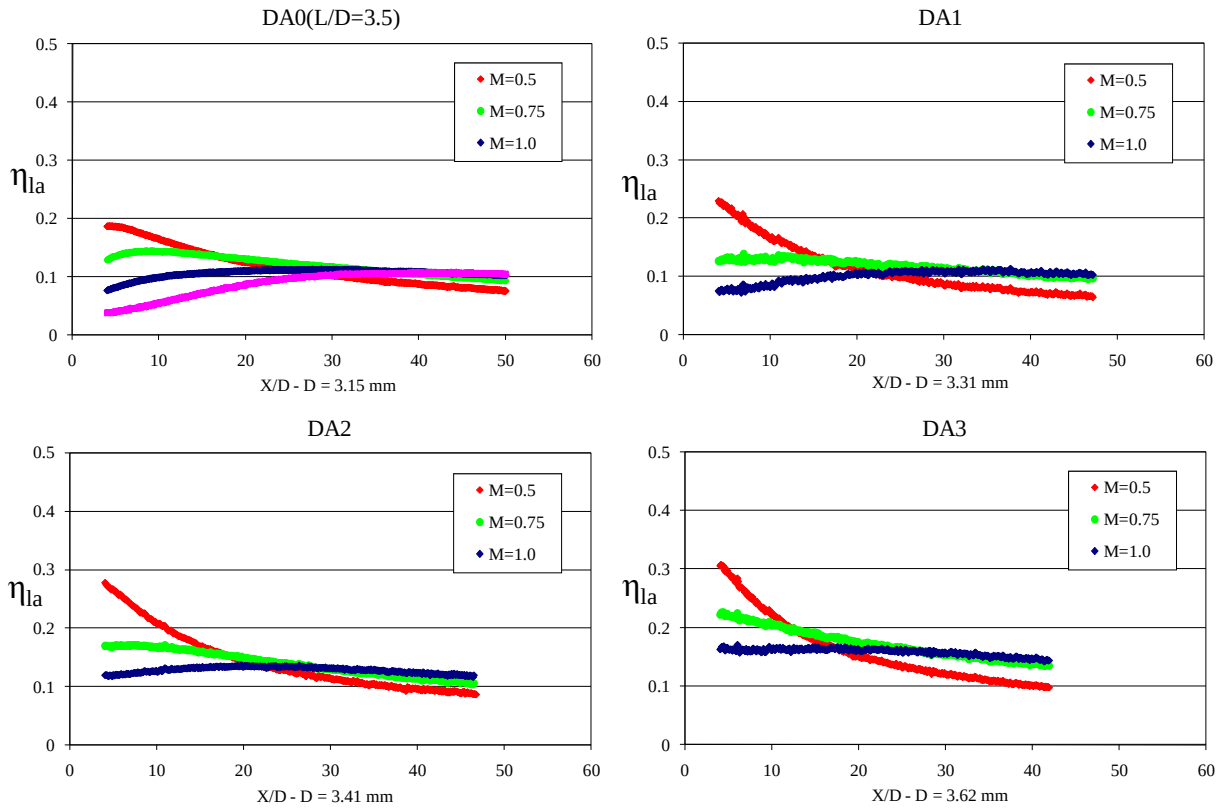

Figure 5.9 Laterally-averaged effectiveness for lower DA plates

In general, DA0 and DA1 behave very similarly, showing comparable values of effectiveness. Perhaps this is due to the closeness of the cone angle values, or that the testing technique is insensitive to such small variations in angle. Looking at DA2 and DA3, we see that they begin to show higher values of laterally-averaged effectiveness. This may be due to the effect of increased lateral spreading of the jets, brought by the higher diffusion angle. This leads to reduced flow momentum at the exit and better coverage.

The trend of higher overall effectiveness at increasing blowing ratios continues for the two coupons in Figure 5.10.

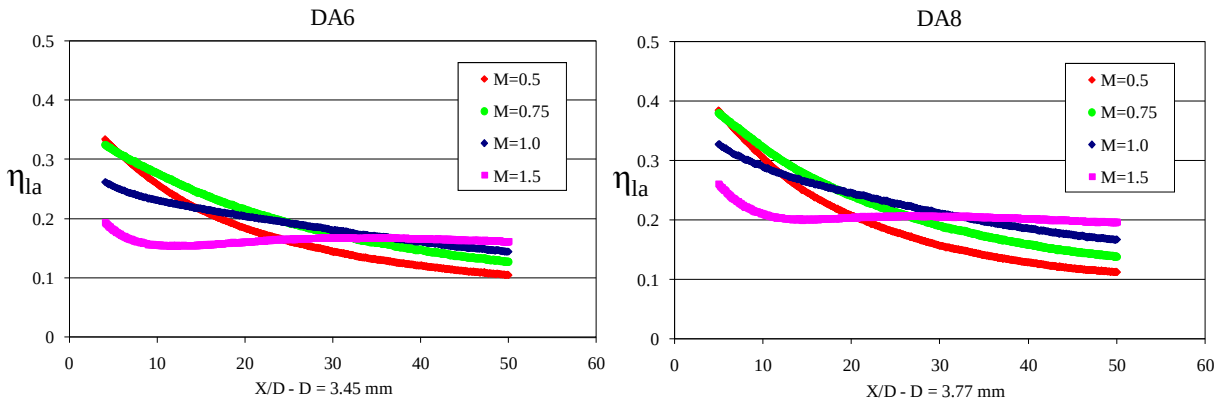

Figure 5.10 Laterally-averaged effectiveness for higher DA coupons

For both plates, a slight dip in effectiveness can be observed at x/D of 10 to 15. There are no signs of detachment for blowing ratios of 1.0 or less, but the increase in effectiveness at the higher blowing ratio of 1.5 suggests enhanced jet interaction downstream of the point of injection.

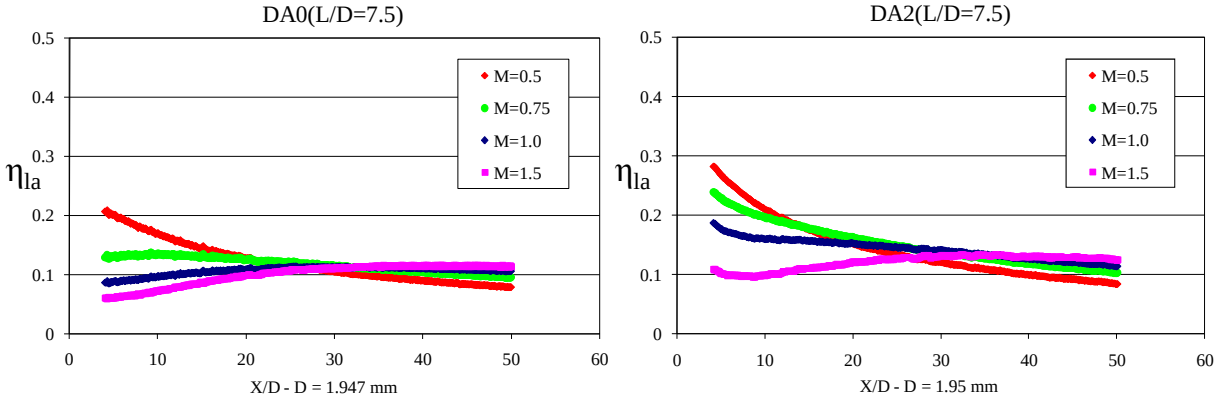

Figure 5.11 Laterally averaged effectiveness of compound holes

For the two sets of data in Figure 5.11, we see that η_{la} for the DA2(L/D=7.5) follows trends very similar in shape to those of the other conical coupons. Its effectiveness is slightly higher at all blowing ratios compared to the nominal DA0(L/D=7.5). In order to understand why this difference is seen it is necessary to separate the effects of entry-length and increased diffusion angle from each other. We need to refer to Figure 5.12. It shows that the only difference in film cooling effectiveness between DA2 and DA2(L/D=7.5) is a slightly higher effectiveness in the near field region (x/D <20), at the higher blowing ratio. Up to that point, the jets should remember the exit geometry, and reflect that, meaning that the jets

from DA2(L/D=7.5) are more diffused compared to the pure conical jets. Hence they have a higher effectiveness over this range. DA2 has a shorter L/D, so the effectiveness is not as high. Thus, we can see that adding an entry length to a conical geometry does not have a negative influence on the values of effectiveness, in fact, it enhances it. Hence, in Figure 5.11, the majority of the gain in performance observed when comparing DA0(L/D=7.5) to DA2(L/D=7.5) is due to the L/D increase, as evident in Figure 5.12.

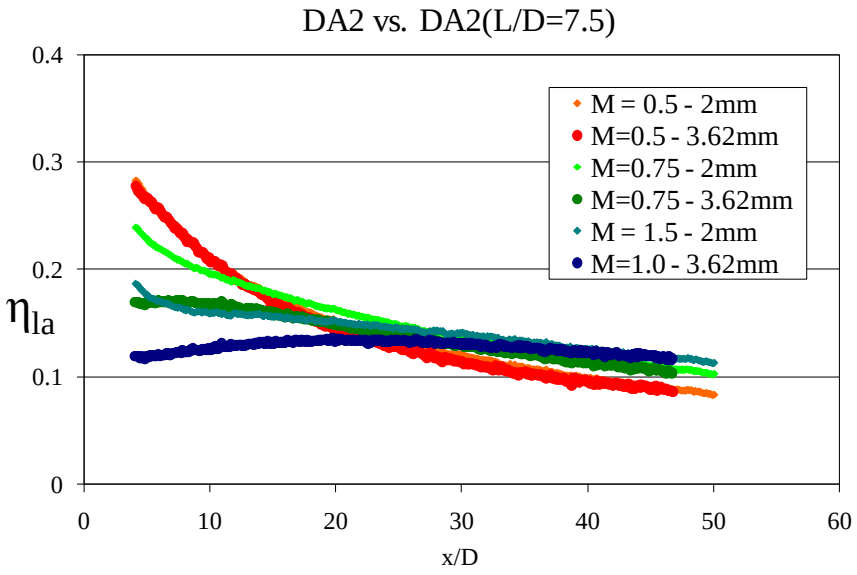

Figure 5.12 Comparison of η_{la} for DA2 and DA2(L/D=7.5)

Figure 5.13 is included for completeness. It shows the performance of DA0 against that of DA0(L/D=7.5).

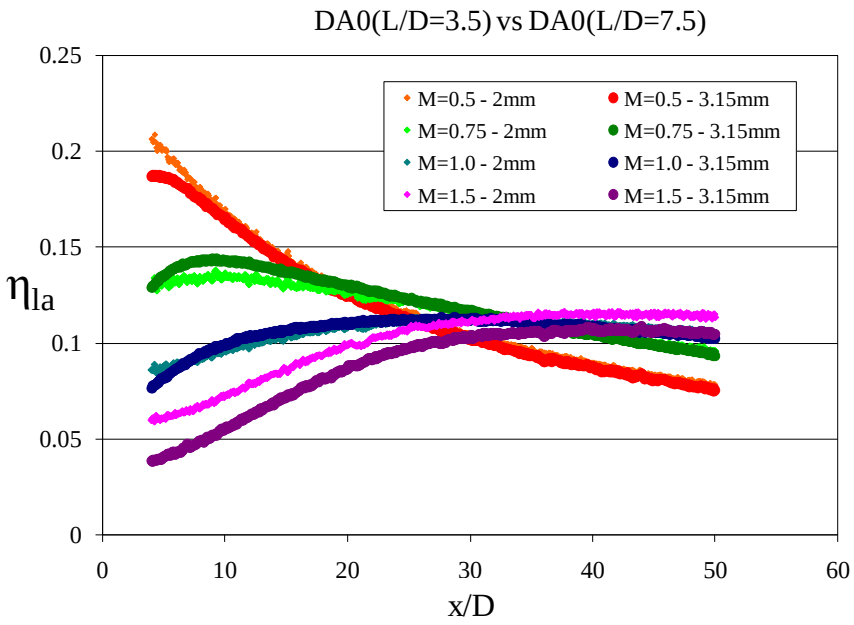

Figure 5.13 Effectiveness comparison for DA0 and DA0(2mm)

The higher effectiveness values for DA0(L/D=7.5) also suggests a more compact jet structure with less momentum than that of the DA0 jets, which helps it retain its cooling ability more effectively.

All of the previous results can be summarized by including them in a single spatially-averaged effectiveness plot for all blowing ratios, as shown in Figure 5.14.

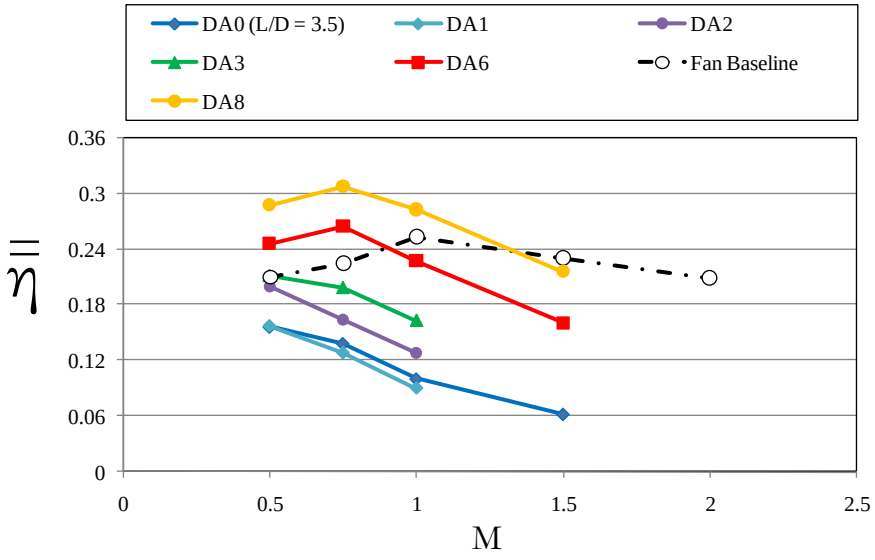

Figure 5.14 Spatially-averaged effectiveness for all blowing ratios

Figure 5.14 shows the spatially averaged film cooling effectiveness from an x/D of 4 to 20. Each curve shown before is collapsed into one point by averaging the effectiveness value over the range of x/D. This is done for every blowing ratio. What is obtained is a picture of the overall performance of each geometry, disregarding local variations. We can see that the slightly lower value of effectiveness for DA1 observed earlier persists for all blowing ratios. We can also see that the effectiveness for DA0 through DA3 all decrease steadily for all blowing ratios studied. The trend changes for DA6 and DA8, in which it is observed that the highest average protection is seen for a blowing ratio of 0.75. Then the values of spatially-averaged effectiveness decline steadily as in the other cases. The effect that is observed can be thought of as a decrease in the effective blowing ratio caused by the increased area ratio of the larger conical holes, manifested as a shift in the curves. Looking at the generic fan-shaped data (discussed later), we can see that at the lower blowing rates, the larger conical holes outperform the fan holes easily. However, once the blowing ratio reaches a value of 1.5 and higher, the fan shaped holes outperform all geometries since they are designed to perform at such high values of M.

What is interesting to see is that the 8-degree holes perform similarly to the fan at M = 1.5, with both holes improving performance by a factor of 4 over the cylindrical baseline. Thus we can see that the larger conical holes on the average provide protection comparable to that of fanshaped holes (at higher M), and significantly better than cylindrical holes and fan holes at the lower blowing ratios. This means that one way to help the gas turbine industry reduce the use of coolant, and improve performance could be by substituting cylindrical holes with flared (conical) holes. At low and moderate blowing ratios, even flaring by 6-degrees would improve performance by 66%. At a blowing ratio of 1.0, the coverage would improve by 100%. At a region in which fan-holes may be difficult to place, a pure flared hole could provide similar protection without the need for an entry length. These are promising results.

Holes Embedded in Trenches

Effect of Pitch-to-Diameter Ratio

Figure 5.15 shows the film cooling effectiveness downstream of the coupons baseline cylindrical hole coupons. These coupons have cylindrical holes at a PI/D of 4. The images are scaled horizontally in order to fit the large distances between holes, especially for the cases of PI/D > 4. For example, if we look at the case CYL1 PI/D = 8, the distance between two hole centerlines is 8 diameters or 16 mm; for the CYL1 P/D = 12, the holes are 24 mm apart. The images squeeze the information in the horizontal direction in order for the reader to see a larger piece of the data in a more manageable size. For all images, the x/D range shown is from 2D to 25.4D, where D is 2 mm.

At the low blowing rates, the P/D = 4 case benefits from the downstream interaction between jets as seen before in the previous section. At the higher blowing ratios, 1.0-2.0, liftoff effects begin to take place and the performance is expected to decrease. For the case of P/D = 8 and 12, there is not really any jet interaction downstream of the holes because of the large distance between holes; the coverage decreases along as PI/D is increased. Thus, it is not common to use these P/D's in practice because of large sections that are unprotected.

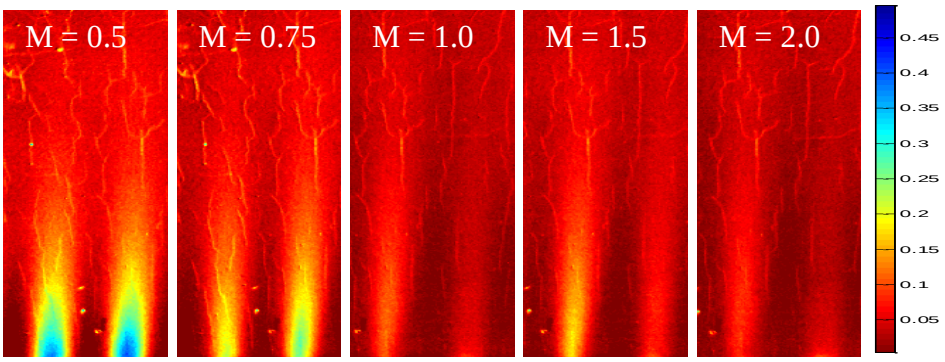

CYL 1, P/D = 4

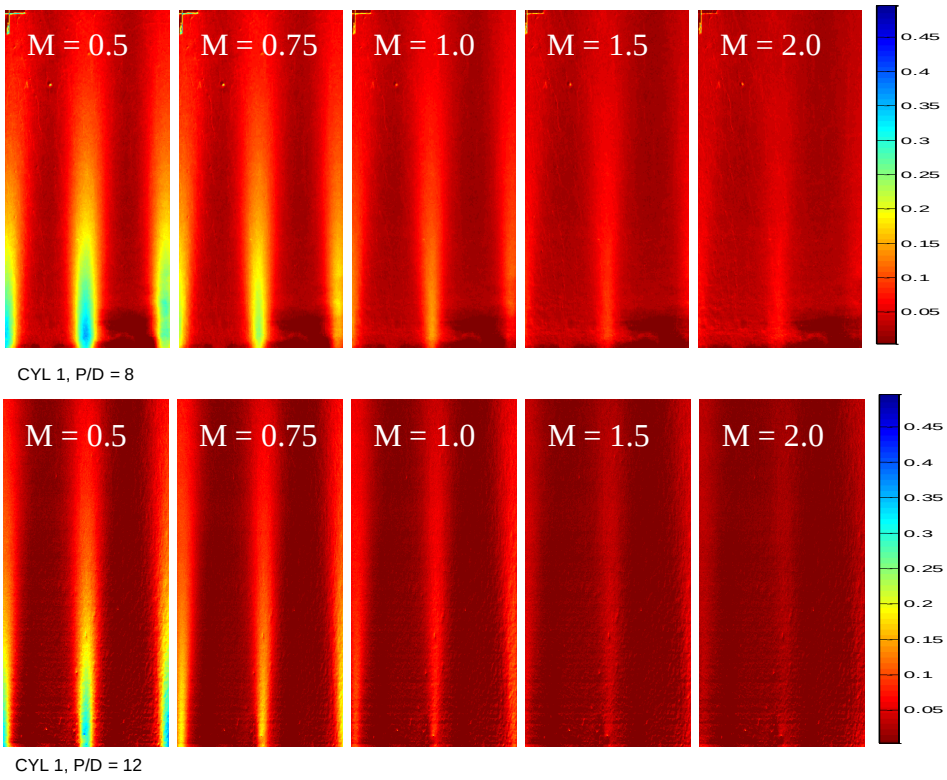

Figure 5.15 Film cooling effectiveness downstream of baseline cylindrical holes

In Figure 5.16, the cylindrical holes are placed in the trench and studied at the same blowing ratios as the baselines. We can observe immediately that there is a substantial increase in the widths of the jets which suggests increased interaction, especially for the PI/D = 4 case. The difference between the PI/D = 4 baseline and the trenched cases are remarkable. At the highest blowing ratios, in which cylindrical holes are of no use, M > 1.0, the trenched holes clearly show protection.

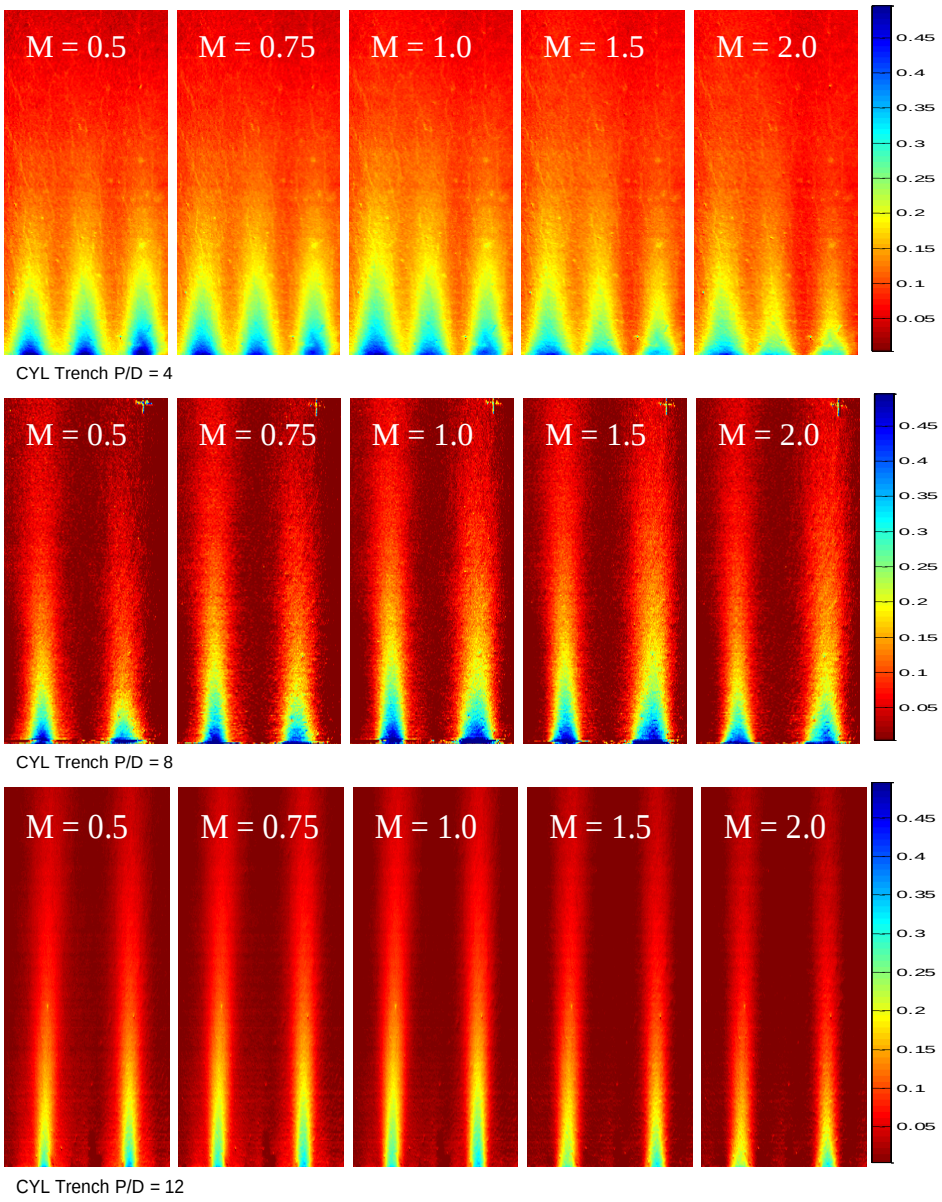

Figure 5.16 Film cooling effectiveness distributions downstream of trenched cylindrical coupons

For the P/D = 8 case, it is hard to tell if the jets are interacting at the exit, but the presence of the trench does increase the visible coverage. Downstream, the jets maintain their individuality. It is interesting to see that the jet widths remains pretty much constant for all blowing ratios in the cases of PI/D = 8 and 12. For the P/D = 12 case, the jets show no interaction, but again they do show an increase in width. Figures 5.17 and 5.18 summarize the previous results quantitatively with the use of span-wise averaging for the lower and higher blowing ratios.

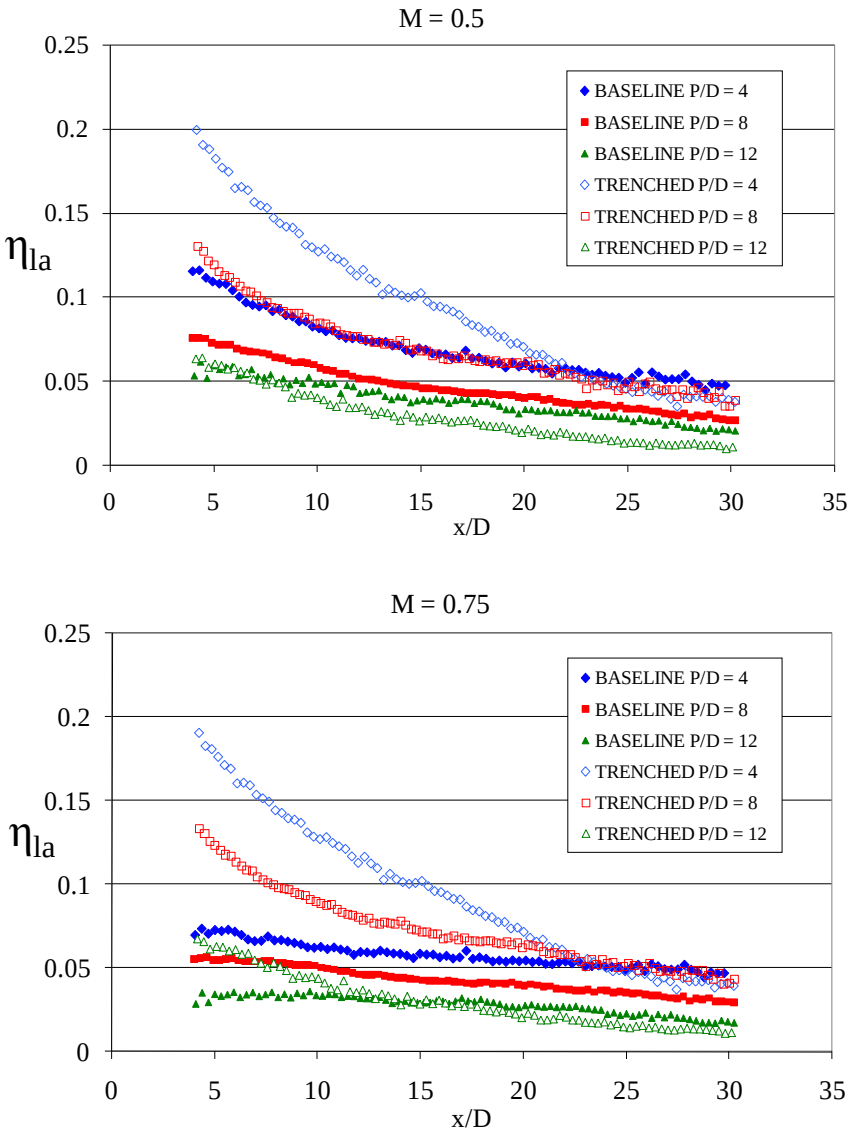

Figure 5.17 Span-wise averaged effectiveness for all cylindrical geometries at lower blowing ratios

Figure 5.17, M=0.5, shows that the trench 4-P/D case outperforms all other configurations. More striking it is to see that the 8-P/D trenched case behaves very much the same as the 4-P/D cylindrical baseline. The trench, as seen in this plot can have the potential to cut the number of holes in half and maintain the same performance as a standard row of cylindrical holes, indicating that the trench somehow lowers the operating blowing ratio of the cylindrical holes. For the 12-PI/D case, the trench appears to hurt the performance slightly, especially downstream since the added diffusion can make the jets lose their cooling mass more quickly than the undisturbed jets. In the case of M = 0.75, the two trenched

configurations outperform the rest. The added diffusion helps the 12-PI/D case in the near-hole region, x/D < 10.

Figure 5.18, M = 1.0 shows the baseline holes beginning to detach, while the performance of the trenched holes has barely diminished. For the case of M = 1.5 and 2.0, the baseline 4-PI/D plate shows the classical detachment and reattachment pattern. This does not happen for the other two baseline cases, and as a result, the effectiveness continues to decrease. One can see at the higher blowing rates that there is no hint of jet detachment for the trench plates. The trench improves performance for the 8-PI/D case, but at the highest blowing rate, the performance drops. Perhaps this is caused by the visible individuality of the jets, which may be far apart to interact.

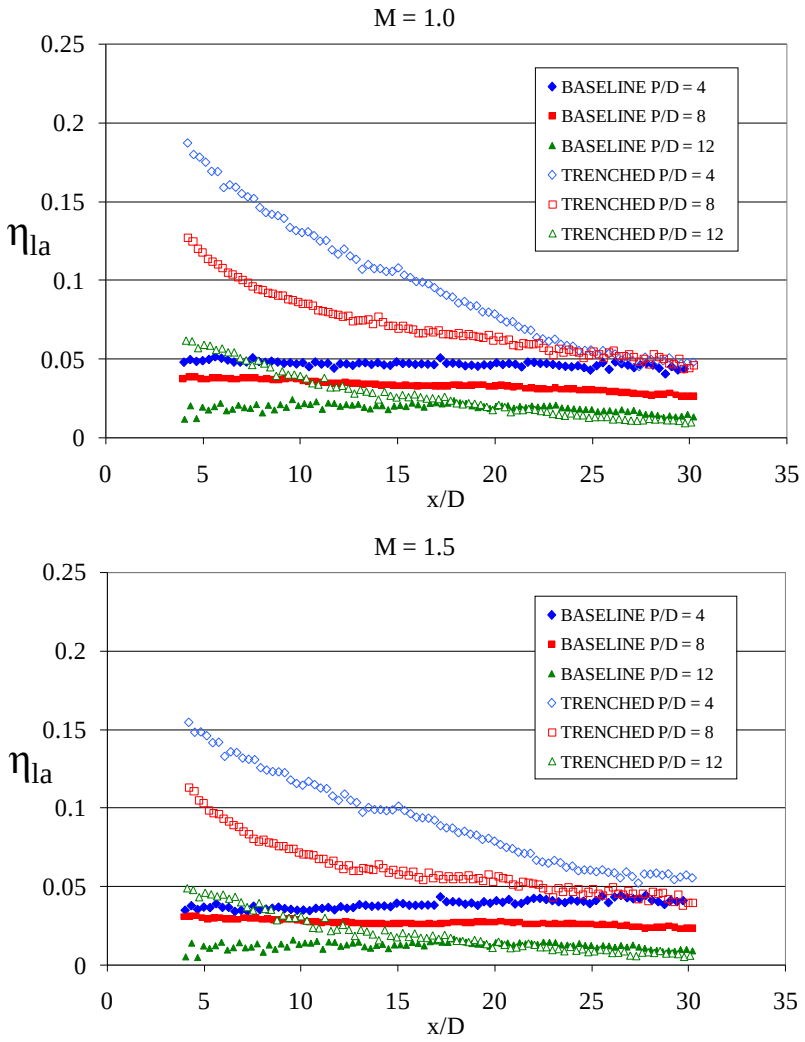

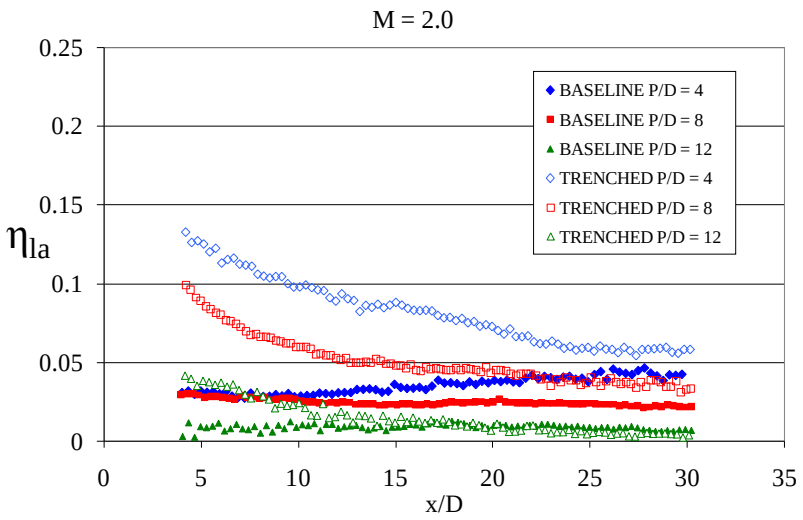

Figure 5.18 Span-wise averaged effectiveness for all cylindrical geometries at higher blowing ratios

Results for fan holes embedded in trenches are discussed next. Figure 5.19 shows the film cooling effectiveness distribution downstream of the baseline fan plates (no trench: top, and trenched: bottom).

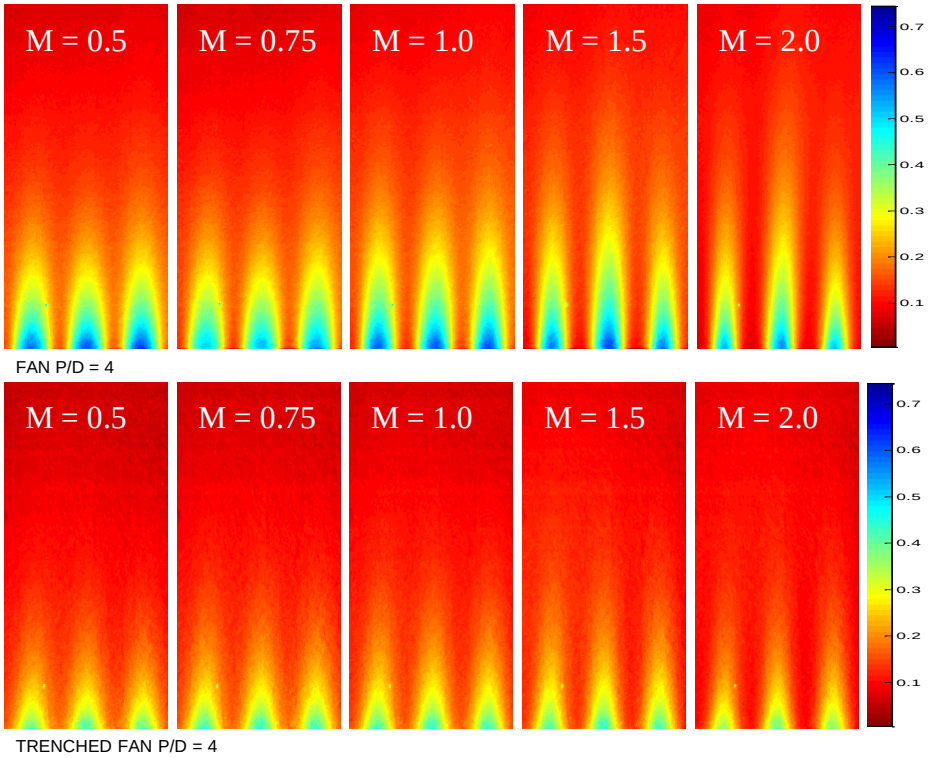

Figure 5.19 Film cooling effectiveness downstream of fan coupons

We can notice that the downstream coverage of the coolant is not as visible for the trenched fan coupon. The reason for this is that the fan geometry already diffuses the flow when it expands. Adding extra diffusion with a trench actually penalizes the flow by promoting even more mixing at the exit. This is evident in the fact that the effectiveness at the center of the trenched jets is more uniform at all blowing rates compared to the baseline fan jets. Diminished performance is a particular concern when fan holes are refurbished. The fact that the coolant flow is being diffused even more as a result of the trench at the exit should be a very critical issue for designers since the parts are not being cooled at the same levels as before, posing serious implications for the lifetime of the component.

The rest of the configurations, omitted from this work, show the same trends, only that the jets are further apart for all configurations and there are no visible benefits to trenching. Figures 5.20 and 5.21 show the spanwise-averaged film cooling effectiveness for the rest of the fan configurations, baseline and trenched. At the lower blowing ratios in Figure 5.20, we can see that the baseline PI/D-4 easily outperforms the rest of the configurations. With an added trench, the PI/D-4 fan effectiveness drops to the level of the baseline at PI/D-8. This translates to a decrease in effectiveness from 25 to 33 percent between x/D of 5 and 15.

For the higher blowing ratios, shown in Figure 5.21, there is a change in the trend as the trenched PI/D-4 performance begins to outperform that of the PI/D-8 baseline. Basically, the PI/D-8 baseline curves begin to flatten out as M increases, since the jets continue to push more flow downstream, but decay slowly. In contrast, the PI/D-4 trenched configuration suggests that some jet interaction begins to happen at the higher blowing rates since this configuration begins to outperform the PI/D-8 holes. It is possible to imagine a point after which the trench intrudes on the high momentum flow to the point that it forces it to spread and interact with the neighboring jets.

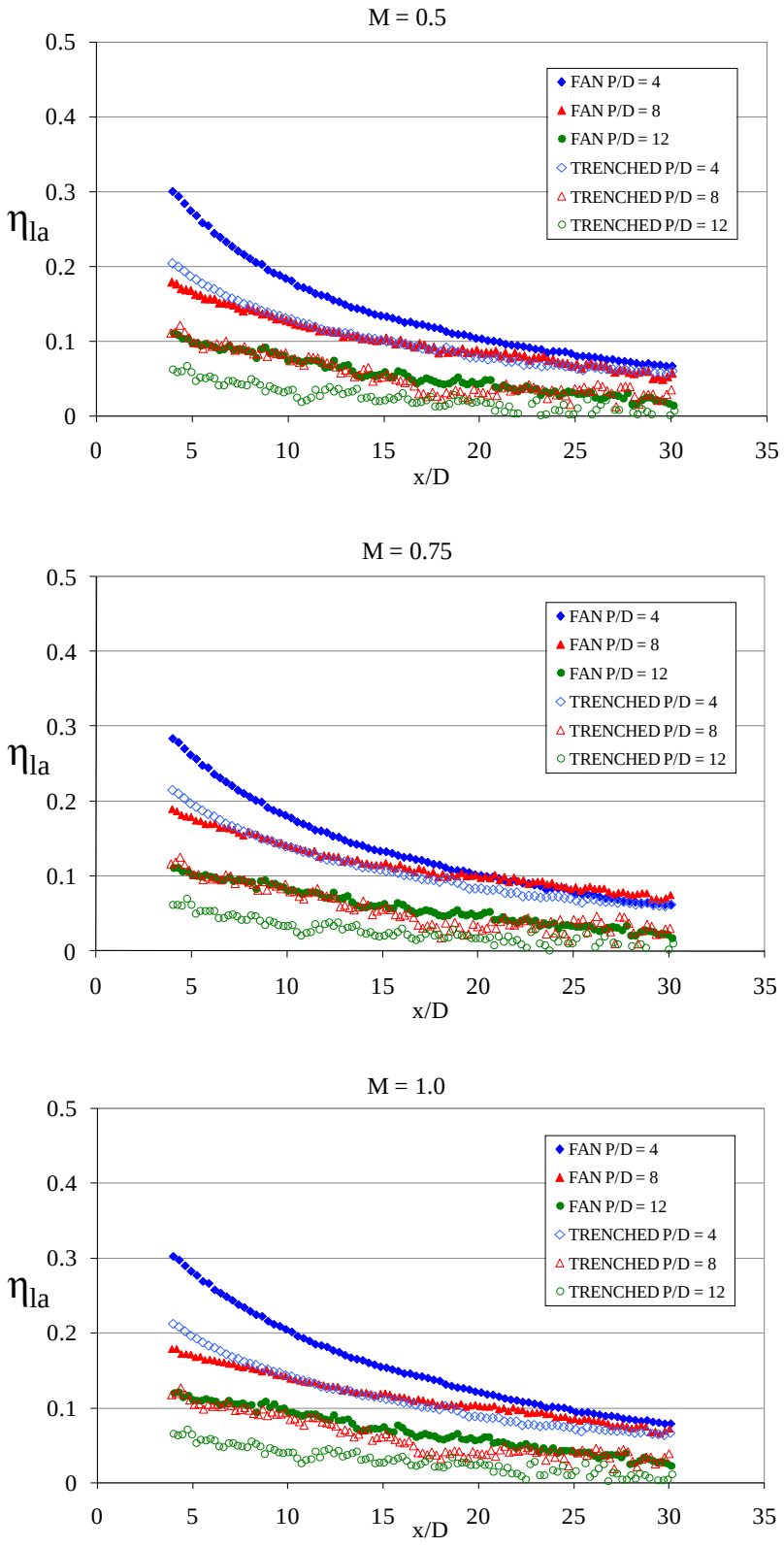

Figure 5.20 Spanwise-averaged film cooling effectiveness for fan holes at lower blowing ratios

While this effect may be present at the lower blowing rates, there is no evidence for it, or it may not be enough to overcome the penalty caused by the trench itself. However, this forced interaction at the highest blowing ratios is not as beneficial as in the case of the cylindrical holes. It is useful to know, though, the fact that placing fan holes inside a trench leads to detrimental effects on their cooling performance. Looking at Figure 5.21, at blowing ratio of 1.5, it can be said that at distances of x/D of 5, 10 and 20, there is a penalty in performance of 35%, 28% and 18%, respectively, in film cooling effectiveness for the trenched configuration PI/D-4 configuration. At a blowing ratio of 2.0, the penalty at x/D of 5 and 10 is reduced to about 25%. Even a modest reduction in performance of 15 to 20% should raise flags to turbine operators since this has implications in future maintenance schedules and estimates of cooling system performance and part life cycle.

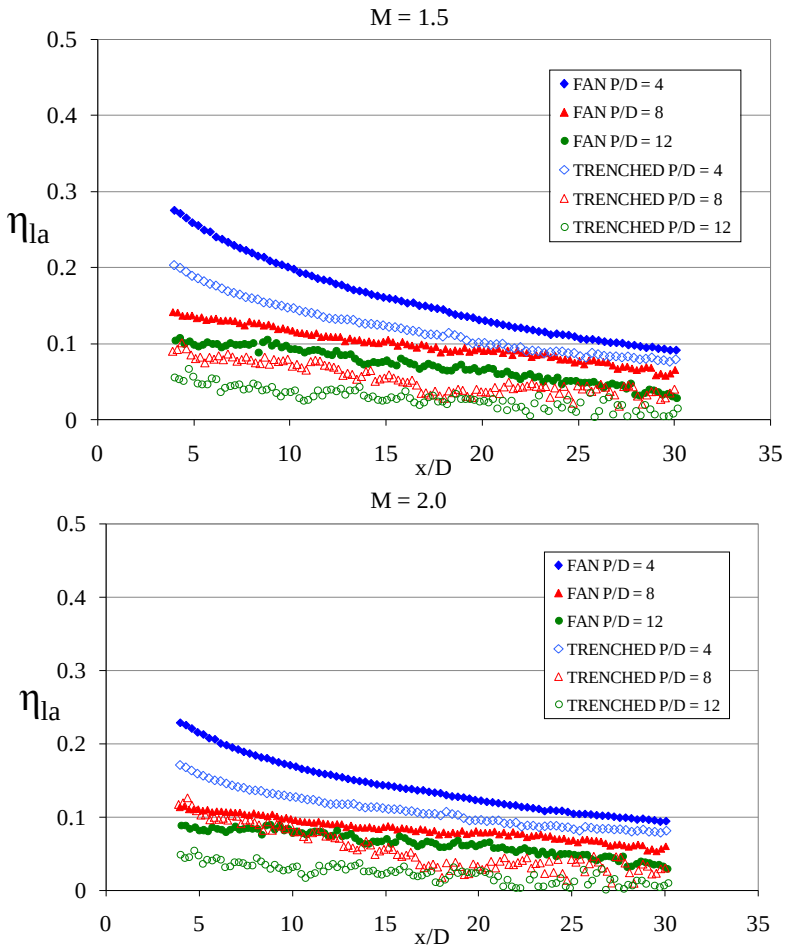

Figure 5.21 Span-wise averaged cooling effectiveness of fans at higher blowing ratios

The next part of the analysis is to all the cylindrical and trenched cylindrical plates in terms of the spatially-averaged effectiveness, shown in Figure 5.22.

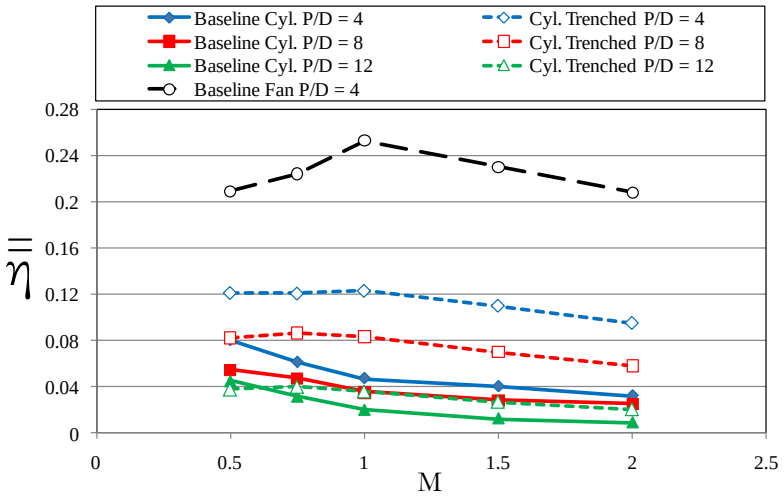

Figure 5.22 Spatially-averaged film effectiveness for all cylindrical holes

The fan data in Figure 5.22 is included as a reference to provide a sense of the magnitude of the enhancement diffusing geometry provide to the film cooling effectiveness. We can immediately see that compared to the (solid blue) 4-PI/D cylindrical baseline and the (solid red) 8-PI/D baseline, the trenched geometry (dotted lines) perform significantly better. In fact, at a blowing ratio of 1.5, when the baseline cylindrical geometry is not useful anymore because of jet detachment, the trenched cylindrical 4-PI/D holes are providing approximately 150% more protection. The trenched 8-PI/D geometry is also providing better coverage, with an increase of about 75%. It is important to point out that this means that the number of holes has been reduced by 50%, they have been embedded in a trench, and the holes' performance still increases by a significant percentage. This sort of performance enhancement is significant. Whether there is jet interaction inside the trench it is unknown. Dorrington et al, 2007 showed that almost doubling the PI/D for the trench geometry decreased performance, and that the effectiveness values observed were lower than a superposition prediction. They conjectured that it was because of lack of jet interaction. However, they did not mention anything about a comparison against a non-trenched, high PI/D cylindrical baseline, so their results in this respect are silent. However, the results shown in this

study, particularly in Figure 5.22 have the potential to be high impact. If there is a jet interaction that spreads the coolant in the space between the holes and can provide acceptable effectiveness values, then the configuration can be used as is, and lead to a 50% reduction of hole and possibly coolant. If the levels of protection are not adequate, which is possible, since a distance of 8 diameters between holes is large, then the trenching could still be used but it would have to be in a multiple-row setup, with the holes intercalated; the space in between two holes would be protected by the row upstream. Another possible solution could be to shape the trench as to encourage the flow to spread even further between the holes. The potential momentum reduction and increased coverage could translate to more than adequate protection downstream of the flow, with much less holes and coolant. These ideas will be further discussed in the conclusion and future work section.

The 12-PI/D geometry follows the performance trend, but its values are so low they are impractical. The same can be said for the 12-PI/D holes embedded in trenches. In that case, we can see that the trench increases performance slightly, but the values are still very low.

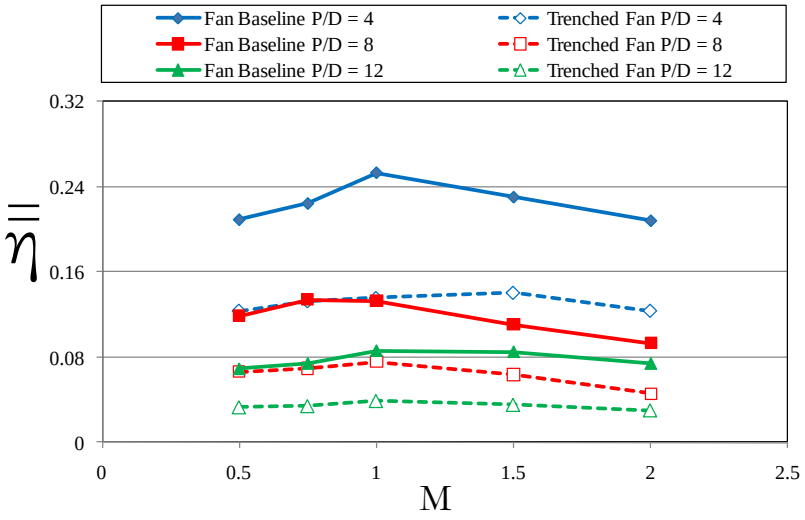

Figure 5.23 Spatially-averaged effectiveness of all fans

Focusing on Figure 5.23 we can see the results for the PI/D effect study on the fan shaped holes. We can see that there is a significant reduction in performance in film cooling effectiveness for all the

trenched fan holes. The value is roughly 50%. It does not seem to matter what the blowing ratio is, performance always decreases. This was expected, as mentioned before since the reader can imagine the flow exiting the fan holes as being diffused by the geometry, forcing it to adhere to the wall more easily. The presence of trench, in this case, disrupts the adhesion process at the exit of the holes and trips the coolant, causing additional mixing. This translates into higher non-dimensional temperature values since the coolant is ingesting the main flow, as evident in the accelerated decay of the effectiveness curves, as seen in Figure 5.20. Thus, it is safe to say that adding a trench with depth of 0.75D to a fan-shaped hole row will decrease the film cooling effectiveness by 50%. This is something that designers should look at more closely since part life estimates are based on metal temperatures and these depend on film cooling performance values. Once a hole configuration is changed because of refurbishing, and the cooling values change, the literature does not provide guidelines for new cooling performance values. This study points to a place to start. More detailed sensitivity studies need to be performed to characterize the decline in performance and to look for ways to lessen the magnitude of the degradation.

The major observations made in this study are various: 1) The performance of cylindrical cooling holes increases inside a trench, as shown in previous studies. However for a given number of cylindrical holes at PI/D-4, doubling the distance between the holes (increasing P/D to 8) and trenching them, yields the same cooling performance. This has the potential to be a viable way to economize coolant, save manufacturing costs, and maintain performance of cylindrical cooling holes. 2) The performance of fan shaped holes decreased as these were trenched. At the lower blowing ratios, the decrease was between 25 and 33%. At the highest blowing ratios, the fans showed that a decrease in cooling performance from 25% to 35% can be expected in the region from x/D from 5 to 20.

Effect of Trench Depth on Shaped Holes

For this next part of the study, the shaped hole data set was expanded to include fan holes inside trenches of varying depths. Figure 5.19, discussed earlier, shows the film cooling effectiveness

downstream of the coupons for the baseline, h/D of 0 and the deepest trench at h/D = 0.75. For all images, the x/D range shown is from 2D to 25.4D.

We can notice that the downstream coverage of the coolant is not as visible for the trenched fan coupon. The reason for this is that the fan geometry already diffuses the flow when it expands. Adding extra diffusion with a trench actually penalizes the flow by promoting even more mixing at the exit. This is evident in the fact that the effectiveness at the center of the trenched jets looks more uniform at all blowing rates compared to the fan jets; i.e. the trenched jets do not have what appears to be a cooler core at the exit, as in the baseline fan images.

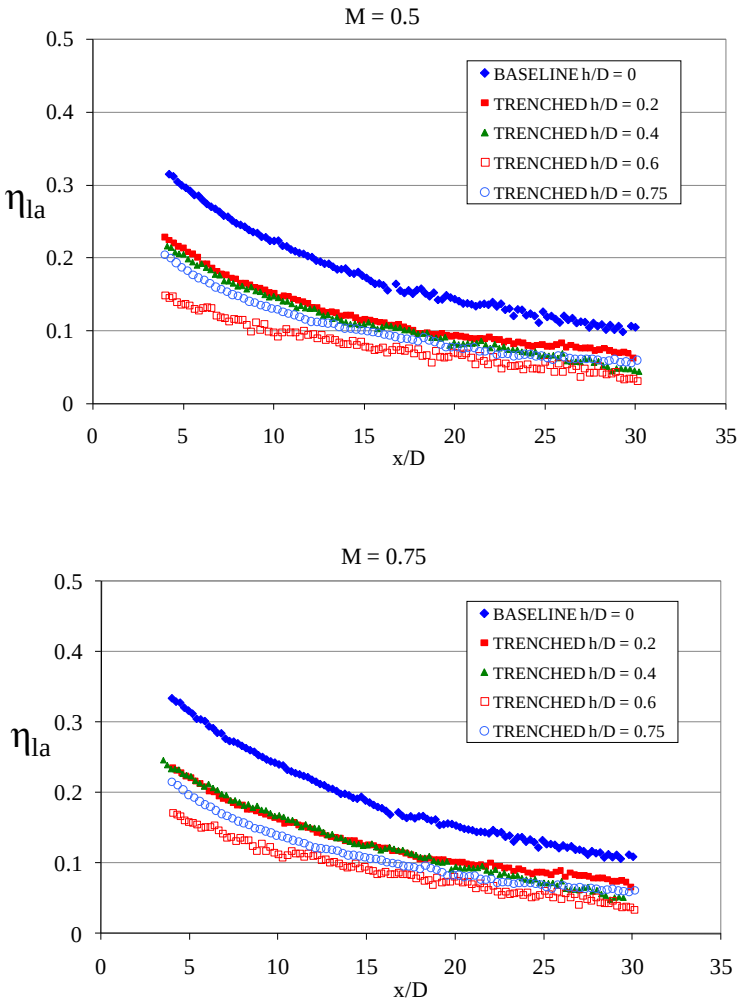

Figure 5.24 Span-wise averaged film cooling effectiveness at lower blowing ratios vs. distance x/D

Figure 5.24 shows the span-wise average effectiveness for all configurations at the lower blowing ratios. One of the salient features of both plots is that the trenched configurations show lower performance than the baseline. At a blowing ratio of 0.75, this difference decreases slightly. The curve for the h/D=0.6 configuration seems slightly lower than the rest. Although this detracts from the general trend, it may just reflect slight testing condition variations. The slope of the curve and its final values are consistent with the trends.

As the blowing ratio is increased to 1.0, the trenched curves as a group tend to go to the same value away from the baseline. This is more apparent at the highest blowing ratios, shown in Figure 5.25, in which the trenched fan curves as a group seem to collapse to the same value. In fact, at blowing ratio of 1.5, it can be said that at distances of x/D of 5, 10 and 20, there is a penalty in performance of 35%, 28% and 18%, respectively, in film cooling effectiveness for all trenched configurations. At a blowing ratio of 2.0, the penalty at x/D of 5 and 10 is reduced to about 25%. Even a modest reduction in performance of 15 to 20% should raise flags to turbine operators since this has implications in future maintenance schedules and estimates of cooling system performance.

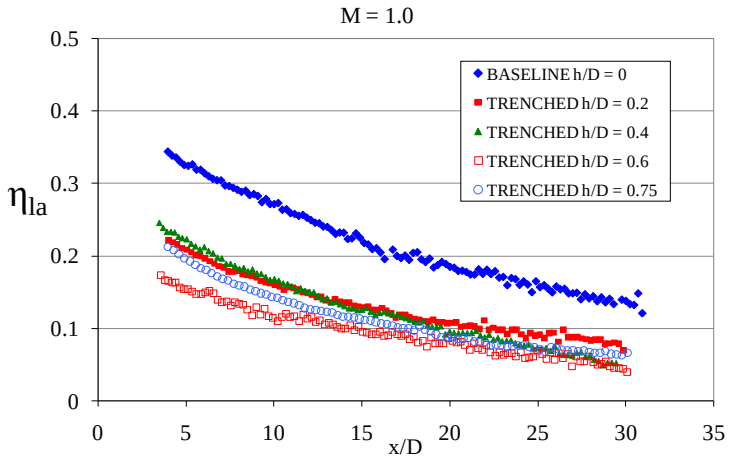

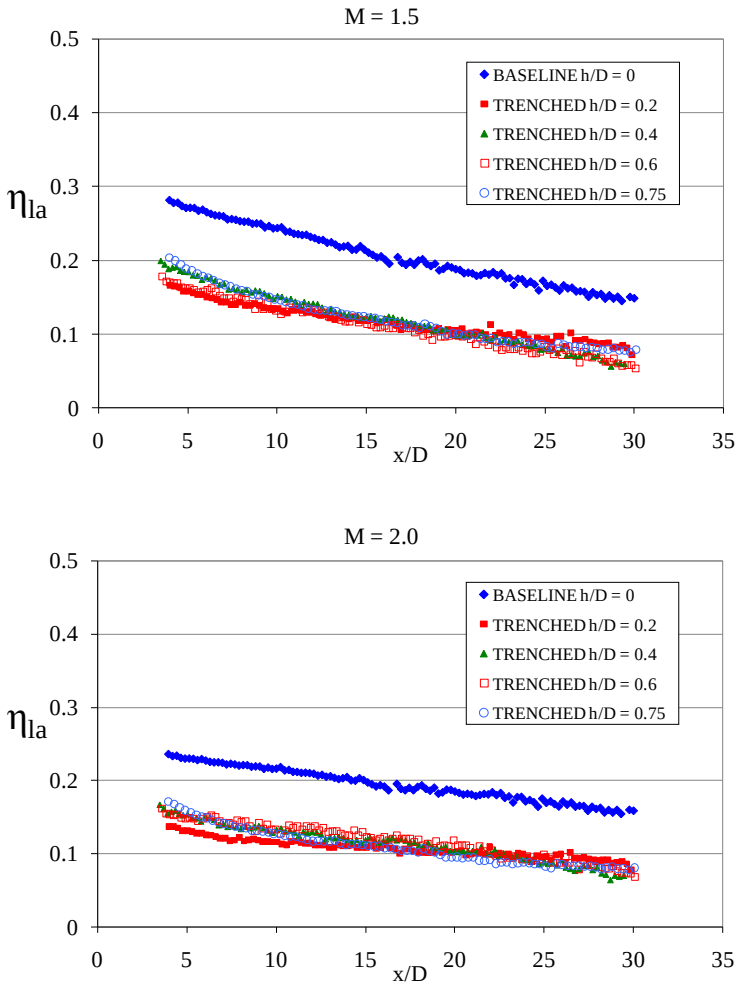

Figure 5.25 Span-wise averaged cooling effectiveness of fans at higher blowing ratios

One of the surprising results of this study is that at the lower blowing rates, there is more differentiation between the specific trench-depth curves, and that this disappears completely at the highest blowing rates. What this indicates is that there may be a way to correlate the decrease in performance at the higher blowing rates which are values at which fan holes normally operate. The focus of the investigation was the effect of trench depth, as this reflects possible changes in fan hole configurations in real engines after undergoing TBC maintenance.

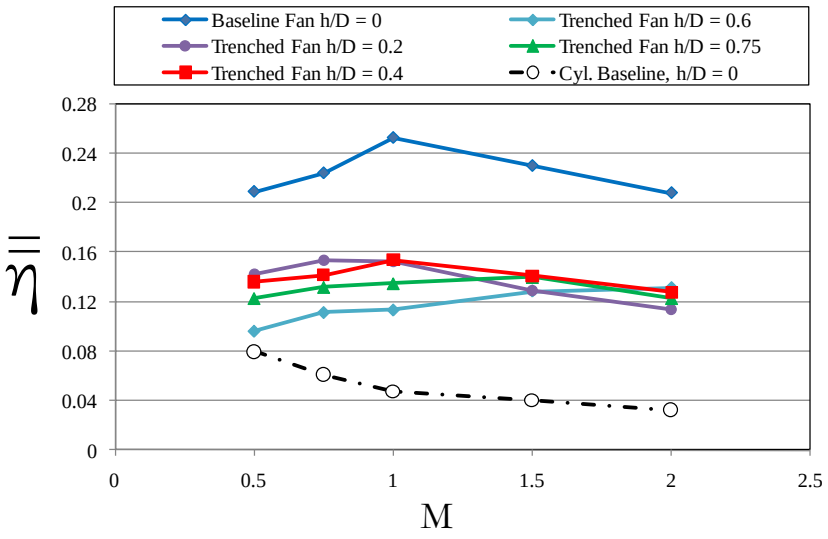

Figure 5.26 Spatially-averaged film effectiveness for all trenched shaped holes

Figure 5.26 summarizes the findings of the previous spanwise-averaged plots. It is easy to see that the baseline fan holes clearly outperform the rest of the configurations. The decrease in performance caused by the addition of a trench at best in the order of 25%; in the worst case, the decrease is about 60%. We saw that the deep trench, at h = 0.75D, decreased performance by 50% for all M. For the case of the 0.6D trench, the decrease is even more. There is not a clear explanation for this observation. The h=0.6D trench data does not fit very well with the data, but it was left for completeness. Future analysis may give hints as to the reason for the deviation.

The major observation in this study is that cooling performance is penalized. This was expected since the trench exit is an obstacle to the already diffused flow emerging from the holes. The steady decline in the effectiveness curves as a function of the distance suggests no increased jet interaction as seen in cylindrical studies, and hints at perhaps the opposite. Another observation is that the values of the film cooling effectiveness for all trenches seem to collapse to the same curve at the highest blowing ratios. Effectiveness values for fan shaped holes have been shown in previous studies to be insensitive to the highest blowing ratios; this may be similar behavior. This study also provided some general Figures for the decline of film effectiveness at the highest blowing ratios for all trenched configurations compared

to the baseline, and showed that a decrease in cooling performance from 25% to 35% can be expected in the region from x/D from 5 to 20.

Shaped Holes with Asymmetric Lateral Diffusion

Figure 5.27 shows contours of effectiveness for an x/D range of approximately 2 to 25. One of the noticeable features of the data sets in Figure 5.24 is that at the lower blowing ratios of 0.5 and 0.75, the distributions look very similar. At a blowing ratio of 1.0, we can observe that the smaller holes begin to show space between the jets, seen as "redder" areas of low effectiveness. This is, of course due to the lower coverage provided by the narrower holes and the shallow lateral diffusion angles.

Figure 5.27 shows only one jet for the 9-7-11 holes. During processing it was noticed that a couple of the jets showed less coolant than others for several plates. The possibility of debris clogging up the holes at the higher blowing rates—though unlikely—was considered and a mesh was installed that would stop debris even smaller than the inlet diameter of the holes. Other sources of error considered were irregular upstream conditions and unsteadiness of the jets. However, if the main flow conditions were so unsteady to the point of significantly skewing the coolant jets at the point of ejection, then this phenomenon would have been observed in all tests, or at least in a noticeable percentage of the tests run throughout the year. But it has not. Thus, the other possibility is the metastable state of the jets. This was actually suggested by Dr. M. Crawford in a conversation.

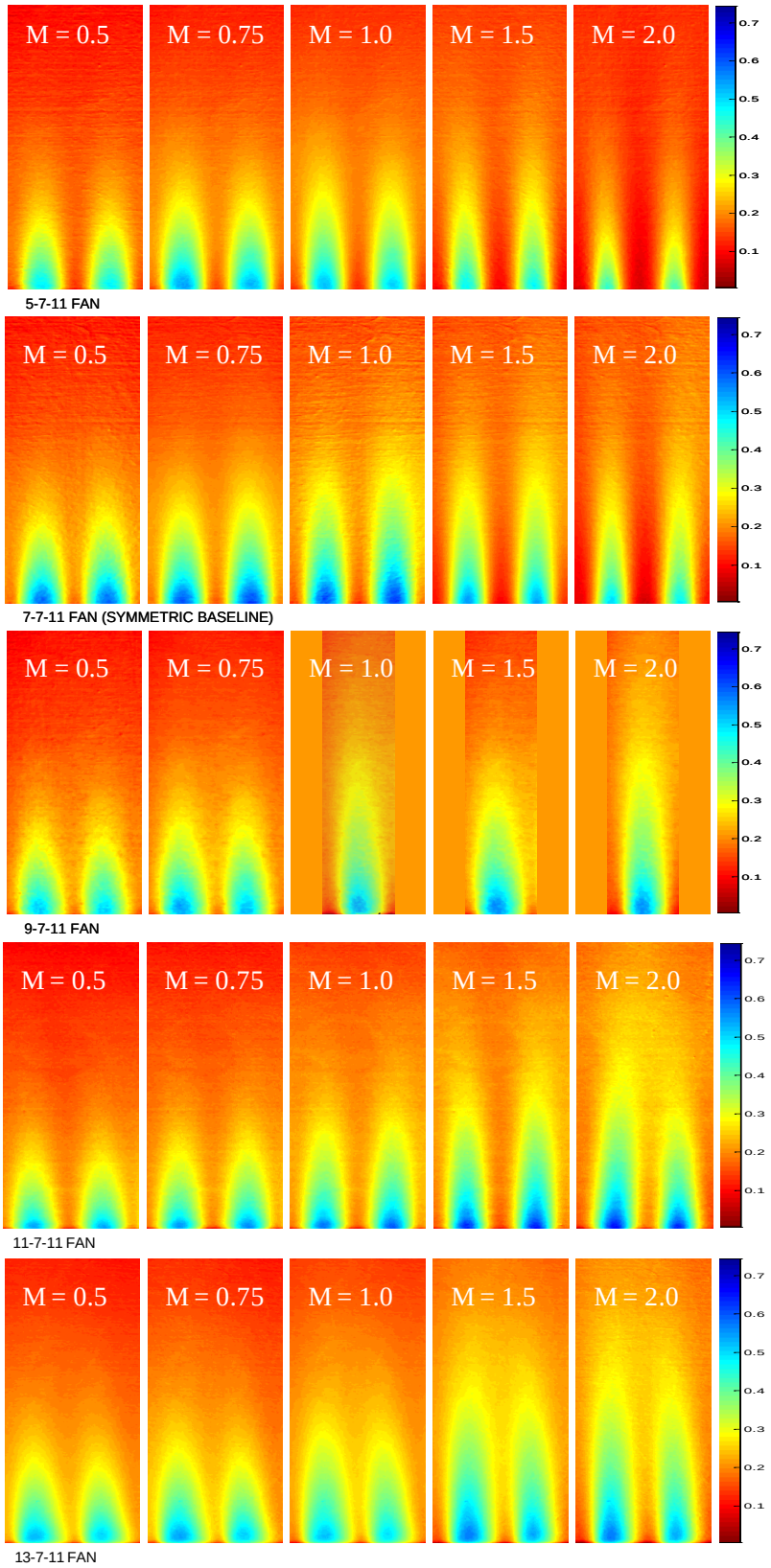

Figure 5.27 Film cooling effectiveness distribution for all coupons at all blowing ratios

He suggests that since the effect that is being studied is the increase of diffusion angle, at some point the geometry would reach a point (near 7°) in which the jets could potentially detach from the angled walls of the diffusers, leading to irregular jet patterns. The jets could be fluctuating between attachment and reattachment or be attached to one side and not the other. The fluctuating jets would not be observable with the TSP since the data collected with TSP is time-averaged. That leaves the possibility of only observing only the jets attached on one side. This is actually a plausible explanation, but more investigation needs to be done. For the 9-7-11 only one of the unaffected jets is shown and the data was reduced from one whole pitch.

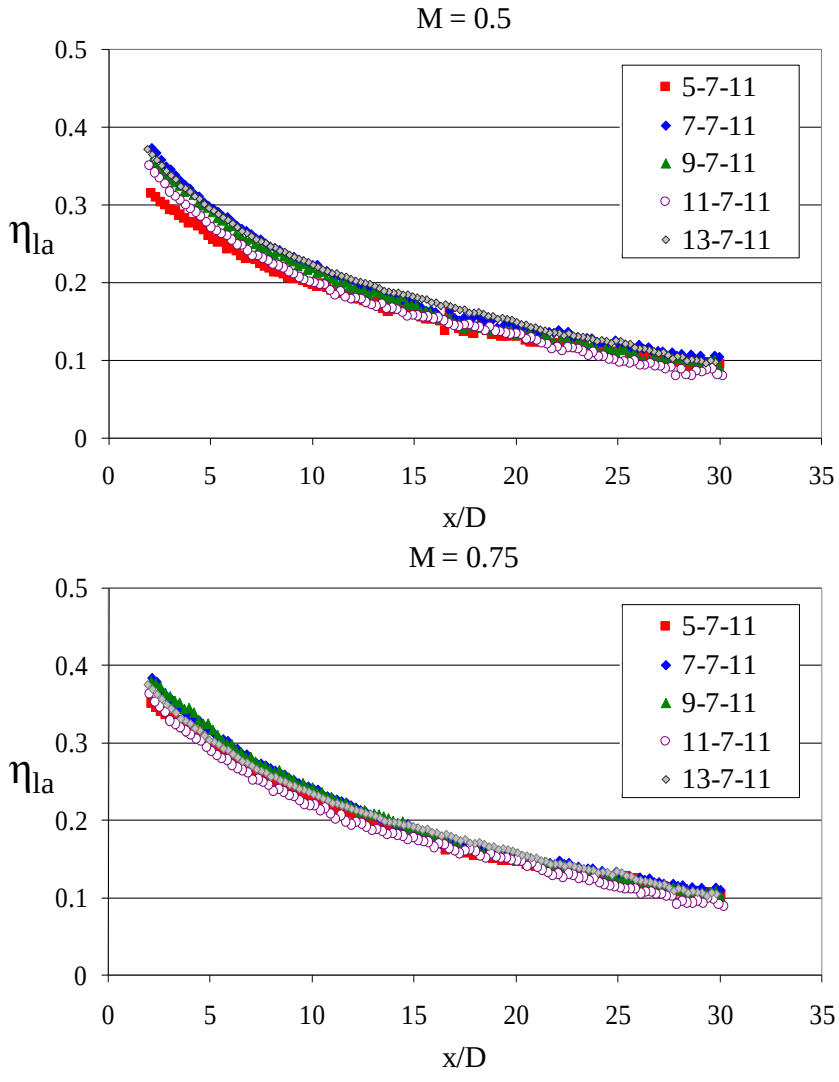

Figure 5.28 Laterally-averaged film cooling effectiveness

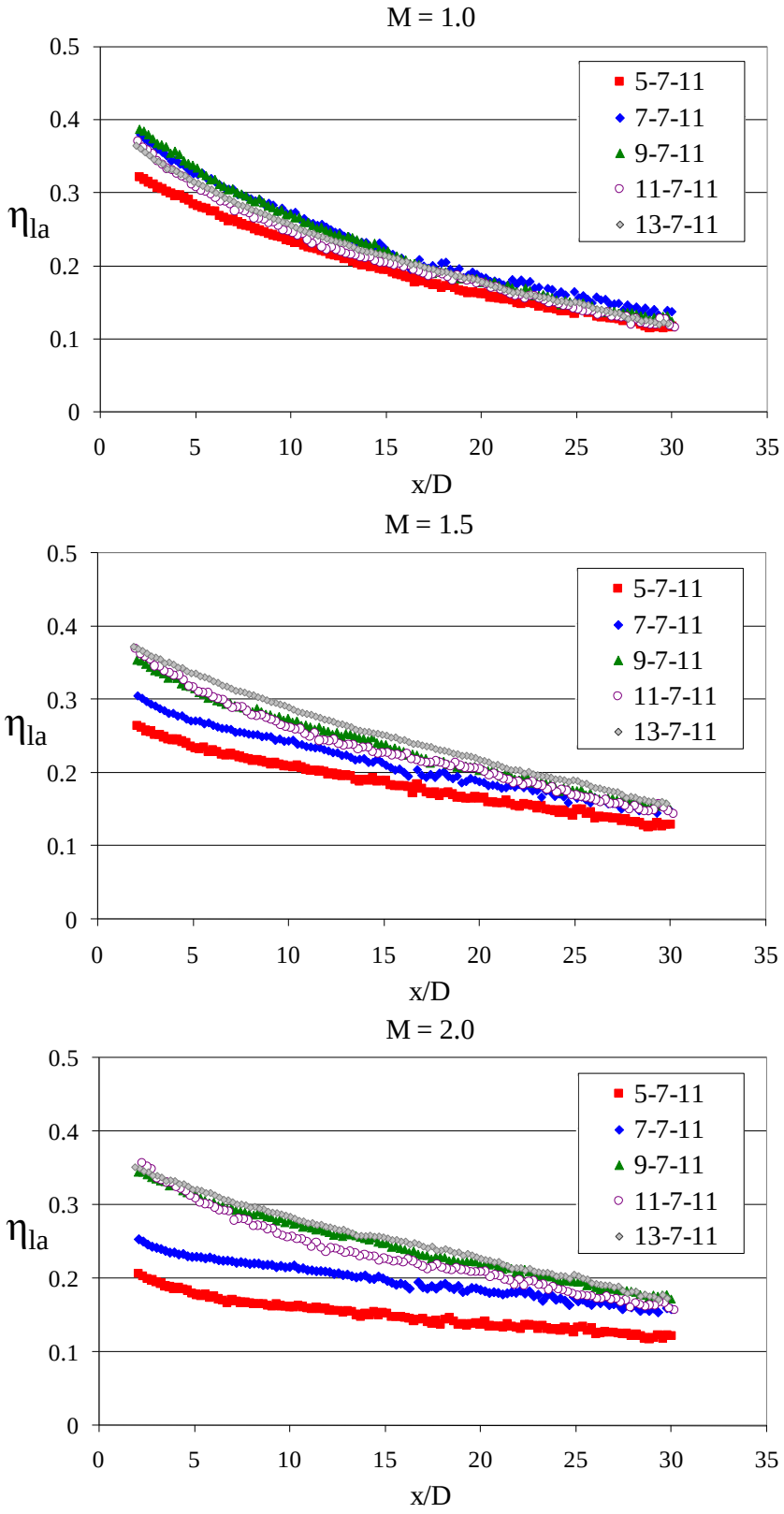

Figure 5.29 Laterally-averaged film cooling effectiveness

As the blowing ratio increases from 1.5 to 2.0, we can notice that compared to the baseline, the larger holes do show a wider coverage and less space between them, which is conducive to more interaction. This is the opposite for the narrower baseline and 5-7-11 cases. Figure 5.28 and Figure 5.29 show the span-wise averaged film cooling effectiveness for the first four blowing rates. As pointed out before, we can see that the holes behave almost identically. And while the differences become apparent at a blowing ratio of 1.0, they crystallize at a blowing ratio of 1.5. Another noticeable feature is that at the higher blowing ratios the performance of the wider holes becomes very similar.

While the overall performance of these fan plates may not be unusual in terms of the average film cooling effectiveness, a closer look at the extreme configurations yields a clue to a very promising application in shroud cooling or regions where the mainstream is turning or accelerating. We can see in Figure 5.30 three of the effectiveness distributions for the 5-7-11, the baseline and the 13-7-11 at the low, mid and high blowing rates. These Figures are shown in a high contrast format to highlight the lopsided nature of the ejected coolant. We are afforded these images because of the high definition of the data captures which is on the average close to 306 pixels per mm^2. To more easily interpret these Figures, we notice that the downstream edges begin in blue at about $\eta = 0.1$ and as we get closer to the hole exit the effectiveness increase to green ($\eta = 0.2$) and then red, and so on. We can see in particular that at the higher blowing rates the jets for the 13-7-11 case appear to be "leaning." This might mean that while the right half of the hole is diffusing the coolant as expected due to the larger area, the jet is somehow able to stay together longer downstream. While the diffusing effect increases the effectiveness in the near hole region ($x/D < 10$), the more intact part of the jet, provided by the narrower side, maintains a higher effectiveness downstream.

The narrower 7-7-11 configuration does not enjoy the benefit of such diffusion and at the higher M shows darker regions of coolant absence leading to lower performance. This is behavior approximating that of forward-diffused cylindrical holes. We could, with more study, envision the highly asymmetrical

holes for use in turning flow applications or in regions that normally “smear” diffused coolant due to hostile conditions.

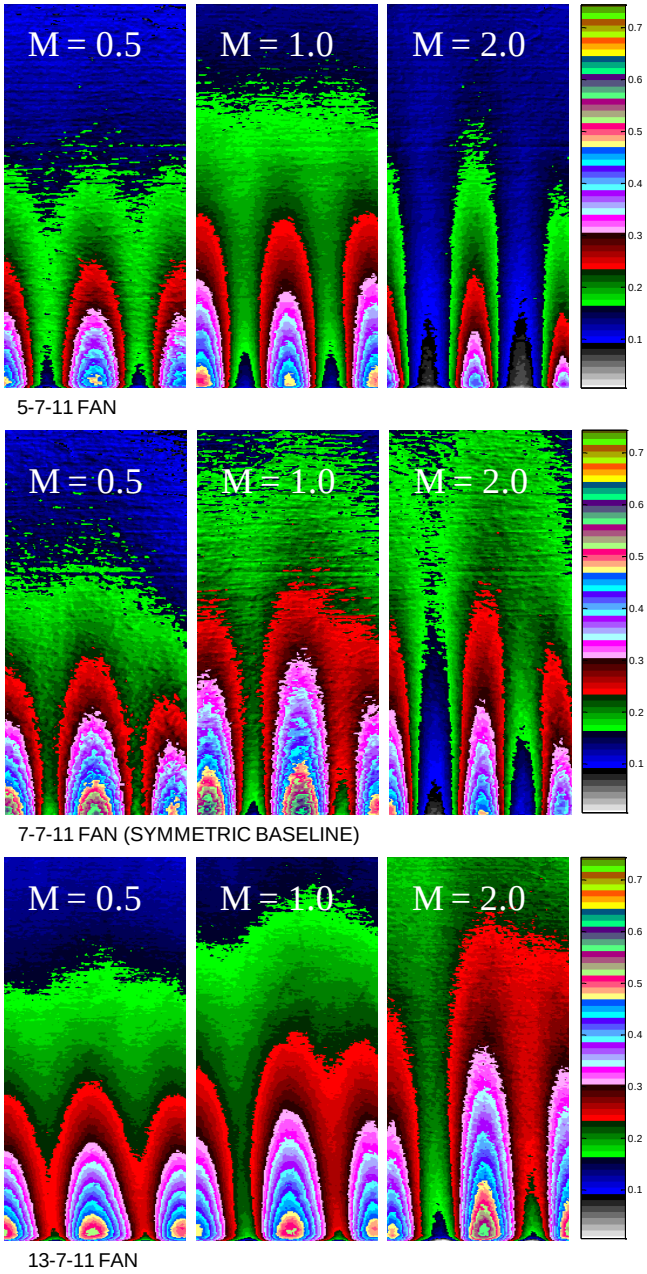

Figure 5.30 High contrast effectiveness plots

CHAPTER SIX: CONCLUSION

The studies conducted show that the temperature sensitive paint technique can be used to study the performance of film cooling holes for various geometries. The studies also show the film cooling performance of novel geometries and explain why, in some cases, such new arrangements are desirable, and in others, how they can hurt performance. The studies also point in the direction of further investigations in order to advance cooling technology to more effective applications and reduced coolant consumption, the main goal of turbine cooling research.

The review of current literature reveals that very few investigations have been done on film cooling effectiveness for uniformly diffusing conical holes. To extend our understanding of effectiveness of conical holes, the present study investigated the effect of increasing diffusion angle, as well as the effect of adding a cylindrical entrance length to a conical hole. The measurements were made in the form of film cooling effectiveness and the technique used was temperature sensitive paint. Eight different conical geometries were tested in the form of coupons with rows of holes. The geometry of the holes changed from pure cylindrical holes, a 0° cylindrical baseline, to an 8° pure cone. The test coupons were tested in a closed loop wind tunnel at blowing ratios varying from 0.5 to 1.5, and the coolant employed was nitrogen gas. Results indicate that the larger conical holes do, in fact offer appropriate protection and that the holes with the higher expansion angles perform similar to a fan-shaped baseline, even at the higher blower ratios. The study was also extended to two other plates in which the conical hole was preceded by a cylindrical entry length. The performance of the conical holes improves as a result of the entry length and this is seen at the higher blowing ratios in the form of a delay in the onset of jet detachment. The results of this study show that conical expanding holes are a viable geometry and that their manufacturing can be made easier with a cylindrical entry length, which in turn will improve the performance of these holes.

Trench cooling consists of having film cooling holes embedded inside a gap, commonly called a trench. The coolant hits the downstream trench wall which forces it to spread laterally, resulting in more

even film coverage downstream than that of regular holes flush with the surface. Recent literature has focused on the effect that trenching has on cylindrical cooling holes only. While the results indicate that trenches are an exciting, promising new geometry derived from the refurbishing process of thermal barrier ceramic coatings, not all the parameters affecting film cooling have been investigated relating to trenched holes. For example, nothing has been said about how far apart holes inside the trench will need to be placed for them to stop interacting. Nothing has been said about shaped holes inside a trench. This dissertation explores the extent to which trenching is useful by expanding the PI/D from 4 to 12 for rows of round and fan holes. In addition the effect that trenching has on fan-shaped holes is studied by systematically increasing the trench depth. Values of local, laterally-averaged and spatially-averaged film cooling effectiveness are reported. It is found that placing the cylinders inside the trench and doubling the distance between the holes provides better performance than the cylindrical, non-trenched baseline, especially at the higher blowing ratios, $M > 1.0$. At these higher coolant flow rates, the regular cylindrical jets show detachment, while those in the trench do not. They, in fact perform very well. The importance of this finding implies that the number of holes, and coolant, can be cut in half while improving performance. The trenched cylindrical holes did not, however, perform like the fan shaped holes. It was also found that the performance of fan-shaped holes inside trenches is actually diminished by the presence of the trench. It is obvious that since the fan diffuses the flow, reducing the momentum of the coolant, the addition of the trench further slows the flow. This, in turn, leads to the quicker ingestion of the main flow by the jets resulting in lower effectiveness.

The major observations in this study are various: 1) The performance of cylindrical cooling holes increases inside a trench, as shown in previous studies. However for a given number of cylindrical holes at P/D-4, doubling the distance between the holes (increasing P/D to 8) and trenching them, yields the same cooling performance. This has the potential to be a viable way to economize coolant, save manufacturing time, and maintain performance of cylindrical cooling holes. 2) The performance of fan shaped holes decrease as these were trenched. At the lower blowing ratios, the decrease was between 25

and 33%. At the highest blowing ratios, the fans showed that a decrease in cooling performance from 25% to 35% can be expected in the region from x/D from 5 to 20.

The next part of the study consisted of systematically increasing the depth of the trench for the fan-shaped holes. The purpose of this part of the study was to quantify the effect of the trench on the film cooling effectiveness. It was found that the presence of the trench significantly reduces the film effectiveness, especially for the deeper cases. At the higher blowing ratios, the overall performance of the fans goes to the same values. The major observation in this study is that cooling performance is penalized. This was expected since the trench exit is an obstacle to the already diffused flow emerging from the holes. The steady decline in the effectiveness curves as a function of the distance suggests no increased jet interaction as seen in cylindrical studies, and hints at perhaps the opposite. Another observation is that the values of the film cooling effectiveness for all trenches seem to collapse to the same curve at the highest blowing ratios. Effectiveness values for fan shaped holes have been shown in previous studies to be insensitive to the highest blowing ratios; this may be similar behavior. This study also provided some general Figures for the decline of film effectiveness at the highest blowing ratios for all trenched configurations compared to the baseline, and showed that a decrease in cooling performance from 25% to 35% can be expected in the region from x/D from 5 to 20.

A recent study suggests that having a compound angle could reduce the protective effect of the film due to the elevated interaction between the non-coflowing coolant jet and the mainstream. Although it has been suggested that a non-symmetric lateral diffusion could mitigate the ill effects of having a compound angle, little has been understood on the effect this non-symmetry has on film cooling effectiveness. The last part of this study investigated the effect of non-symmetric lateral diffusion on film cooling effectiveness by systematically varying one side of a fan-shaped hole. For this part of the study, one of the lateral angles of diffusion of a fan-shaped hole was changed from 5° to 13°, while the other side was kept at 7°. It was found that a lower angle of diffusion hurts performance, while a larger diffusion angle improves it. We have seen that as the symmetry of a jet is disrupted, the film cooling

effectiveness is indeed affected, in particular at the higher blowing rates. Jets that are highly asymmetric with larger diffusion angles enjoy sustained performance at the higher blowing rates, while narrower diffusion angle holes see their performance decline as the main stream enters the space between holes. At the lower blowing rates, the performance of all configurations is nearly identical. However, the more significant result was that the jet seemed to be slightly turning. This suggests that the jets actually have two regions: one region with reduced momentum, ideal for protecting a large area downstream of the point of injection; and another region with more integrity which could withstand more aggressive main flow conditions.

The author has theorized that a balance between high diffusion of the coolant on one side of the hole and higher jet integrity on the other could be responsible for the sustained performance of the 13-7-11 configuration over the range of blowing rates. Such ability could be used for situations in which the main stream is highly hostile, even for common fan shaped cooling holes. The unexpected behavior of several of the wider jets at the higher blowing ratios, in which a few showed less coolant than others for no apparent reason, will be further explored. Such occurrences were not observed for the narrower holes, even though the testing conditions were identical for all cases. A further study should be conducted for this geometry at compound angles with the main flow to test this theory.

APPENDIX: MEASUREMENT UNCERTAINTY AND REPEATABILITY

The uncertainties reported were estimated taking into consideration the approaches described by Kline and McClintock (1953), Moffat (1988), Holman (1994) and Wheeler and Ganji (2004). The formulas used to describe the process, including most of the nomenclature, are taken from Wheeler and Ganji (2004).

The general idea is to take a result, R, which is a function of n measurable variables $x_1, \ldots, x_n$ and quantify the effect that small changes in x have on small changes on R. That is, how the different δx's affect δR. Where,

$$R = f(x_1, x_2, \ldots, x_n)$$

A series expansion of the above relation leads to the expression:

$$\delta R = \delta x_1 \frac{\partial R}{\partial x_1} + \delta x_2 \frac{\partial R}{\partial x_2} + \cdots + \delta x_n \frac{\partial R}{\partial x_n} = \sum_{i=1}^{n} \delta x_i \frac{\partial R}{\partial x_i}$$

Since R is a calculated result based on x_i's, the value of δx_i's can be substituted by the uncertainty in the variables—stated as U_{xi}. Then, δR is rewritten as U_R. Since the values of ∂R/∂can be positive or negative, to measure the total uncertainty of a calculated quantity, the total must be forced to become positive. Taking the absolute would be a good way to accomplish this, but it opens the possibility of numbers cancelling out and yielding zero uncertainty. Thus, the accepted method of doing so is by taking the root of the sum of the squares, yielding

$$U_R = \sqrt{\sum_{i=1}^{n} \left(U_{xi} \frac{\partial R}{\partial x_i} \right)}$$

The restrictions on this expression, for it to be valid, are that the confidence level in all x_i's uncertainties be the same, and that the measured variables be independent of each other.

In our case, taking place of R is the film cooling effectiveness defined as:

$$\eta = \frac{T_{rec} - T_{aw}}{T_{rec} - T_c}$$

The effectiveness as defined as a non-dimensional temperature difference is used to find the derivatives in the uncertainty equation:

$$U_\eta = \sqrt{\left(\frac{\partial \eta}{\partial T_c} U_{Tc}\right)^2 + \left(\frac{\partial \eta}{\partial T_{rec}} U_{Trec}\right)^2 + \left(\frac{\partial \eta}{\partial T_{aw}} U_{Taw}\right)^2}$$

Where,

$$\frac{\partial \eta}{\partial T_{aw}} = \frac{1}{T_c - T_{rec}}$$

$$\frac{\partial \eta}{\partial T_{rec}} = \frac{T_{rec} - T_c}{(T_{rec} - T_c)^2}$$

and

$$\frac{\partial \eta}{\partial T_c} = \frac{T_{rec} - T_{aw}}{(T_{rec} - T_c)^2}$$

In this case, U_{Trec} and U_{Taw}, corresponding to the uncertainties in the recovery and adiabatic wall temperatures are equal since both are obtained with TSP, calibrated with thermocouples. Their value is ±0.8ºC, as obtained by Liu, 2006.

U_{Tc} is ± 0.25 ºC, which is the uncertainty in the coolant temperature, as measured with the plenum thermocouple set up. The bias error for these thermocouples was ± 0.25 °C, provided by Omega®. In order to obtain the precision error value, a set of tests was taken in which repeated measurements with the thermocouples were taken with the help of a thermocouple calibration box. The precision uncertainty was then determined to be ±0.05 °C.

Figure A.1 shows a sample of the effectiveness calculations as performed on a spreadsheet. Each row of the spreadsheet represents data from one pixel row of temperature data. The derivatives are calculated numerically between two points, and the U_η formula is carried out at every row, as well.

Unc. For M = 0.5						see plot below		
dn/dTrec	dn/dTaw	dn/dTc	0.8*dn/dTrec^2	0.8dn/dTaw^2	0.25*dn/dTaw^2	U	n+U	n-U
0.01214461	-0.0129917	0.00084711	9.43945E-05	0.000108022	4.48501E-08	0.014228902	0.079433048	0.05097524
0.01214679	-0.0129848	0.000838	9.44285E-05	0.000107907	4.38902E-08	0.01422601	0.078762998	0.05031098
0.01215805	-0.0129847	0.00082664	9.46036E-05	0.000107905	4.27083E-08	0.014232063	0.077894679	0.04943055
0.01214098	-0.012972	0.00083098	9.43381E-05	0.000107694	4.31575E-08	0.014215311	0.078274702	0.04984408
0.01214102	-0.0129689	0.00082784	9.43388E-05	0.000107642	4.28322E-08	0.014213515	0.078046227	0.0496192
0.01212898	-0.0129626	0.00083361	9.41518E-05	0.000107538	4.34313E-08	0.014203293	0.078511979	0.05010539
0.01213852	-0.0129614	0.00082287	9.43E-05	0.000107519	4.23196E-08	0.014207775	0.077693975	0.04927843
0.01214552	-0.0129647	0.00081913	9.44088E-05	0.000107573	4.19361E-08	0.014213491	0.077395432	0.04896845
0.01217061	-0.0129746	0.00080401	9.47993E-05	0.000107738	4.04023E-08	0.014232986	0.076201108	0.04773514
0.01217868	-0.0129851	0.00080644	9.4925E-05	0.000107913	4.0647E-08	0.014243532	0.076348784	0.04786172
0.01219581	-0.0129978	0.00080203	9.51921E-05	0.000108124	4.02029E-08	0.014260304	0.075964918	0.04744431
0.01219331	-0.0129963	0.00080302	9.51531E-05	0.000108099	4.03029E-08	0.014258063	0.076046513	0.04753039
0.01219872	-0.0130044	0.00080564	9.52376E-05	0.000108233	4.05659E-08	0.014265717	0.076217177	0.04768574
0.01219624	-0.0130066	0.0008104	9.51988E-05	0.000108271	4.10473E-08	0.014265708	0.076572722	0.04804131
0.01219615	-0.0130076	0.00081144	9.51975E-05	0.000108286	4.11518E-08	0.014266218	0.076648012	0.04811558
0.01219601	-0.0130063	0.00081026	9.51953E-05	0.000108264	4.10323E-08	0.014265367	0.076562795	0.04803206
0.01218302	-0.0129959	0.00081288	9.49927E-05	0.000108092	4.12989E-08	0.014252224	0.076801527	0.04829708
0.01217488	-0.0129868	0.00081193	9.48657E-05	0.000107941	4.12022E-08	0.014242455	0.07676226	0.04827735
0.01216051	-0.0129808	0.00082034	9.46419E-05	0.000107841	4.20595E-08	0.014231141	0.077427077	0.04896479
0.01214703	-0.0129677	0.00082072	9.44322E-05	0.000107624	4.20985E-08	0.014216127	0.077505215	0.04907296
0.01215525	-0.012973	0.00081778	9.456E-05	0.000107712	4.17982E-08	0.014223693	0.077260939	0.04881355
0.01216393	-0.0129753	0.00081139	9.46952E-05	0.00010775	4.1147E-08	0.014229757	0.076763006	0.04830349

Figure A.1 Sample uncertainty calculation for a DA0 at M = 0.5

The values of U_η are evaluated at every point on the η_{la} curve, the derivatives are calculated between points and the temperature uncertainties are multiplied in leading to the uncertainty band shown in Figure A.2.

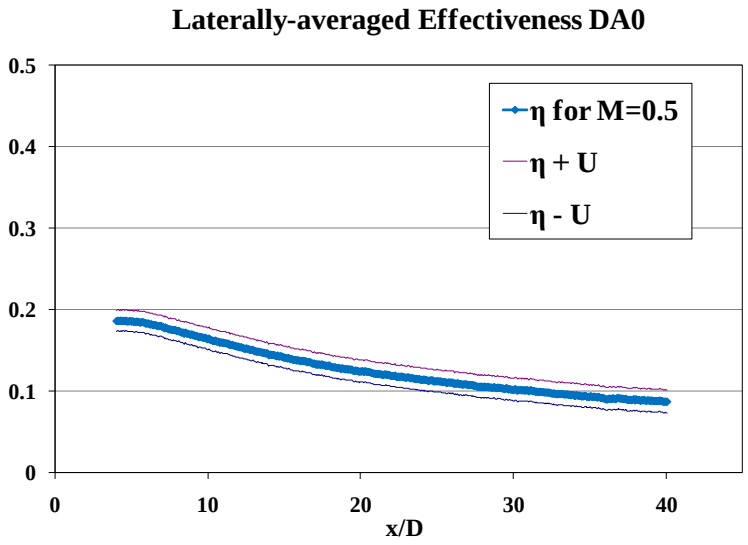

Figure A.2 Baseline effectiveness with uncertainty bands

The thickness of the error band is pretty much constant. For an effectiveness value of 0.1, the estimated error is then ±0.0139, or 13.9%. For an effectiveness value of 0.2, the error decreases to ±0.013, or 6.96%. For higher values of effectiveness, the percent error is even lower.

Part of the reliability of data is the ability to reproduce it. The experiments for this study were conducted over a period of approximately 15 months. During that time, there were opportunities to repeat several tests, and choose the results for which the data yielded seemed to have better resolution, or to have a longer range. Such is the case presented in Figure A.3, in which the test labeled Test 1, showed results within acceptable uncertainty, but there had been questions about the cleanliness of the data, as well as the extent of the range over which it was presented. Thus, the test was repeated months later, over a longer stretch of TSP for the current study. Two weeks later, the test was repeated again and the data is shown for a blowing ratio of 0.75. For that case, a completely new layer of TSP was used, and the results were identical.

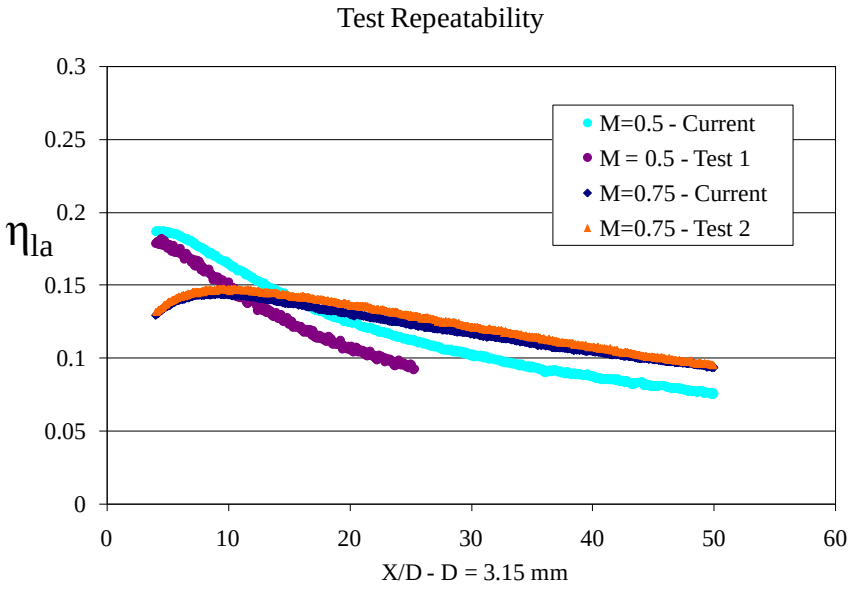

Figure A.3 Data from current study vs. repeats and older tests

For a given set of data, multiplying the maximum x/D by the diameter of the hole yields the maximum distance downstream of the exit; the shorter the value, the older the test. When observing the plots in the next section, the age of the tests does not seem to affect the trends, only the range.

LIST OF REFERENCES

Abdel-Messeh, W., Tibbott, I. and Subhash Arora, 1998, Cooling Passages for Airfoil Leading Edge, US patent number 5,779,437.

Ames, F. E., 1997, "The Influence of Large-Scale High-Intensity Turbulence on Vane Heat Transfer," ASME Journal of Turbomachinery, 119, pp. 23–30.

_____, 1998, “Aspects of Vane Film Cooling with High Turbulence: Part II - Adiabatic Effectiveness,” ASME Journal of Turbomachinery, Vol. 120, pg. 777.

Baldauf, S., Scheurlen, M., Schulz, A., and Wittig, S., 1997, ‘‘An Overall Correlation of Film Cooling Effectiveness From One Row of Holes,’’ ASME Paper 97-GT-46.

_____, 2002, “Correlation of Film-Cooling Effectiveness from Thermographic Measurements at Enginelike Conditions,” ASME Journal of Turbomachinery, 124, pp. 686–698.

Bell, C.M., Hamakawa, H., Ligrani, P.M. (2000), "Film cooling from shaped holes", *Journal of Heat Transfer*, Vol. 122 pp.224-32.

Bons, J. P., MacArthur, C. S., and Rivir, R. B., 1996, "The Effect of High Free-Stream Turbulence on Film Cooling Effectiveness," ASME J. Turbomach., 118, pp. 814–825.

Burd, S. W., Kaszeta, R. W., and Simon, T. W., 1996, "Measurements in Film Cooling Flows: Hole L/D and Turbulence Intensity Effects," ASME Paper No. 96–WA/HT–7.

Bunker R. S., 2002, “Film Cooling Effectiveness due to Discrete Holes Within a Transverse Surface Slot” Paper No. GT-2002-30178, IGTI Turbo Expo, Amsterdam, Netherlands.

Bunker, R.S., 2001, “A Method for Improving the Cooling Effectiveness of a Gaseous Coolant Stream”, US Patent 6,234,755.

_____, 2005, “A Review of Shaped Holes Turbine Film Cooling Technology”, ASME J. Heat Transfer, 127, pp. 441–453.

Bunker, R. S., Bailey, J. C., Lee, C-P., and Nesim Abuaf, 2001, Method of Improving the Cooling Effectiveness of a Gaseous Coolant Stream, and Related Articles of Manufacture, US Patent number 6,234,755 B1.

Çengel, Y. A. and M. Boles, *Thermodynamics: An Engineering Approach*, 6th ed. New York, 2008.

Clark, D. and Phillpot, S. R., 2005, "Thermal Barrier Coating Materials", Materials Today.

Crawford, Michael, 2009, Private Communication.

Cho, H. H., Rhee, D. H. and Kim, B. G., 1999, "Film Cooling Effectiveness and Heat/Mass Transfer Coefficient Measurement around a Conical-Shaped Hole with a Compound Angle Injection," the 44th ASME Gas Turbine and Aeroengine Technical Congress, Exposition and Users Symposium, June, Indianapolis, USA, 99-GT-038.

Dittmar, J., Schulz, A., Wittig, S., 2003, "Assessment of Various Film-Cooling Configurations Including Shaped and Compund Angle Holes Based on Large-Scale Experiments", ASME J. Turbomachinery., 125, pp. 57–64.

Dorrington, J.R. and Bogard, D.G., 2007, "Film Effectiveness Performance for Coolant Holes Embedded inVarious Shallow Trench and Crater Depressions", ASME paper GT-2007-27992.

Eriksen, V. L., and Goldstein, R. J., 1974, "Heat Transfer and Film Cooling Following Injection Through Inclined Circular Tubes", ASME J. Heat Transfer, 96, pp. 239–245.

Foster, N. W., and Lampard, D., 1980, "The Flow and Film Cooling Effectiveness Following Injection Through a Row of Holes", ASME J. Eng. Power, 102, pp. 584–588.

Fric, T. F and A. Roshko, "Vortical structure in the wake of a transverse jet," J. Fluid Mech. 279, 1 (1994).

Fric, T. F. and Robert P. Campbell, Method for Improving the Cooling Effectiveness of a Gaseous Coolant Stream which Flows through a Substrate, and Related Articles of Manufacture, US Patent number 6,383,602.

Goldstein, R. J., Eckert, E. R. G. and Ramsey, J. W., 1968. "Film Cooling with Injection Through Holes: Adiabatic Wall Temperatures Downstream of a Circular Hole," ASME Paper 68–GT–19.

Goldstein, R.J. 1971 Film Cooling. In *Advances in Heat Transfer* (edited by T.F. Irvine, Jr. and J.P. Hartnett), Vol. 7, 321-379, Academic Press, New York.

Goldstein, R. J., and Taylor, J. R., 1982, "Mass Transfer in the Neighborhood of Jets Entering Crossflow," ASME J. Heat Transfer, 104, pp. 715–721.

Gritsch, M., Colban, W., Schär, H. and Döbbeling, K., 2005. "Effect of Hole Geometry on the Thermal Performance of Fan-Shaped Film Cooling Holes," Transactions of the ASME, 127, pp. 718–725.

Gritsch, M., Schulz, A. and Wittig, S., 1998, "Adiabatic wall Effectiveness Measurements of Film-Cooling Holes with expanded Exits", ASME J. Turbomachinery., 120, pp. 549–556.

_____, 1998, "Discharge Coefficient Measurements of Film-Cooling Holes with Expanded Exits," ASME Journal of Turbomachinery, 120, pp. 557–563.

Haas, W., Rodi, W., and Schönung, B., 1991, "The Influence of Density Difference Between Hot and Coolant Gas on Film Cooling by a Row of Holes: Predictions and Experiments", ASME Paper 91-GT-255

Halila, E. E.; Lenahan, D. T.; Thomas, T. T., 1982, "Energy efficient engine high pressure turbine test hardware detailed design report", NASA-CR-167955.

Han, J. C., S. Dutta., and S. Ekkad. Gas Turbine Heat Transfer and Cooling Technology. Great Britain: Taylor & Francis, 2001.

Harrison, K.L. and Bogard, D.G., 2007, "CFD Predictions of Film Cooling Adiabatic Effectiveness for Cylindrical Holes Embedded in Narrow and Wide Tranverse Trenches," Paper No. GT-2007-28005, IGTI Turbo Expo, Montreal, Canda.

Haven, B.A. and M. Kurosaka (1997). Kidney and anti-kidney vortices in crossflow jets. Journal of Fluid Mechanics, 352 , pp 27-64

Hay, N., and Lampard, D., 1995. "Discharge Coefficient of Flared Film Cooling Holes." ASME Paper 96-GT-492.

Haven, B. A., Yamagata, D. K., Kurosaka, M., Yamawaki, S., and Maya, T., 1997, "Anti-Kidney Pair of Vortices in Shaped Holes and Their Influence on Film Cooling Effectiveness", IGTI Turbo Expo, Orlando, Paper 97–GT–45.

Haven, B. A., Kurosaka, M., 1997, "Kidney and anti-kidney vortices in crossflow jets", J. Fluid Mechanics, 352, pp. 27–64.

Holman, J. P., Experimental Methods for Engineers, 6th ed., McGraw-Hill, Inc., Highstown, NJ, 1994.

Jackson, D. J., Lee, K. L., Ligrani, P. M., Johnson, P. D., and Soechting, F. O., 1999, "Transonic Aerodynamic Losses Due to Turbine Airfoil Suction Surface Film Cooling", IGTI Turbo Expo, Indianapolis, Indiana, Paper 99–GT–260.

Jovanović, M., de Lange, A. and van Steenhoven, A., 2005, "Influence of LASER Drilling imperfection on Film Cooling Performances," IGTI Turbo Expo, Reno-Tahoe, Nevada, Paper GT–2005–68251.

Kadotani, K., and Goldstein, R. J., 1979. "On the Nature of Jets Entering a Turbulent Flow Part A—Jet-Mainstream Interaction," ASME Journal of Engineering for Power, 101, pp. 459–465.

_____, 1979. "On the Nature of Jets Entering a Turbulent Flow Part B—Film Cooling Performance," ASME Journal of Engineering for Power, 101, pp. 466–470.

Kiesow, H. J. and J. Kapat, 2008, “Thermal Barrier Coatings”, Lecture Course *Turbines for Sustainability* at the University of Central Florida.

Kline, S., and McClintok, F., 1953, “Describing Uncertainties in Single-Sample Experiments,” Mechanical Engineering, 75, pp. 3–8.

Kohli, A., and Bogard, D. G., 1998, "Effects of Very High Free-Stream Turbulence on the Jet-Mainstream Interaction in a Film Cooling Flow," ASME Journal of Turbomachinery, 120, pp. 785–790.

Leylek, J.H., Zerkle, R.D. (1993), "Discrete-jet film cooling: a comparison of computational results with experiments", ASME Paper 93-GT-207.

Liu, Q., Kapat, J. S., Douglass, C. J., and Qiu, J., 2003, “Applicability of Temperature Sensitive Paints for Measurement of Surface Temperature Distribution,” IGTI Turbo Expo, Atlanta, Georgia, Paper 2003-GT-38591.

Liu, Quan. Study of Heat Transfer of Impinging Air Jet Using Pressure and Temperature Sensitive Luminescent Paint, Ph.D. Dissertation, University of Central Florida, 2005.

Lu Y., Dhungel A., Ekkad, SV, and Bunker R, 2007, “Effect of Trench Width and Depth on Film Cooling from Cylindrical Holes Embedded in Trenches”, Paper No. GT-2007-27388, IGTI Turbo Expo, Montreal, Canada.

Lu, Y., Nassir, H., Ekkad, S. V., 2005, “Film Cooling from a Row of Holes Embedded in Transverse Trenches,” ASME Paper GT2005-68598.

Lutum, E., Johnson, B. V., 1999, “Influence of the Hole Length-to-Diameter Ratio on Film Cooling With Cylindrical Holes”, ASME J. Turbomachinery, 121, pp. 209–216.

Moffat, Robert J., 1998, Describing Uncertainties in Experimental Results, Experimental Thermal and Fluid Science, Vol. 1, pp. 3–17.

Moustapha, H., M. Zelesky, N. Baines, and D. Japikse. Axial and Radial Turbines. United States: Concepts NREC, 2003.

Pedersen, D. R., Eckert, E. R. G., and Goldstein, R. J., 1977. "Film Cooling with Large Density Difference between the Mainstream and the Secondary Fluid Measured by the Heat-Mass Transfer Analogy, "ASME J. Heat Transfer, 99, pp. 620–627.

Saumweber, C., Schulz, A., and Wittig, S., 2003, "Free-Stream Turbulence Effects on Film Cooling With Shaped Holes," ASME Journal of Turbomachinery, 125, pp. 65–73.

Sen, B., Schmidt, D. L., and Bogard, D. G., 1996, ''Film Cooling With Compound Angle Holes: Heat Transfer,'' ASME J. Turbomach., **118**, pp. 800–806.

Sinha, A. K., Bogard, D. G., and Crawford, M. E., 1991, "Film Cooling Effectiveness Downstream of a Single Row of Holes with Variable Density Ratio", ASME J. Turbomachinery, 113, pp. 442–449.

Sinha, A.K., Bogard, D.G. and Crawford, M.E. 1991 Gas Turbine Film Cooling: Flowfield Due to a Second Row of Holes, J. Turbomach. 113, 450–456.

Taslim, M. E. and Ugarte, S., 2004. "Discharge Coefficient Measurements for Flow Through Compound-Angle Conical Holes with Cross-Flow," International Journal of Rotating Turbomachinery, 10, pp. 145–153.

Thole, K, Gritsch, M., Schulz, A. and Wittig, S, 1998, "Flowfield Measurements for Film-Cooling Holes with Expanded Exits", ASME J. Turbomachinery., 120, pp. 327–336.

Wang T., Chintalapati S., Bunker R., and Lee CP, 2002, "Jet Mixing in a Slot," Experimental Thermal and Fluid Science, **22**, pp. 1-17.

Waye S. K., Bogard D.G., 2006, "High Resolution Film Cooling Effectiveness Measurements of Axial Holes Embedded in a Transverse Trench with Various Trench Configurations" Paper No. GT-2006-90226, IGTI Turbo Expo, Barcelona, Spain.

Wheeler, Anthony J. and Ahmad R. Ganji, Introduction to Engineering Experimentation, 2d ed., Pearson Prentice Hall, Upper Saddle River, NJ, 2004.

York, W. D., Leylek, J. H., 2003. "Leading-Edge Film-Cooling Physics—Part III: Diffused Hole Effectiveness," ASME Jorunal fo Turbomachinery, 125, pp. 252–259.

Yu, Y., Yen, C.-H., Shih, T. and Chyu, M. K. and Gogineni, S., 2002. "Film Cooling Effectiveness and Heat Transfer Coefficient Distributions Around Diffusion Shaped Holes," ASME Journal of Heat Transfer, 124, pp. 820–827.